NEW STUDY OF THE CERRO SECO RHYOLITE, VALLES CALDERA, NEW MEXICO

A Thesis

Presented to the faculty of the Department of Geology

California State University, Sacramento

Submitted in partial satisfaction of
the requirements for the degree of

MASTER OF SCIENCE

in

Geology

by

Robin L. Wham

SPRING
2018

NEW STUDY OF THE CERRO SECO RHYOLITE,

VALLES CALDERA, NEW MEXICO

A Thesis

by

Robin L. Wham

Approved by:

_____, Committee Chair
Lisa Hammersley

_____, Second Reader
Amy Wagner

_____, Third Reader
Fraser Goff

_____
Date

Student: Robin L. Wham

I certify that this student has met the requirements for format contained in the University format manual, and that this thesis is suitable for shelving in the Library and credit is to be awarded for the thesis.

_____, Department Chair _____
Tim Horner Date

Department of Geology

Abstract

of

NEW STUDY OF THE CERRO SECO RHYOLITE,

VALLES CALDERA, NEW MEXICO

by

Robin L. Wham

Cerro Seco is one of six post-caldera rhyolite domes in the northern moat of the Valles Caldera, New Mexico. This study presents detailed mapping as well as petrographic and geochemical analysis of Cerro Seco's eruptive units and surrounding lacustrine deposits. Cerro Seco's eruptive members were previously mapped as three separate units: two flow units (lavas Qvse1 and Qvse2), and a pyroclastic unit Qvset. This study has revealed that the pyroclastic unit should be classified as two units: one ignimbrite and one hydromagmatic tuff. Outcrop morphology and pumice clast morphology support a hydromagmatic eruption for the newly classified unit; geochemical analysis illustrates that significant post-emplacement alteration involving water also occurred. This new study offers an in-depth characterization of Cerro Seco and a model for it its eruptive behavior, with primary focus on the hydromagmatic tuff; a new designation of Qvshy is proposed for the hydromagmatic unit. These findings are important because they identify Cerro Seco as the only eruptive center in the Valles caldera that produced a

hydromagmatic eruption. Findings and conclusions put forth by this study have not been identified until now, and are unique within the Valles caldera system.

.
_____, Committee Chair
Dr. Lisa Hammersley

_____
Date

ACKNOWLEDGMENTS

I express my gratitude to my departmental advisor, Dr. Lisa Hammersley, of California State University, Sacramento, for her direction since this work started in 2015. Dr. Hammersley has guided me with her critical thinking and editorial skills during the course of this project, and I thank her for taking me in and keeping me on track.

I am indebted to Dr. Fraser Goff, a remarkable scientist and field geologist, and undisputed expert on the geology and many other aspects of the Valles Caldera, New Mexico. His tireless enthusiasm for the project, and his dedication to both my education and the Valles are an inspiration. I thank him for his introduction to, and companionship in one of the most geologically beautiful field areas I have experienced, and for all his direction in the writing of this thesis.

I also express thanks to Amy Wagner, for her support and kindness over the past two years. My gratitude goes to Cathy Goff, whose geological insights, hospitality and support were immeasurable contributions to my wellbeing during this project. To Dr. Ken Wohletz, your keen eye, knowledge and experience, both in the field and through our exchanges, have been invaluable. Special thanks go to Matt O'Neal for his technical help and friendship, and for sharing his expertise with ArcMap.

Additionally, I would like to thank Christopher Farrar for his voluntary position as my field assistant. His field support, geologic curiosity and ability to digest publications are respectable behaviors that inspired me in the field. I will always treasure the many great memories we created in the Valles.

I thank my thesis committee: Dr. Lisa Hammersley, Dr. Fraser Goff and Dr. Amy Wagner for their time, patience, and guidance in reviewing my work. In the department, Dr. Barb Munn and Dr. Greg Wheeler were always there for me. I thank them for their petrographic skills and steady support.

Finally, immense gratitude goes to my family and friends for their continued love, and whose patience and support raised me up to this achievement.

This project was funded in part by a Graduate Student Scholarship received from the National Association of Geoscience Teachers, Far Western Section in 2015. I give thanks to Dr. Robert Parmenter of the Valles Caldera National Preserve for his kind attention in obtaining a research permit, and to Dr. Matthew Zimmerer at the New Mexico Geochronology Research Laboratory for his extra assistance in determining $^{40}Ar/^{39}Ar$ dates for this project.

TABLE OF CONTENTS

Page

LIST OF TABLES

Tables Page

LIST OF FIGURES

LIST OF ILLUSTRATIONS

Plate Page

CHAPTER 1

INTRODUCTION

The Valles caldera (1.25 Ma) of north-central New Mexico consists of a 22-km diameter collapse depression that contains the central resurgent dome Redondo peak, and a concentric ring of 15 post-caldera dome and flow eruptive centers that represent the climactic and terminal stage of volcanism in the Jemez Mountains (Bailey et al., 1969). Of these, Cerro Seco, the primary focus of this study, is the only rhyolite dome in the northern caldera moat that erupted a significant amount of pyroclastic material.

The Valles caldera, named for the many valleys within it, is one of the world's most studied calderas, and is considered to be the type location of a resurgent caldera. This distinction is due to its well-defined topographic expression of multiple discrete domes along a circular ring-fracture zone, its excellent exposures, and to its relatively little-eroded state. Additionally, it has been drilled to reveal an understandable subsurface picture, and exhibits a clear mechanism by which resurgence occurred (Smith and Bailey, 1968; Self et al., 1986; Goff et al., 2011). Stratigraphy of the Valles caldera spans the Proterozoic to the Cenozoic, and is diverse; the most recent geologic map of the Valles caldera documents 140 map units.

Smith et al. (1970) mapped the northern moat eruptive centers as one unit of "domes and flows", named at that time as the Valle Grande member, and identified one subunit of "tuffs" in the northern moat associated with the domes (SAM, CS, SL, SR, CA and DM in Figure 1) (Gardner et al., 2010).

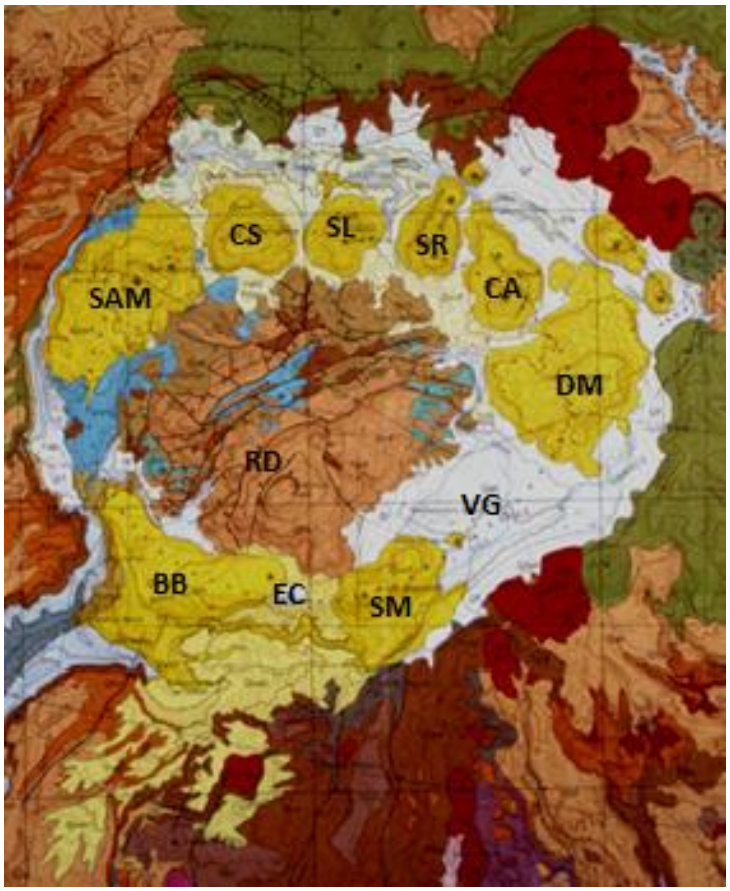

Figure 1. Photograph of the central part of the geologic map of the Jemez Mountains, New Mexico (Smith et al., 1970) showing the Valles caldera. RD = resurgent dome, mostly orange; VG = Valle Grande. Moat rhyolites are shown in dark yellow: DM = Cerro del Medio; CA = Cerros del Abrigo; SR = Cerro Santa Rosa; SL = Cerro San Luis; CS = Cerro Seco; SAM = San Antonio Mountain; BB = Banco Bonito; EC = El Cajete; SM = South Mountain. Pale yellow surrounding northern moat rhyolites designate "tuffs" and other deposits too small to show in detail.

More recent mapping and analysis has led to separate identification of the northern moat eruptive units. Goff et al. (2006; 2011) mapped each dome as a distinct lithologic unit, identifying one pyroclastic unit in the northern apron of Cerro Seco, neither separating the pyroclastic members, nor differentiating between ignimbrite and any hydromagmatic units (Figure 2, Figure 3). The detailed geologic map of the Valles caldera by Goff et al. (2011) describes 140 lithologic units, revises the nomenclature, and

regroups units within the Valles caldera by age and composition. In its accompanying document, "Description of Map Units", the Cerro Seco Member is described as two rhyolite lava flow units based on morphology, and one pyroclastic deposit consisting of ignimbrite and dry surge near the vent, to probable hydromagmatic surge distally. The goal of this study is to fully characterize Cerro Seco's pyroclastic deposits and determine (1) whether there are indeed two distinct pyroclastic units and (2) if there is any evidence for a hydromagmatic origin for any of the pyroclastic deposits.

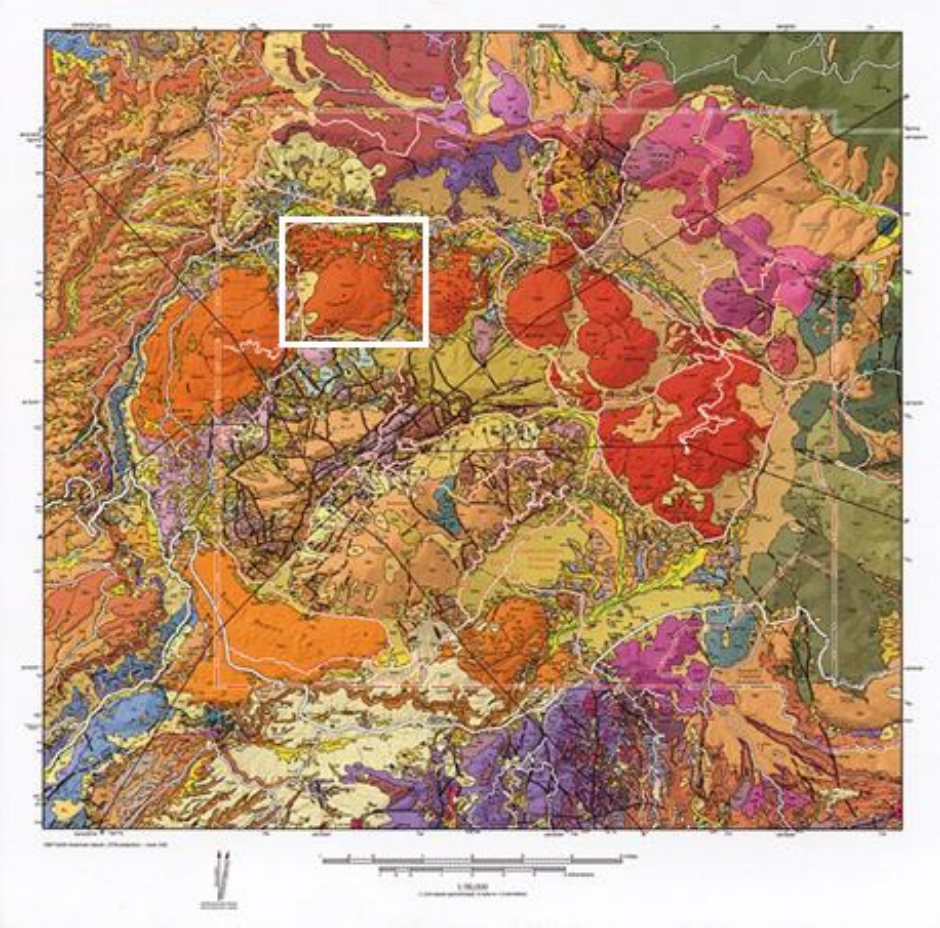

Figure 2. Most recent geologic map of the Valles caldera, Jemez Mountains, New Mexico (from Goff et al., 2011), with boxed Cerro Seco field area. The map's accompanying explanation describes 140 lithologic units.

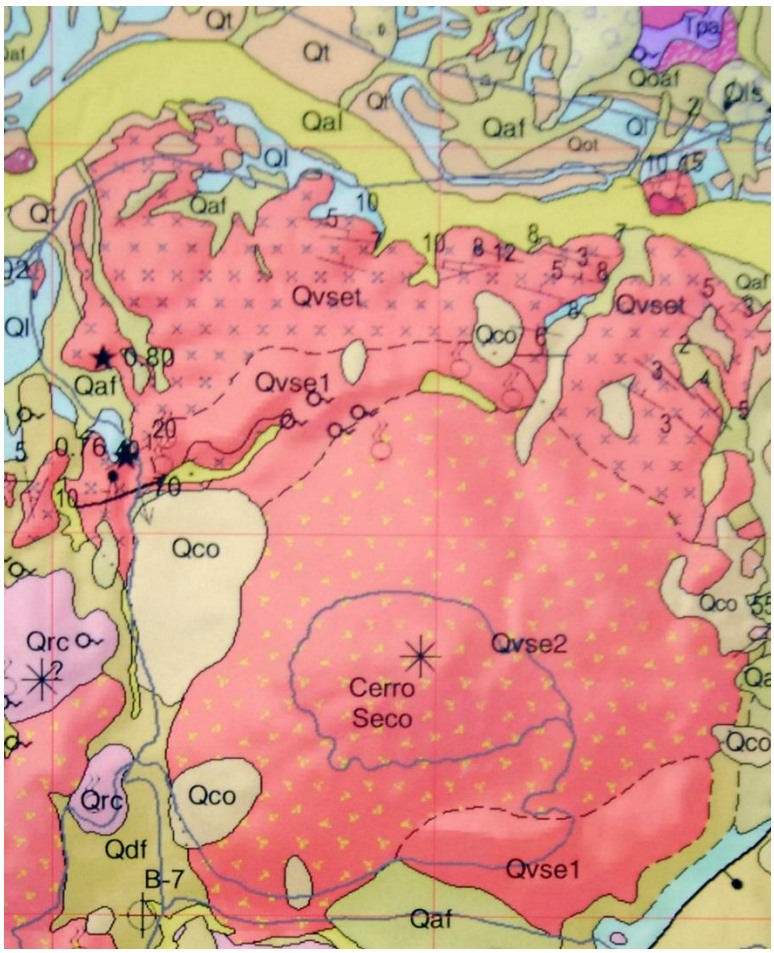

Figure 3. Detail of Cerro Seco from the geologic map of the Valle San Antonio quadrangle (from Goff et al., 2006). Relevant abbreviations: Qvset = pyroclastic rocks, undivided, produced during early phase of Seco eruption; Qvse1 and Qvse2 = later dome lavas; Ql = lacustrine deposits; Qdf = early caldera-fill debris flow; Qrc = Redondo Creek rhyolite; B-7 = geothermal well Baca-7.

Aside from the basic mineralogy, Ar/Ar dates, and gross description associated with the geologic map, little has been specifically written about the Cerro Seco post-resurgent dome eruption. This study provides detailed mapping of Cerro Seco, petrographic and geochemical analyses that characterize it more fully and contribute to our understanding of the timing and mechanism for eruption of the Cerro Seco dome.

1.1 Geologic Background and Previous Work

The earliest work in the Valles caldera was done by C.S. Ross, R.L. Smith and R.A. Bailey of the USGS, from the 1920's through the 1960's. It was Smith and Bailey who developed the classic 7-stage model of resurgent caldera formation (Figure 4).

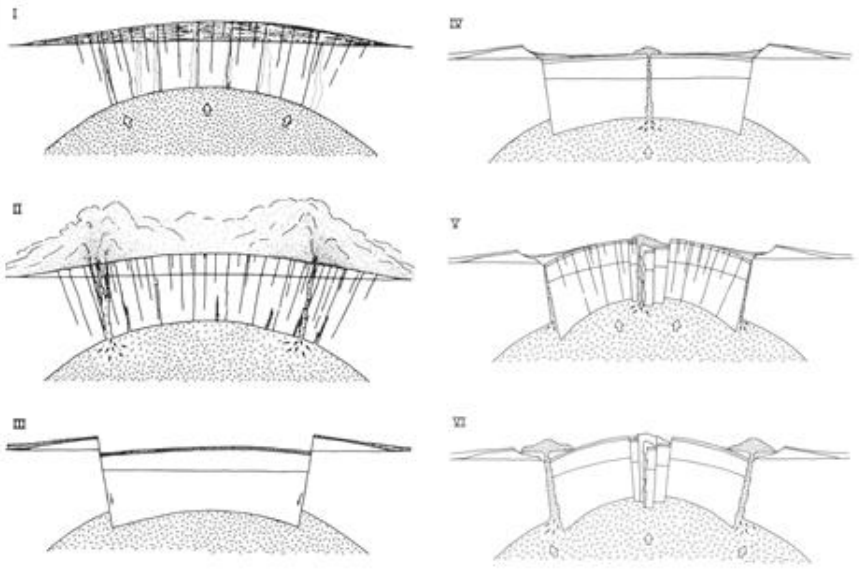

Figure 4. Major stages in the resurgent caldera cycle, based on the Valles caldera (Smith and Bailey, 1968): I Regional tumescence and ring-fracture development; II Caldera-forming eruption; III Caldera collapse; IV Preresurgence volcanism and sedimentation; V Resurgent dome formation; VI Ring- fracture volcanism. Not shown is Stage VII Post caldera hydrothermal alteration.

Further detailed geologic mapping and volcanological studies of the Jemez volcanic field in the 1980's refined the stratigraphic and temporal relations of major units on a regional scale, and obtained over 100 radiometric dates (Gardner et al., 1986). These studies revealed that the inception of volcanism in the area began by about 16.5

Ma with episodic eruptions of alkaline basalts, progressing to olivine tholeiite and high-silica rhyolite (ca. 10 Ma), then to andesitic, dacitic, and rhyolitic rocks from 10 to 2 Ma, finally to eruption of large volume rhyolitic ignimbrites by less than 2 Ma (Gardner et al. 1986). The latter coincides with the 1.64 to 1.24 Ma time frame for creation of the Toledo and Valles calderas, the whole sequence illustrating a typical compositional evolution within caldera systems.

The most recent dates for the Cerro Seco Member of the Valles Rhyolite are 0.77 ± 0.03 Ma and 0.78 ± 0.04 Ma on pumice from the two units that Goff et al. suggested make up the pyroclastic deposit (Goff et al., 2006, 2011; Kelley et al., 2013), and 0.80 ± 0.007 for the youngest dome lava (Spell and Harrison, 1993). New dates for the two units of the pyroclastic deposit and for Qvsl1 from adjacent Cerro San Luis are pending.

Exploration drilling and studies of the evolution of the geothermal system in the Valles caldera revealed a mature hydrothermal system that remains hot, and that contains a classic geothermal configuration (Goff and Gardner, 1994). Through various dating methods, they conclude that the system was created at about 1.0 Ma, and although it has been continuously active to the present, the size of the hydrothermal system has shrunk since initial formation. While the wells were not utilized commercially, they did produce a wealth of stratigraphic and geochemical data, which aided in the understanding of caldera geologic history. For example, well Baca-7 drilled just SW of Cerro Seco, has a lithologic log extending down to 1700 m (Lambert and Epstein, 1980), the data from which augments this study's cross section (Plate II and Appendix A, Table 7).

1.2 Tectonic Setting and Regional Geology

The Jemez Volcanic Field (JVF) contains basalts, andesites, dacites and rhyolites from a variety of eruptions beginning at 16.5 Ma, and dominated by eruption of rhyolitic ignimbrites less than 2 Ma, the most notable of which created the Valles caldera (Gardner et al., 1986). The JVF sits at the intersection of the Jemez lineament and the Rio Grande rift (Figure 5).

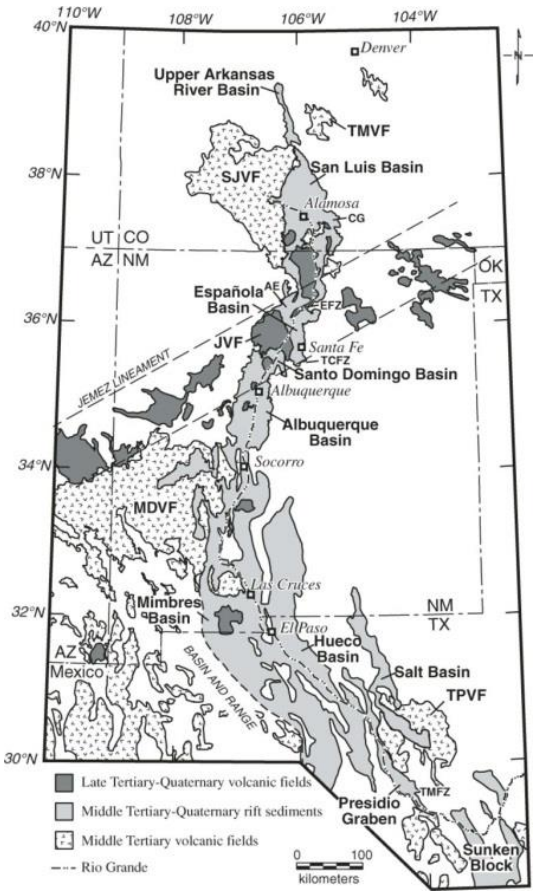

Figure 5. Geographic extent and main features of the Jemez lineament and the Rio Grande rift (from Hudson and Grauch, 2013). Relevant abbreviations: JVF=Jemez Volcanic Field; SJVF=San Juan Volcanic Field; MDVF=Mogollon-Datil Volcanic Field.

The Jemez lineament is a ~50-km wide, northeast-trending (N52E) tectonically active crustal flaw that extends from eastern Arizona through northern New Mexico into Colorado and Oklahoma, and comprises an alignment of late Cenozoic volcanic fields. Its location coincides with the southeastern border of the Colorado Plateau, also with a Precambrian province boundary (Aldrich, 1984; Karlstrom and Humphreys, 1998). Researchers have long speculated that the lineament is a long-lived basement weakness that influenced rift development and was a conduit for magma in Cenozoic time (Aldrich and Laughlin, 1984; Hudson and Grauch, 2013). Because no systematic progression of age has been identified within the lineament rocks, hotspot tectonism has been ruled out (Lipman, 1980). The Rio Grande rift is a 1000 km-long intraplate series of asymmetrical grabens extending from central Colorado through New Mexico, to Chihuahua, Mexico, thought to be the result of passive extension (West et al., 2003) (Figure 5).

1.3 The Valles Caldera

The magmatic volume of the 1.62 Ma Otowi eruptions that created Toledo caldera is estimated within a range of 216 to 550 km^3 (Goff, 2009; Cooke et al., 2016). At 1.25 Ma in a nearly coincident event the Valles caldera was formed when 400 km^3 of ash-flow tuff erupted, nearly obliterating the Toledo caldera. The pyroclastic flows produced collectively by the Toledo and Valles eruptions are called the Bandelier Tuff, with a combined eruptive volume of 800 km^3.

1.4 Resurgence and Post-resurgent eruptions

After the Valles caldera formed and the Tshirege Member of the Bandelier tuff was emplaced, the caldera floor collapsed, the caldera was filled with a lake, and small volume rhyolite domes, flows and tuffs (Deer Canyon Member of Valles Rhyolite) were erupted into the lake (Smith et al., 1970; Gardner et al., 2010; Goff et al, 2011). Almost coincident with these events, buoyant residual magma began to lift the central caldera floor (Smith and Bailey, 1968). The entire resurgence event occurred over roughly 30,000 years to produce the elliptical dome, present day Redondo Peak, 1000 m above the original caldera floor (Phillips et al., 2007; Goff et al., 2011)(Figure 6). Although small volumes of crystal-rich rhyodacite lavas were erupting during mid- to late resurgence, the Redondo Peak resurgent dome is a structural uplift, not a volcanic dome (Smith and Bailey, 1968; Goff, 2009).

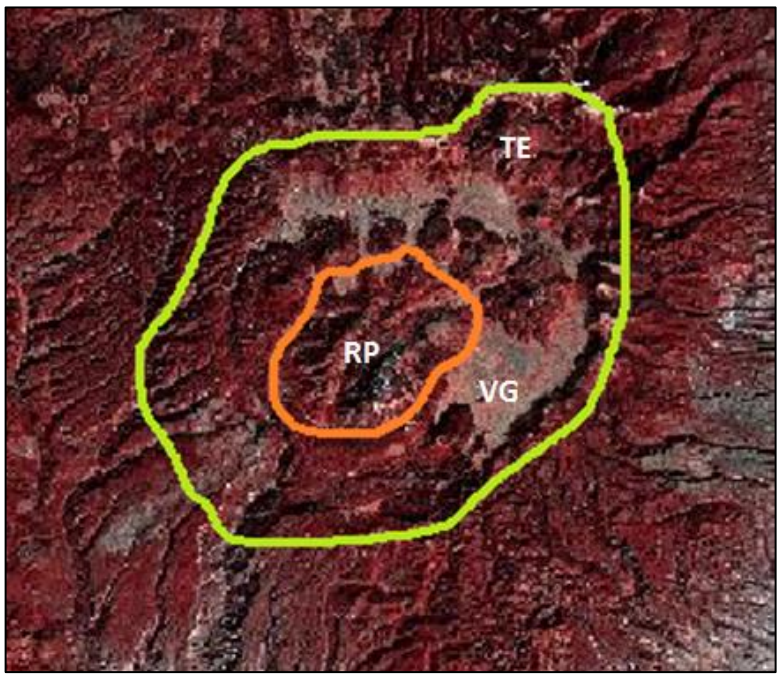

Figure 6. False-color Landsat photo of Valles caldera (outlined in green), showing central resurgent dome Redondo Peak (RP, outlined in orange) and concentric ring of moat rhyolites. TE = Toledo embayment; VG = Valle Grande (modified from Goff et al., 2011; photo from www.ece.rice.edu).

Following resurgence six large rhyolite domes erupted sequentially in the moat between the resurgent dome and the northern caldera walls. The first moat rhyolite to erupt was Cerro del Medio at 1.23 ± 0.017 Ma, followed by Cerros del Abrigo (0.97 ± 0.010 Ma), Cerro Santa Rosa (0.93 – 0.79 ± 0.015 Ma), Cerro San Luis (0.80 ± 0.003 Ma), Cerro Seco (0.80 ± 0.007 Ma) and San Antonio Mountain (0.56 ± 0.004 Ma) (Spell and Harrison, 1993; Singer and Brown, 2002; Goff et al., 2011). Moat rhyolite volcanism then shifted to the southern ring-fracture zone of the caldera, when the South Mountain Member (0.52 ± 0.01 Ma) and East Fork Member (El Cajete, Battleship Rock Ignimbrite, VC-1 rhyolite and Banco Bonito Flow) erupted until c.a. 70 ka (Spell and Harrison, 1993; Toyoda et al., 1995; Reneau et al., 1996; Ogoh et al., 1993; Phillips et al., 1997; Goff and Gardner, 2004; Lepper and Goff, 2007; Zimmerer et al., 2016).

Cerro Seco is the only lava dome of the northern group that exhibited significant pyroclastic eruptions; only small volumes of pyroclastic rocks have been identified in some of the other domes. The most current description of the Cerro Seco Member defines three units: Qvset, the earliest pyroclastic deposit, and Qvse1 and Qvse2, two morphologically defined rhyolite lavas (Goff et al., 2011).

1.5 Hydromagmatism

One of the main goals of this study is to determine whether the second unit of Qvset suggested by Goff has a hydromagmatic origin. Generally, any interaction of water and magma or magmatic heat with an external source of water can be defined as hydromagmatic. In the literature, the terms hydrovolcanic, hydromagmatic, phreatomagmatic, phreatoplinian or hydroclastic are also used when referring to an

eruption caused by the mixing of magma with water; the terms have slightly distinct meanings. For this study, the general term hydromagmatic is used. The water-magma interaction may occur in a variety of terrestrial or marine environments, and results in the explosive expansion of volatile materials (Figure 7). The development of hydromagmatic phenomena in the wake of magma-water interaction is governed by the duration of the initial contact of external water with erupting magma and the mass ratio of water to magma (Sheridan and Wohletz, 1983).

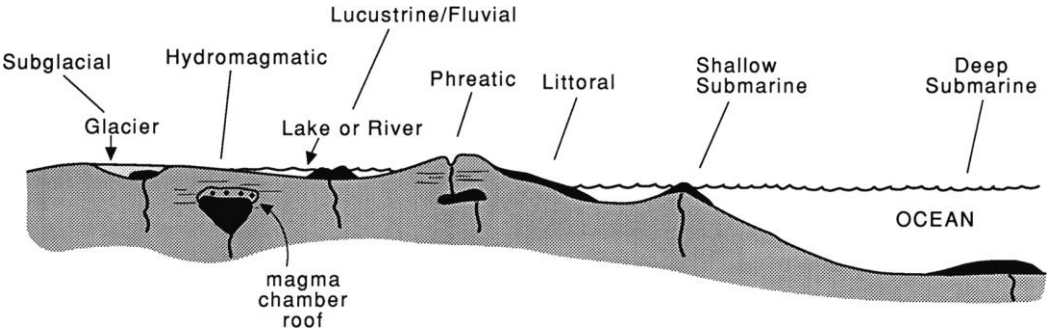

Figure 7. Common environments for hydromagmatism (from Wohletz et al., 2012).

The most common volcanic edifices associated with hydromagmatic activity are tuff rings and tuff cones, formed subaerially and/or in shallow water (Vespermann and Schmincke, 2000) (Figure 8c). Whether a tuff ring or a tuff cone is formed depends on if the erupting lateral blasts (called surges) were dry (superheated steam media) or wet (condensing steam media) (Wohletz, 1998). Tuff rings are commonly less than 50 m high, have shallow craters with small depth-to-width ratios, and have beds dipping <25° (Vespermann and Schmincke, 2000). Tuff rings encounter water at a shallow depth,

leading to central craters that are at or above ground level. This study illustrates that Cerro Seco's pyroclastic phase included a hydromagmatic eruption that resulted in a tuff ring.

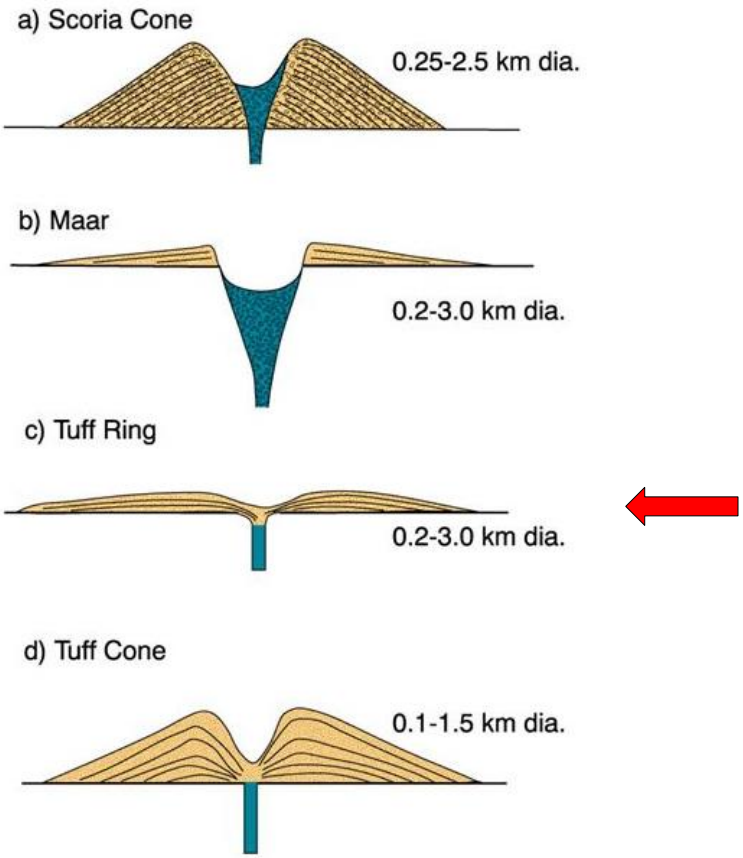

Figure 8. Hydromagmatic landforms with comparison to tuff ring morphology (red arrow) with other (after Wohletz and Sheridan, 1983).

CHAPTER 2

METHODS

This study included geologic mapping, petrography, geochemical analyses, and (pending) $^{40}Ar/^{39}Ar$ dating analyses. Refer to Appendix A for specific information about mapping, petrographic, and geochemical methods.

Detailed geologic mapping was conducted in 2016 and 2017 in the north central part of the Valle San Antonio 7.5-minute topographic quadrangle, and focused on mapping the lithologic units of the Cerro Seco rhyolite lava dome. Other related volcanic rocks, pre-eruptive rocks and Quaternary non-volcanic units were also mapped (Plate 1). Special attention was given to contacts, map unit distribution in the field, bedding attitudes, features and thickness, and other volcanic and sedimentary features useful for establishing stratigraphic, structural, and magmatic relationships.

Thirty-one standard 30-micron thin-sections were analyzed petrographically. Of these, eleven new slides were made by Steve Rounds at California State University, Sacramento, from hand samples gathered in 2016. Another fifteen slides had been previously made but were unstudied, and provided by Dr. Fraser Goff for this study. The latter were made by David Mann of High Mesa Petrographics, who also made five new thin sections from hand samples gathered in 2017. Detailed petrographic descriptions of multiple units were recorded from these thin-sections, including mineralogy, modal percentages, colors, presence of lithic fragments, and textures from volcanic and depositional processes (Appendix B).

Whole-rock and pumice samples of ash-flow tuffs, lavas, and pyroclastic units representative of igneous activity at Cerro Seco underwent complete geochemical analysis at ALS Mineral in Reno, Nevada. Ten samples were analyzed using ICP-AES and ICP-MS instrumentation. New radiometric dates for three units - Qvset-2 (the proposed Qvshy) and Qvse1 from Cerro Seco, and Qvsl1 from adjacent Cerro San Luis - are being calculated from measured $^{40}Ar/^{39}Ar$ of sanidine phenocrysts using an Ar-Ar total fusion method. These ages are being determined by Matt Zimmerer at the New Mexico Geochronology Research Laboratory, but are incomplete as of this publication.

CHAPTER 3

RESULTS

3.1 Geologic Mapping and Stratigraphy of Cerro Seco and Associated Map Units in the Northern Moat

The majority of the floor of the Valles caldera collapse depression sits at or above an elevation of 2560 m (8,400 ft). Resurgence uplifted the central floor of the caldera to form Redondo Peak, which at 3430 m (11,254 ft) marks the highest elevation in the caldera. The caldera footprint within the ring fracture zone is nearly circular with a diameter of 13.6 km, occupying an area of roughly 145 km^2. This project's mapping area may be generally described as a central-northwest sixth of the northern moat of the Valles caldera, an area of roughly 30 km^2. Refer to Plate 1, Geologic Map of Cerro Seco for correlation to this section.

In this section the focus is field mapping results, with particular attention given to the Cerro Seco pyroclastic unit and two lava flow units. However, other lithologic units in the area, both adjacent to and underlying Seco, afford a deeper understanding of Seco's history and character, also described in this section.

3.1.1 Post-caldera debris flow and gravels

The substrate through which all post-caldera moat rhyolite units erupted is associated with resurgence, and a variety of landslide, slump, alluvial and colluvial identified as Qdf, a matrix-supported conglomerate of early post-caldera rhyolites, Bandelier Tuff, precaldera volcanic rocks, Miocene to Permian sandstone, Pennsylvanian limestone and Precambrian crystalline rocks (Goff et al., 2011) (Figure 9 and Plate 2).

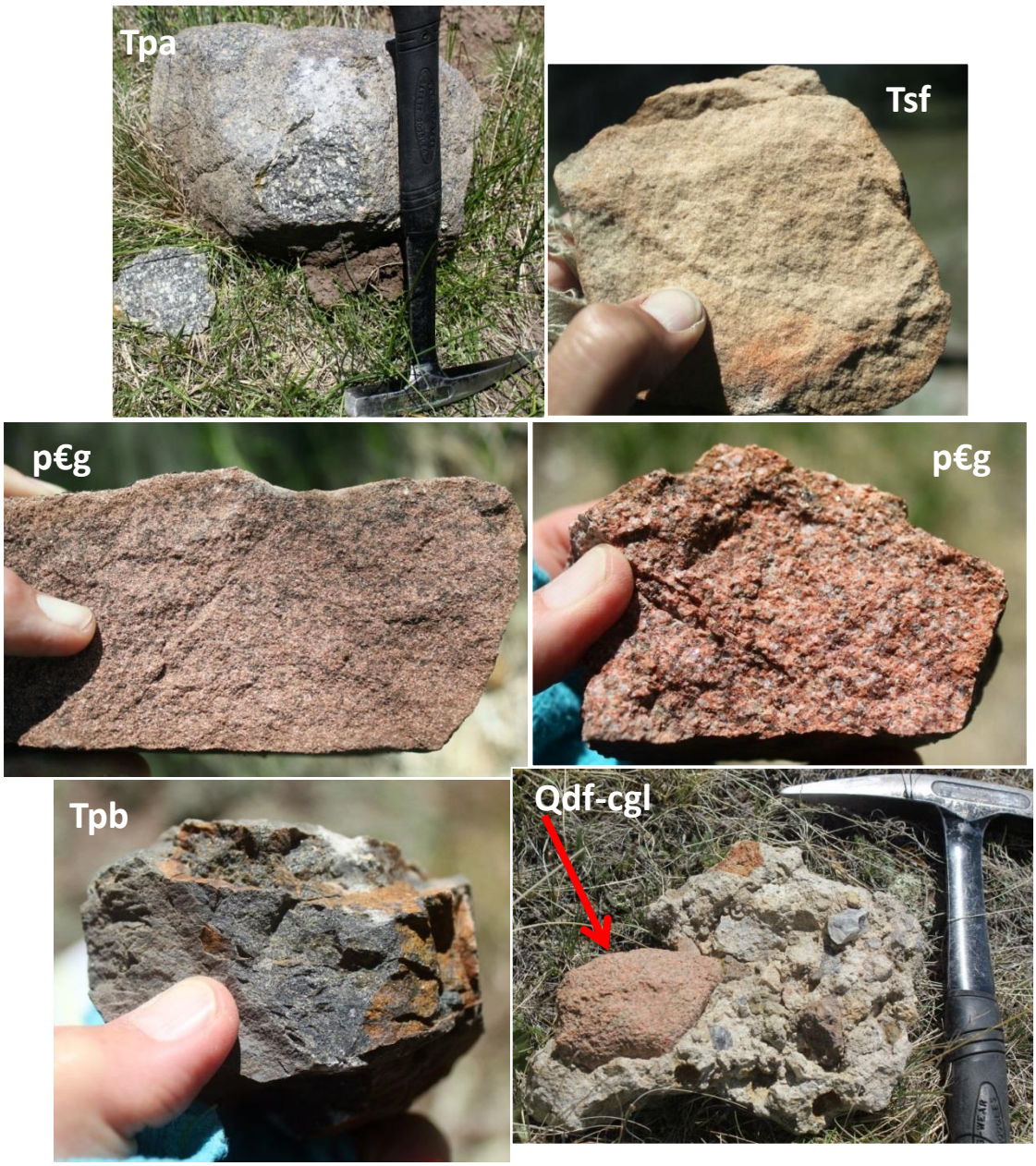

Figure 9. Composite photograph of some constituents of **Qdf***, the early caldera-fill debris flow unit, consisting of (clockwise from top left): boulder of **Tpa***, porphyritic andesite from Paliza Canyon Formation, Keres Group; **Tsf***, sandstone of Santa Fe Group; **p€g**, Precambrian granite; **Qdf-cgl**, conglomeratic clast of debris-flow unit with ashy groundmass, showing variety of clast types; **Tpb***, fine-grained basaltic andesite from Paliza Canyon Formation, Keres Group; **p€g**. fine-grained Precambrian granite or granite gneiss**.** Red arrow points to clast of coarse-grained p€g. See text for details. ***Nomenclature after Goff et al., 2011.

The debris flow and gravel deposits of Qdf were emplaced as a result of the uplift erosional processes since caldera formation. The unit incorporates a wide variety of pre-caldera rocks with compositions and ages that constituted the crust at the time of caldera formation, and it is mixed with eroded products of the early caldera (Bandelier Tuff and early post-caldera rhyolite lavas and tuffs). This unit exists in the mapping area as loose cobbles and boulders, rarely visible in place within its finer-grained matrix, although whole-rock evidence is seen in the field (Figure 9: Qdf-cgl). The age assigned to the heterogeneous Qdf unit is 1.25 to 1.0 Ma (Goff et al., 2011), though the fact that it is interbedded with and overlies all other units on the resurgent dome renders the lower age inexact.

3.1.2 Lacustrine deposits

The Valles caldera has contained multiple lakes since its formation and resurgence at ≥1.2 Ma. The current understanding holds that three large lakes (each >20 km^2 in area) formed when drainages were dammed during the three youngest episodes of volcanism, but it is likely that earlier volcanism similarly blocked drainages and allowed lakes to form (Reneau et al., 2007). Intracaldera lakes have been dated at 55 ka, 520 ka, 560 ka, 800 ka and 1.25 Ma (Goff and Goff, 2005). The lake at 1.25 Ma formed soon after caldera formation, consistent with the original caldera evolution model proposed by Smith and Bailey (1968) (Figure 10).

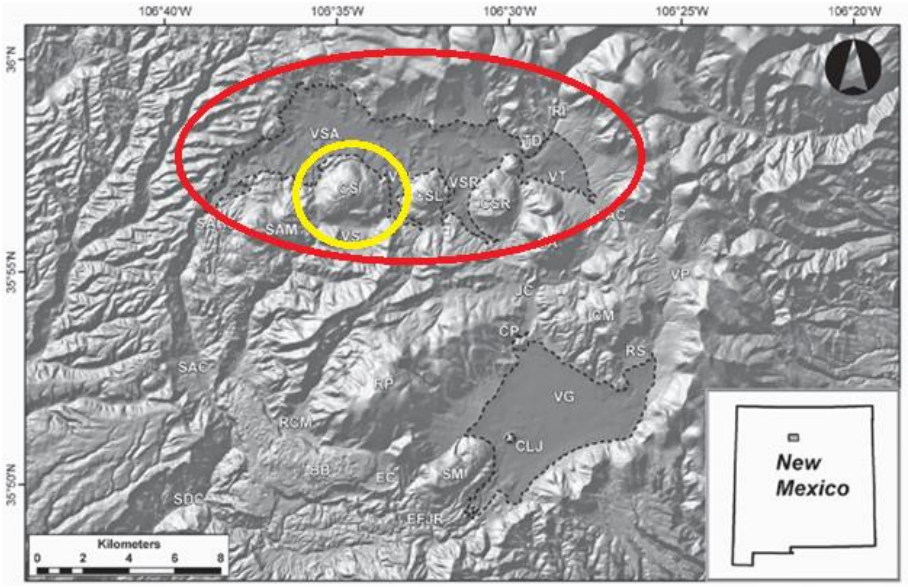

Figure 10. Digital elevation model of the Valles caldera showing estimated maximum lake extent in Valles San Antonio (VSA-circled in red) and South Mountain Lake in Valle Grande (VG). Cerro Seco (CS) is circled in yellow. For other abbreviations see text. After Reneau et al., 2007.

One of the large post-resurgent lakes occupied much of the northern moat, and was formed when thick flows of rhyolite from San Antonio Mountain (at ca. 557 ka; Spell and Harrison, 1993) abutted the west wall of the caldera, thus forcing San Antonio Creek to cut a course between the lava and weaker Bandelier Tuff, blocking San Antonio Creek (Reneau et al., 2007) (Figure 10). The most extensive outcrops of lacustrine sediment in the Valles caldera occur in the northern moat along San Antonio Creek and its tributaries, site of the previous San Antonio Lake (Reneau et al., 2007).

Lacustrine deposits both underlie and overlie Cerro Seco deposits, indicating that there was another lake in the northern moat before 0.8 Ma. These deposits are found at elevations from 2567 m to 2706 m at points around all but the southwest quadrant of Cerro Seco dome (Plate 1 and Table 1).

Location (by WP)	Elevation (m)	Description
WP-144	2567	opalized, strongly bedded
WP-100	2580	unconsolidated, weakly bedded
WP-123	2590	opalized, strongly bedded
WP-024	2595	opalized, strongly bedded
WP-028	2638	pink "beach sands"
WP-013	2639	pink "beach sands"
WP-139	2674	pink "beach sands"
WP-129	2706	consolidated, presence of crystals

Table 1. Lacustrine deposits around Cerro Seco by waypoint location, listed in ascending elevation in meters. Note similar elevations for pink “beach sands”.

Lacustrine deposits (Ql) are described as finely laminated clay, silt and very fine sand, often interlayered with coarser sand and gravel (Goff, et al., 2011). They are seen in the field typically as light-colored, poorly consolidated, sandy outcrops, well exposed in ravines or low hillsides (Figures 11A and B), but are also found as white, strongly laminated and consolidated beds (Figure 11C).

Figure 11. Lacustrine deposits (Ql), typically fine-grained clay, silt and very fine sand

A. Lacustrine deposits near site WP-100 in ravine alongside road VC09 within northern moat area. Red bar = 1 m.

B. Unconsolidated "beach sands" of Ql deposit on road VC08 near site WP-144, field assistant for scale.

C. Consolidated, laminated and weakly cross-bedded Ql at site WP-144, thumb for scale.

Another unit potentially classified as lacustrine was originally mapped by Goff et al. (2011) as Qso, an older intracaldera sandstone. Described as a weakly indurated, moderate to well-sorted, subrounded, medium-grained reddish-tan quartz lithic sand, the unit underlies portions of the second Seco lava in the eastern mapping area (Goff et al., 2011). Unconsolidated pink "beach sands" are also found in zones measuring 10 m by 50 m in the field area at similar elevations (Figure 12 and Table 1).

Figure 12. Pink "beach sands." Mapped by Goff et al. (2011) as Qso, an older sandstone. This outcrop on the eastern edge of mapping area is at elevation 2674 m and is roughly 30 m thick.

In other lacustrine outcrops (site WP-123), bedding is more conspicuously indurated and opalized, and may represent other sedimentary features such as preserved mudcracks (Figure 13A and B).

Figure 13. Opalized lacustrine deposits.

A. Broken pieces of Ql in opalized, indurated form at outcrop near site WP-123.

B. Opalized blebs of lacustrine sediments found near site WP-123, mapped as Ql, tentatively interpreted to be mudcracks with opaline infill.

While this project did not constitute an in-depth study of the several lacustrine environments and chronology within the northern moat, the complexity of the relationship between volcanism of Cerro Seco and the lakes that have existed here is noted, and merits further study. Lacustrine deposits were mapped as they were encountered, as were water-altered and water-related features and deposits relating to the Cerro Seco volcanic rocks.

3.1.3 Cerro San Luis Member

Although not the primary focus of this project, the stratigraphic relationship of Cerro San Luis members (lavas Qvsl1 and Qvsl2) to those of Cerro Seco is important for interpretation of Seco's eruptive sequence. The two San Luis lavas together occupy a surface area of roughly 10 km^2 comprising the dome of Cerro San Luis. The first lava (Qvsl1) immediately underlies the ignimbrite of Cerro Seco in the easternmost margin of the field area (Plate 1). The second lava of San Luis (Qvsl2) has yielded an $^{40}Ar/^{39}Ar$ date of 0.800 ± 0.003 Ma (Spell and Harrison 1993) (Table 2). A date for the first San Luis lava is pending. The Cerro San Luis Member is a flow-banded porphyritic rhyolite lava containing phenocrysts of sanidine, quartz and biotite, and achieves a maximum exposed thickness of 325 m (Goff et al, 2011). It was previously mapped as two flow units (Qvsl1 and Qvsl2) based on morphology.

Map Unit	Age (Ma)	Sample	Description
Qvsl1	pending	RWVC17-043	San Luis first lava
Qvsl2	0.800 ± 0.003	-	San Luis second lava (Spell and Harrison 1993)
Qvset-1	0.78 ± 0.04	F05-137	pumice of Seco ignimbrite (Goff et al., 2006, 2011; Kelley et al., 2013)
Qvset-1	pending	RWVC16-132	Seco whole-rock ignimbrite, WP-16-132
Qvset-2	0.77 ± 0.03	JG05-15C	Seco hydromagmatic deposit (Goff et al., 2006, 2011; Kelley et al., 2013)
Qvse1	pending	RWVC16-116	Seco first lava - WP-16-116
Qvse2	0.800 ± 0.007	-	Seco second lava (Spell and Harrison 1993)

Table 2. **Radiometric ($^{40}Ar/^{39}Ar$) dates of selected northern moat volcanic rocks from Cerro Seco and associated Cerro San Luis in millions of years.** A (-) symbol indicates that no sample number was reported. All listed dates were obtained on sanidine phenocrysts (see Spell and Harrison, 1993 and Kelley et al., 2013, Table 1 for analytical details).

3.1.4 Cerro Seco Pyroclastic Unit

The focus of this project is Cerro Seco, one of six northern moat rhyolite domes in the Valles caldera, which produced pyroclastic and lava flow deposits. Goff (2011), when describing the pyroclastic unit Qvset, notes that it is likely composed of two separate units, one with a possible hydromagmatic origin. Field observations confirmed that there are two pyroclastic units that can be clearly distinguished from one another. For the sake of clarity, these two units will be referred to in this section as Qvset-1 and Qvset-2. Qvset-1 refers to the ignimbrite deposit already described by Goff, and Qvset-2 refers to the second unit, which Goff hypothesized may have a hydromagmatic origin.

The Cerro Seco ignimbrite Qvset-1 crops out at the furthest east and west extents of the northern half of the field area (Plate 1.) Geologic mapping shows that Cerro San Luis lava Qvsl1 erupted before the Cerro Seco ignimbrite, as seen on the eastern map edge where the ignimbrite overlies the first lava of Cerro San Luis as a channel-filling deposit (Figures 14A-B). Pumice in the Cerro Seco ignimbrite yielded an $^{40}Ar/^{39}Ar$ date of 0.77 ± 0.03 Ma, from outcrop WP-102 near the western access road VC09 (Goff et al., 2006, 2011; Kelley et al., 2013) (Table 2). In the western field area the ignimbrite persists as three relatively narrow, elliptical outcrops. The northernmost mapped outcrop of ignimbrite is inferred from float at site WP-137 that includes numerous 10-cm size pumice clasts, and pieces of bedded Seco pyroclastics. The broader eastern outcrops are inferred from the localized and concentrated presence of pumice, just west of the bedded, channelized deposit overlying San Luis lava.

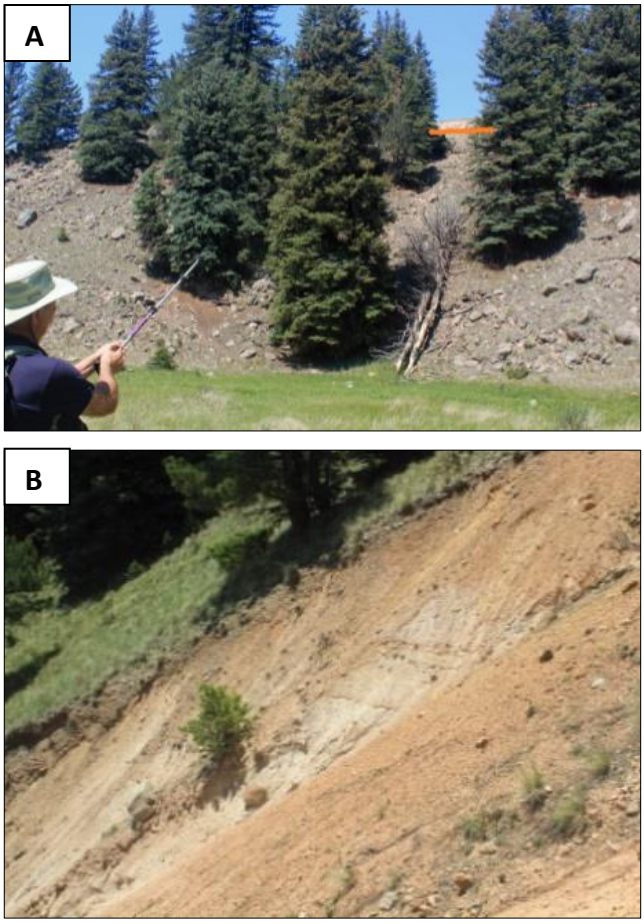

Figure 14. A. Cerro Seco ignimbrite overlying Cerro San Luis lava in eastern field area, contact highlighted in red.

B. Close-up of Seco ignimbrite channel-filling deposit.

The ignimbrite is inferred to cover a surface area of almost 14 km^2 with an estimated volume of 0.82 km^3, calculated from mapped unit distribution and an average thickness of 0.120 km (Refer to section 4.2 and sketch in Appendix A). At the point of exit from the vent, the ignimbrite is at its most uniform thickness, though in the absence of well data and measurable outcrop near the vent, true maximum thickness of the Seco pyroclastic deposits is not known. Further complicating the thickness determination is that the ignimbrite erupted onto a sloping substrate, created when the resurgent dome shed the debris flow Qdf during uplift.

The ignimbrite volume calculation is a rough estimate based on broad assumptions, given that the unit could have been planed off by a second pyroclastic eruption or eroded by wave action of a subsequent lake; it was also covered by two later lava eruptions, adding to potential error in the volume calculation. However, thickness can be estimated, and is constrained somewhat by well data from geothermal well Baca-7 (Figure 15, Plate II and Appendix A, Table 7). The continuous sequence of early rock types encountered in Valles Caldera is typically represented in Baca-7, an almost completely sampled well, and data nearest to Seco (Lambert and Epstein, 1980). This well reaches a total depth of 1687 m; a modified columnar section showing rock types found in Baca-7 well cuttings appears in the geologic cross-section, Plate II.

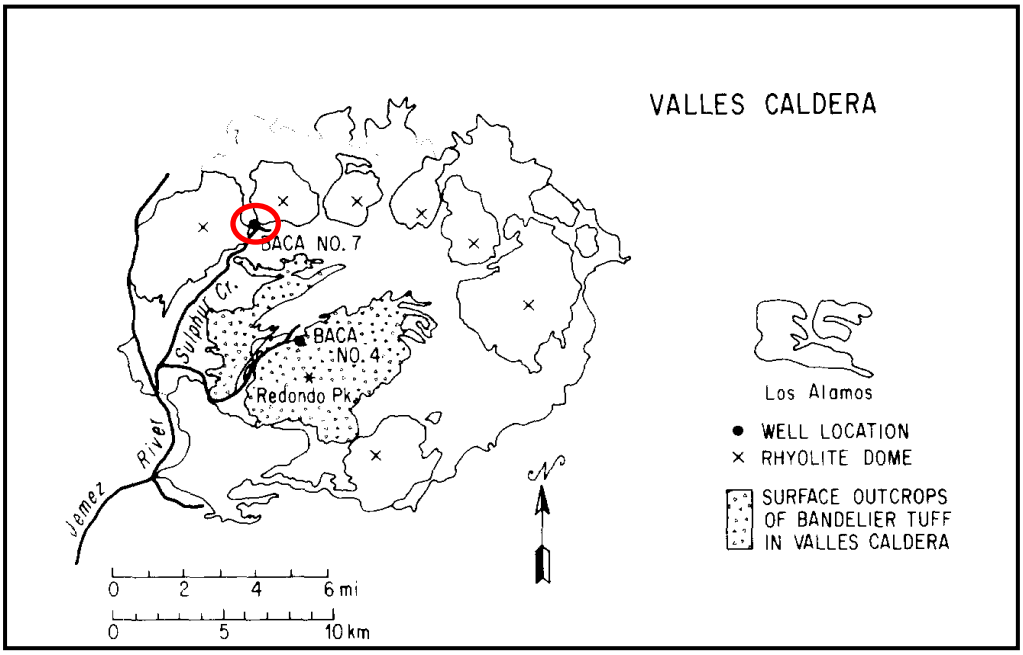

Figure 15. Map of Valles caldera showing location of geothermal well Baca-7 (circled in red) and areal extent of intracaldera outcrops of Bandelier Tuff. Modified from Lambert and Epstein, 1980.

The only surface exposures of the base of the ignimbrite occur 1) near site WP-102 on road VC08 near the intersection of road VC10 in the western map area, where it sits on lacustrine deposits of the northern moat, 2) at site WP-132, across from Warm Springs Dome near San Antonio Creek, and 3) where the ignimbrite rests on Cerro San Luis lava (Fig. 14). No exposures of ignimbrite are found in the broad central field area, now occupied by the Seco second pyroclastic and lava deposits. The ignimbrite is pink to tan, massive, poorly sorted, variably vesicular and cross-bedded, sub-vertical and generally seen as elliptical walls 3 to 7-meters high, although one outcrop (WP-138) is a one-meter high ground-level mound (Figures 16A and B).

Figure 16. Cerro Seco ignimbrite outcrop morphology.

A. Characteristic elliptical sub-vertical morphology ignimbrite outcrops.

B. Ignimbrite outcrop at site WP-138 exhibiting mound morphology.

Some lenses within outcrops are more vesicular and/or more heavily jointed, and weathered surfaces provide substrate for a blue-green lichen (Figure 17A and B).

Figure 17. Variable textures of Cerro Seco ignimbrite.

A. Vesicular interval. Red bar = 1 m.

B. Heavily jointed (lower) layer. Red bar = 1 m.

Qvset-2 is distinct in appearance from the ignimbrite (Qvset-1) and other volcanic units in the mapping area. Fresh surfaces typically have a tan to light orange color, and weathered surfaces are darker rusty-brown. Bedding and cross-bedding on the 10- to 30-cm scale, and a typically well-sorted, (angular) clast-supported texture distinguish it from the ignimbrite. An $^{40}Ar/^{39}Ar$ date on this unit provides an age of 0.78 ± 0.04 Ma, from an

outcrop near site WP-107 in the western mapping area (Goff et al., 2006, 2011; Kelley et al., 2013) (Table 2).

The distribution of Qvset-2 creates a pyroclastic east-west apron north of the Cerro Seco dome that mostly covers the earlier-erupted ignimbrite (Plate 1). The unit appears to mantle pre-existing topography, exhibiting smooth, undulating surfaces and variable attitudes and dip directions in the field (Figure 18 and Appendix E).

Figure 18. "Undulatory" outcrop morphology of Qvset-2, field assistant for scale. Note unique mantling appearance.

Strong bedding and cross-bedding dominate deposits of Qvset-2, at both fine- and coarse-grained scales. Pinch-and-swell features are also observed, and refer to a laterally variable bed thickness from vent to distal outcrops (Figure 19).

Figure 19. Coarse-grained cross-bedded outcrop of Qvset-2 at site WP-017, illustrating a pinch-and-swell feature, an example of surge deposition.

The thickest stratigraphic section of Qvset-2 measured for this study is 46 m minimum thickness, at site WP-132 (Plate 6), which is approximately 2 km from the vent. Estimated surface area covered by Qvset-2 is 14 km^2; estimated eruptive volume is 0.49 km^3, based on an average thickness of 74 m (Refer to Appendix A). The northernmost evidence of Qvset-2 exists as abundant float of fine-grained bedded Seco pyroclastic deposits near Road VC09. Detailed stratigraphic sections measured at waypoints -141, -136, -049 and -132 (Plate 3, Plate 4, Plate 5 and Plate 6) illustrate the character and variability of the Qvset-2 deposits.

Three common lithofacies of this unit are exhibited in the field: fine-grained surge (typically cross-bedded), coarse-grained planar (may be cross-bedded as in Figure 19), and even coarser-grained conglomeratic lenses. The lithofacies' change in thickness and appearance is influenced by distance from source: distally, beds consist of better sorted, more fine-grained, pumice-poor and lithic-rich deposits (Figure 20). This facies is consistent with a water-fluidized, farther-travelled and more "winnowed" deposit of hydromagmatic surge.

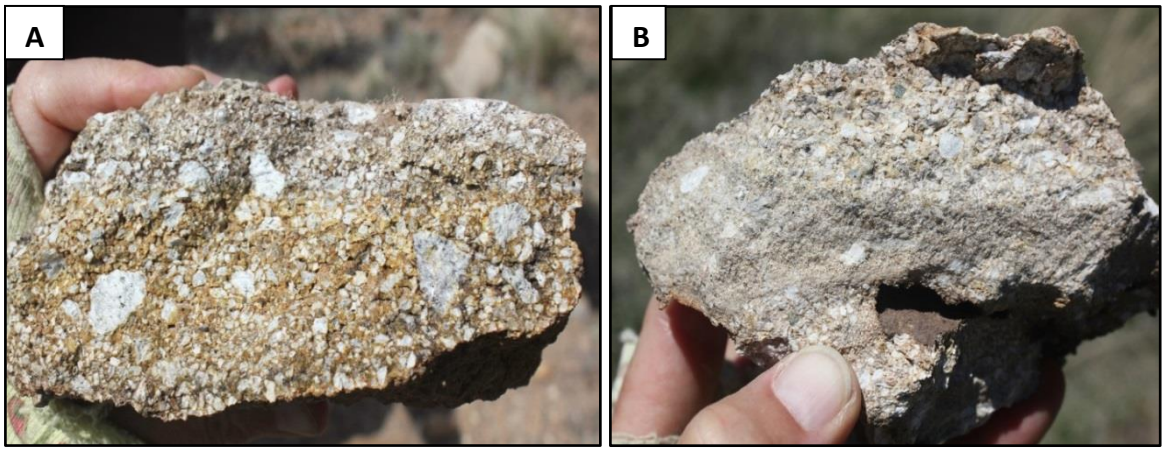

Figure 20. Hand samples from deposits of Qvset-2 from two different sites to illustrate lithofacies change with distance from the eruptive source, thumb for scale. **A.** Site WP-121, 2.4 km from source. **B.** Site WP-136, most distal outcrop of Qvset-2, 3.6 km from source.

Fine-grained surge deposits of the unit Qvset-2 are best exemplified in the section at WP-141 (Plate 3 and Figure 21). Interbeds of fine-grained angular white to light grey glassy particles resemble lacustrine deposits, which overly other packages of beds with lapilli-sized crystals and lithic grains. Low-angle cross-bedding is characteristic of the basal 2.5 m of this section (Figure 21). These fine-grained deposits contain 5-10% crystals by volume, typically less than 1.5 mm in size. Pumices in the fine-grained layers

are up to 2.5 mm in size. Individual layers vary from 1-10 cm in thickness, and are interpreted as surge deposits.

Figure 21. Fine-grained cross-bedded Cerro Seco surge deposit at base of outcrop at site WP-141, hammer for scale.

Coarse-grained layers in the section contain 10-15% crystals by volume, with crystal size up to 3 mm, angular lithic fragments and pumices up to 9 mm; these layers range from 8-25 cm in thickness, and may be planar bedded, cross-bedded or channelized (Figure 22). These layers occupy the majority of the outcrop as a whole by a ratio of two

to one over the fine-grained surge deposits. This description of coarse-grained lithofacies fits the general description of other Qvset-2 beds throughout the mapping area.

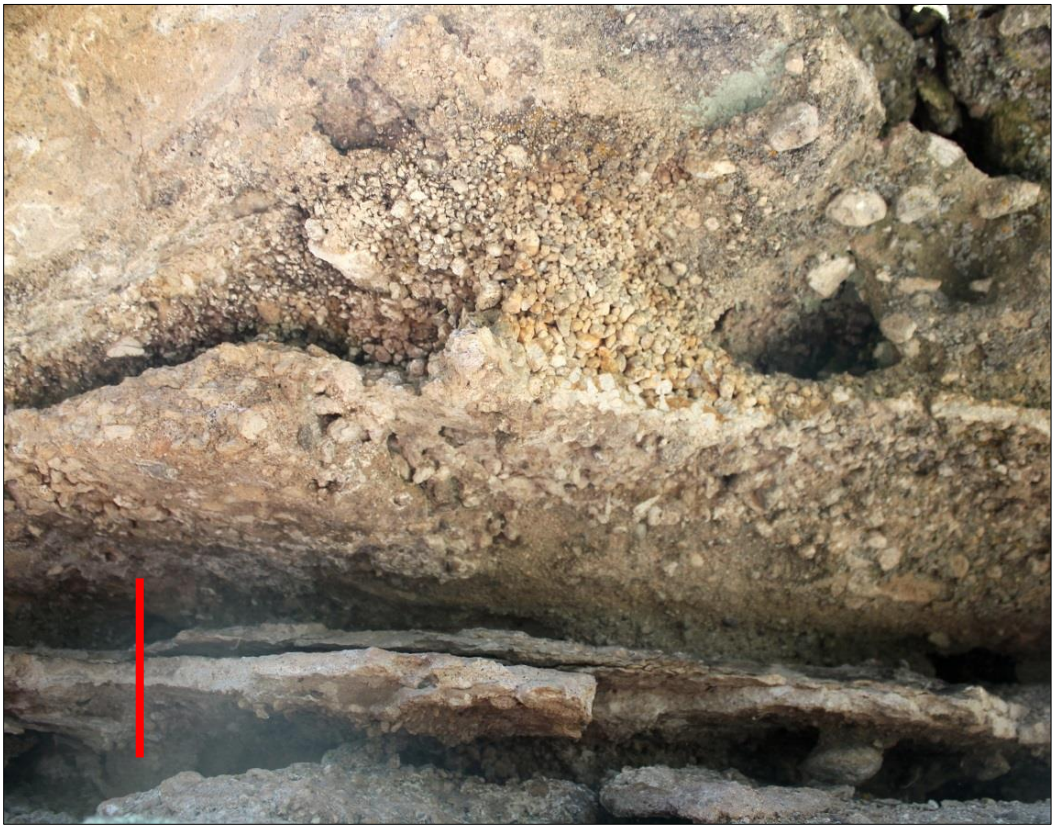

Figure 22. Coarse-grained lithofacies of Cerro Seco unit Qvset-2 at site WP-141, showing channel feature within bedding. Red bar = 10 cm.

Conglomeratic intervals in the field area occur along a specific topographic horizon spanning a ground distance of approximately 2.5 km, and between 50-150 m (1-3 contour lines) above the valley floor, relatively low in the stratigraphy of Qvset-2 (Plate 1). The conglomeratic intervals contain 40% groundmass, 25-30% subangular to rounded lithic fragments (up to 3 cm) and 15-20% crystals by volume (up to 2 mm in

size) (Figure 23A). Most of the lithic fragments consist of porphyritic rhyolite, dacite, and andesite; tan sandstone and Precambrian crystalline rocks.

In outcrops exposed near the southern margin of San Antonio Creek, Qvset-2 deposits include sparse clasts of aphyric obsidian (Figure 23B) resembling the obsidian facies of Cerro del Medio (1.17 Ma; Goff et al., 2011), the easternmost northern moat rhyolite of the caldera. This clast type is distinctive and is found in various older sedimentary deposits along and within the drainage system of San Antonio Creek.

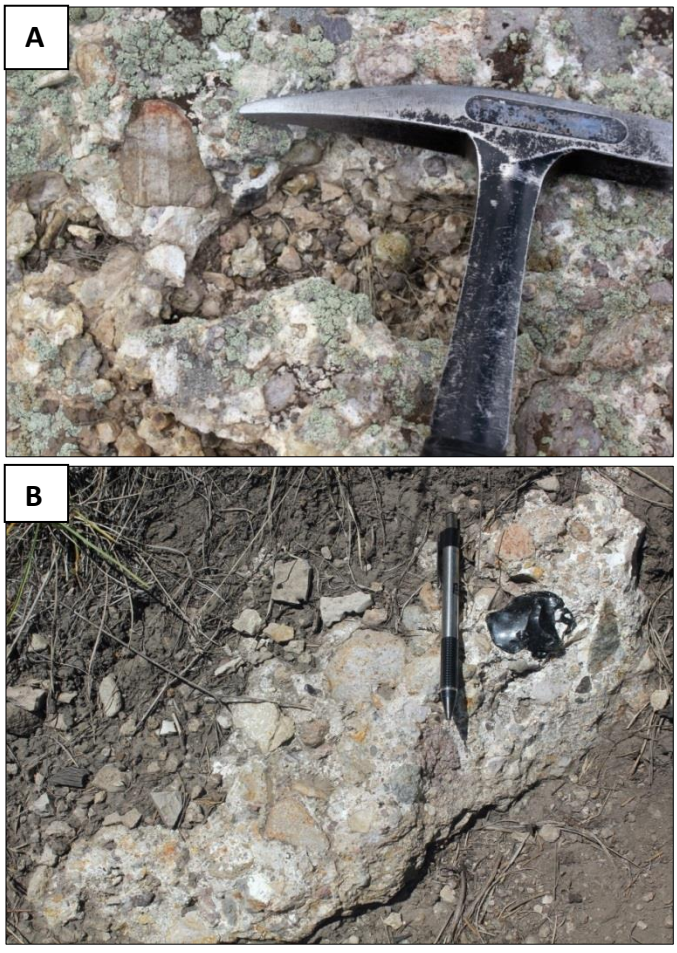

Figure 23.
A. Conglomeratic lithofacies of unit Qvset-2 at site WP-125, showing large lithic clast of rhyolite, dacite and andesite, Precambrian granite and sandstone, hammer for scale.

B. Conglomerate at site WP-017 with aphyric obsidian clast, pencil for scale.

The three different lithofacies of Qvset-2 form deposits ranging in thickness from less than one meter at sites distal to the source, to 46 m. The unit covers an area of approximately 22 km^2. Inferred from the map, proximal deposit thickness could be up to 75 m, leading to an estimated erupted volume of 0.34 km^3 (Refer to section 4.2 for details on volume calculations.)

3.1.5 Cerro Seco Lavas

The two Seco lavas Qvse1 and Qvse2 were initially mapped based on morphology, the contact placed at an obvious slope break where definite lobate map patterns suggested separate flows (Goff et al., 2011). Mapping, petrography and chemistry done as a part of this study confirm the placement of earlier mapped contacts, and that the two Seco lava flows are indeed distinct. The first lava flow (Qvse1) immediately overlies Qvset-2 described above, but in many places in the field, the contact is covered. The western lava-ignimbrite contact, where the first lava appeared to have flowed up to a subvertical tuff outcrop and ponded to a steep border, has an estimated thickness of 100 m, taken directly from map topographic lines. Maximum exposed thickness of the second lava is 275 m.

In outcrop, Seco lavas are dark grey on weathered surfaces, and light grey to pinkish to white on fresh surfaces (Figure 24A). Both lavas are flow-banded, massive to slightly vesicular, and contain quartz crystals that are often pink (Figure 24B).

Figure 24. **A**. Outcrop of first Seco lava Qvse1 at site WP-040, showing massive and flow-banded form.

B. Hand sample of Seco lava Qvse1. Pencil for scale, pointing to pink quartz crystal.

Sanidine from the second lava Qvse2 yielded an $^{40}Ar/^{39}Ar$ age of 0.800 ± 0.007 Ma (Spell and Harrison, 1993) (Table 1). A date on the first lava is pending, but the timing between the two lava eruptions is likely very close, given the lack of evidence of a cooling break, rubble piles or soil development at contacts between flows, and because timing is constrained by the known age of the preceding Qvset-2 eruption (0.78 Ma).

The ages in Table 1 suggest that Qvse2 is older than Qvset-2, but the ages are within the analytical errors of the various laboratories. The San Antonio Mountain Member produced an $^{40}Ar/^{39}Ar$ age of 0.557 ± 0.004 Ma (Spell and Harrison 1993), leaving the range of 0.223 Ma for eruption of the two Seco lavas to have occurred. There is also the possibility that these ages are consistent because all Cerro Seco lava eruptions are indistinguishable in age from the ignimbrite and any subsequent pyroclastic unit themselves; eruptions of all Seco units were closely timed. However, the analytical uncertainties are consistent with the post-ignimbrite lavas being as many as tens of thousands of years younger than Seco pyroclastic members.

In summary, field observations confirm that Cerro Seco should be characterized as four eruptive units – two pyroclastic and two lava flows, with an eruptive sequence of Qvset-1, Qvset-2, followed by two lavas (Qvse1 and Qvse2) (Table 3). With pyroclastic products totaling 1.31 km^3 of material, Seco's volcanic explosivity index (VEI) is 4-5.

Deposit	Surface area (km^2)	Thickness (km)	Volume (km^3)
Ignimbrite-Qvset-1	14	0.120	0.82
Qvset-2	14.5	0.074	0.49
lava-Qvse1	5.1	0.100	0.37
lava-Qvse2	5.3	0.275	0.52
Total pyroclastic products		1.31 km^3	
VEI		4-5	

Table 3. Estimated Volumes of Cerro Seco Eruptive Products

3.1.6 Terrace Gravels and Other Overlying Lithologies

In addition to the interlayered pre- and post-eruption lacustrine units, a wide range of fluvial-colluvial lithologic units post-date the Cerro Seco deposits. The San Antonio quadrangle map by Goff et al., (2006) describes 16 such units; this project limited them to two: combined alluvium-colluvium (Qa, Qc) and a combined terrace-older terrace deposit (Qto, Qt). The Qt unit is a younger stream terrace of sand, gravel and silt bordering present streams, and in this study includes older stream terraces of sand, gravel and silt that underlie higher terraces. Generally, the older stream terraces post-date the large valley-filling lakes of the caldera, so sit on higher platforms, and may also contain various volcanic rocks in addition to rare Precambrian clasts and Banco Bonito rhyolite (Goff et al., 2011) (Figure 25).

Figure 25. Photo illustrating profile of older terrace (Qto) morphology; red line above terrace surface traces the profile. This terrace sits at an elevation of 2500-2600 m (view is to the East); terrace is of lower elevation to North/left in photo). The red arrow points to the dome of Cerro San Luis east-southeast in the distance.

3.2 Petrography

Introductory Comments

The prior petrographic classification of Cerro Seco grouped the lithologic units under the Cerro Seco Member, Qvse, which included sub-members Qvset (pyroclastic deposits), and two lava flow units Qvse1 and Qvse2. Mapping of Qvset, as described above, confirms that it comprises two distinct units, referred to herein as Qvset-1 and Qvset-2. In this section, detailed petrographic descriptions are provided for each of the four Cerro Seco units.

Petrography

Detailed petrographic descriptions of 30 samples from within and around Cerro Seco are recorded in Appendix B. Data include points counted during petrographic analysis, modal percentages with voids and void-free, groundmass and glass content, presence of lithic and pumice fragments, total phenocrysts, phenocryst assemblages and textures. Of the 30 samples analyzed, 16 are thin sections of samples collected during this study, and 14 are existing sections, provided by Fraser Goff, that had not previously been analyzed. Grains less than 0.5 mm in length were considered elements of groundmass; grains greater than 0.5 mm were counted as phenocrysts. Unless otherwise noted, the photomicrographs below were taken at 4X power. Refer to Appendix A for details about petrographic methods used.

An abbreviated overview of phenocryst assemblage, modal percentages and major phenocryst size of the Cerro Seco volcanic suite, is presented in Table 4. Data in Table 4

are based on thin section analysis, and are grouped by deposit type. A sample of vitrophyre from the ignimbrite is also included.

Sample Number	Unit	Phenocryst % (by volume)	Phenocrysts	Major phenocryst size (mm)
Ignimbrite				
RWVC16-02	Qvset-1-vitrophyre	27.0	qtz, sa, pl, bt, hbl	0.25 -1.5
RWVC16-24	Qvset-1	17.9	qtz, sa, pl, ksp	0.25 -3.5
RWVC16-132	Qvset-1	15.0	qtz, sa, pl, hbl	0.25 - 2.5
RWVC16-132P	Qvset-1	13.2	qtz, sa	0.5 - 2.25
RWVC16-102	Qvset-1	17.5	qtz, sa, pl, bt	0.6 - 1.5
F05-137 ("Qvset")*	Qvset-1	15.0	qtz, sa, pl, ksp	0.25 -2.0
Hydromagmatic				
RWVC16-03	Qvset-2	24.0	qtz, pl, bt, hbl	0.25 -2.0
RWVC16-10	Qvset-2	20.2	qtz, sa, pl	0.15 -2.0
RWVC16-12	Qvset-2-cgl	18.0	qtz, sa, pl	0.25 -2.0
RWVC16-14	Qvset-2	30.8	qtz, sa, pl, bt, hbl, ksp	0.25 -2.0
RWVC16-16	Qvset-2	29.1	qtz, sa, pl, bt, ksp	0.25 -1.75
RWVC16-28	Qvset-2	5.5	qtz, sa, pl, bt	0.15-1.5
RWVC17-136	Qvset-2	11.1	qtz, sa, pl, bt	0.35 - 2.25
F95-45a ("lg-gr")*	Qvset-2	15.3	qtz, sa, pl, bt, ksp	0.5 -2.0?
F95-45b ("sm-gr")*	Qvset-2	25.6	qtz, sa, pl, bt	0.25 -1.75
F05-151 ("West")*	Qvset-2	14.6	qtz, sa, pl, bt, ksp	0.15 -1.75
F05-154 ("fossil")*	Qvset-2	19.6	qtz, sa, pl, bt, ksp	0.2 -2.0
Lava				
RWVC16-21	Qvse1	25.0	qtz, sa, pl, bt, hbl*	0.15 - 2.15
RWVC17-050	Qvse2	26.9	qtz, sa, pl, ksp	0.1 - 1.85

*Previous Slides *hbl seen in slide

TABLE 4. Generalized petrography of the Cerro Seco volcanic suite. Phenocryst percentages were determined from point-counting 200 points per slide. Abbreviations: sa – sanidine; pl – plagioclase; qtz – quartz; bt – biotite, hbl – hornblende, ksp – potassium feldspar.

Cerro Seco ignimbrite (Qvset-1) samples RWVC16-132, -132P, -102 and -24 are similar in both phenocryst assemblage and percentages (Refer to Appendix B).

Phenocrysts of quartz, sanidine and plagioclase are seen in all the ignimbrites, with sample RWVC16-132 containing green hornblende, and sample RWVC16-102 containing biotite. Phenocryst percentages range between 13.2% and 17.9%, with the exception of the vitrophyre sample, which contains 27.0% crystals. Major phenocryst size is generally between 0.25 and 2.25 mm, although sample RWVC16-24 contains phenocrysts up to 3.5 mm (Figure 26). Compared to the other ignimbrites, this sample also had the highest phenocryst content at 17.9%, the highest lithic fragment content at 19.4%, and the highest pumice content at 22.4%. The pumice clasts of RWVC16-24 are large, up to 2.5 mm, and contain abundant large crystals of quartz and sanidine. In the Seco ignimbrite samples, groundmass is pinkish and glassy with some minor devitrification in some samples. No welding is observed in any of the Seco ignimbrites.

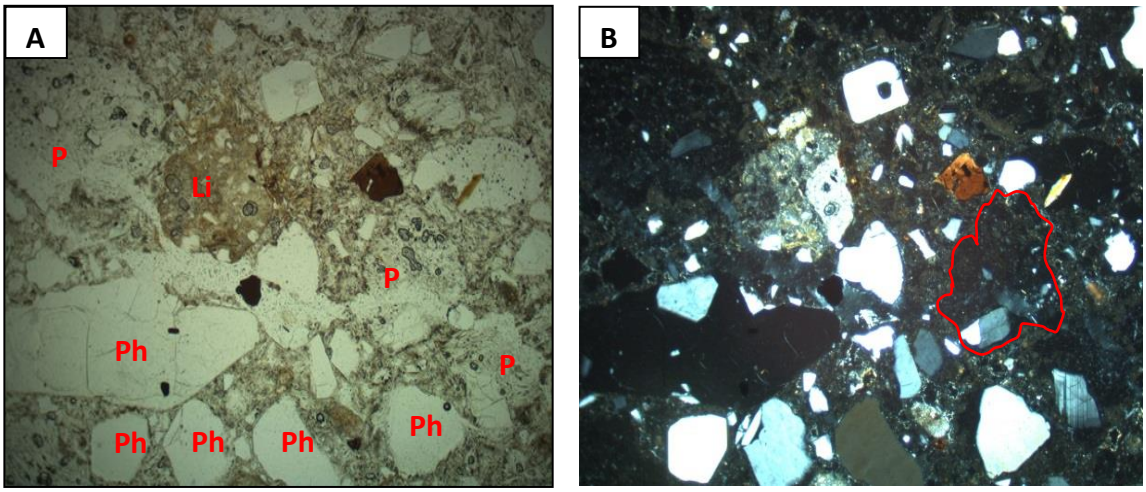

Figure 26. Photomicrograph of the Cerro Seco ignimbrite Qvset-1, sample RWVC16-24 from site WP-138. Red scale bar=1 mm. Abbreviations, in red: P=pumice; Ph=phenocryst; Li=lithic fragment. Red outline in (**B**) illustrates a single pumice clast. Note variety and abundance of constituents within this tuff. (**A**) Plane-polarized light. (**B**) Cross polarized light.

Crystals within the pumices of both pyroclastic units were also counted, and show a wide variation in abundance (Appendix B).

Qvset-2 is the least petrographically homogeneous of all the units studied. Phenocryst percentages vary widely within the lithofacies, from 5.5% to 30.8%. The most distal outcrops of Qvset-2 (sample RWVC16-28) are fine-grained and contain 5.5% phenocrysts ranging in size from 0.15 to 1.5 mm. In contrast, coarse-grained conglomeratic sample RWVC16-12 contains 30.8% phenocrysts of 0.25 to 2.0 mm size. Multiple outcrops of this conglomeratic lithofacies of Qvset-2 contain fragments of obsidian and clasts of the early caldera-fill debris flow unit Qdf. These gravels may contain Precambrian crystalline rocks, Miocene to Permian sandstones, and basaltic andesites from the Paliza Canyon Formation, previously discussed older lithologies through which Cerro Seco erupted (Figure 27).

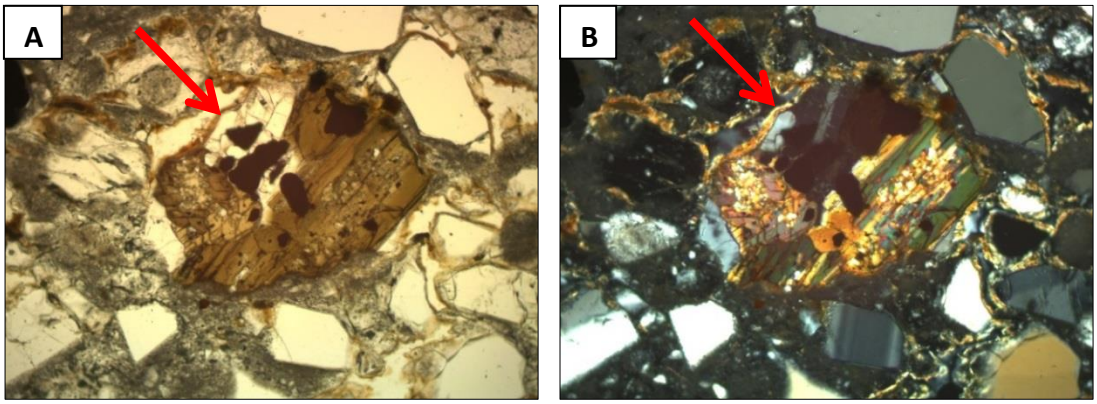

Figure 27. Photomicrograph of sample F95-45b, Qvset-2 containing clasts of Qdf, early caldera-fill debris flow, red arrow showing Precambrian crystalline constituent. (**A**) Plane-polarized light. (**B**) Cross polarized light.

Pumices in Qvset-2 generally exhibit low vesicularity, and are notably dense in hand sample. This is in contrast to the large open-vesicle, frothy texture associated with the pumices within the ignimbrite Qvset-1. The juvenile clasts are also blocky and equant, showing fracture-controlled surfaces. Many of the bedded outcrops of Qvset-2 show a characteristic pumice-rich, clast-supported texture, well represented by sample RWVC16-03 from site WP-049, with 51.8% pumice, and interstitial spaces filled by opaline clay (Figure 28). These opaline rinds are observed in many Qvset-2 hand samples, as well as in thin section. Quartz comprises 19% of the rock, and is rimmed and showing undulatory extinction in many of the points counted.

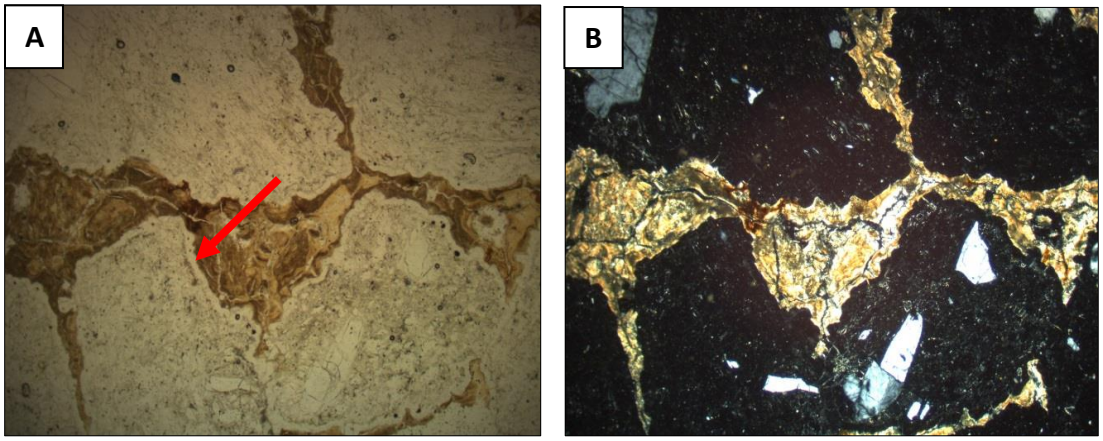

Figure 28. Characteristic texture of the Seco pyroclastic unit Qvset-2: blocky and equant clast-supported, pumice-rich with opaline-clay-filled interstices, sample RWVC16-03 from site WP-049. Red arrow points to opaline rind surrounding pumice clast. (**A**) Plane-polarized light. (**B**) Cross polarized light. Photographed at 10X power.

Notably, sample RWVC16-14, a coarse-grained variant of Qvset-2, contains the highest volume percent of lithic fragments and phenocrysts of any of the Qvset-2 variants, as well as the most variable phenocryst assemblage (Figure 29). Phenocysts and groundmass crystals include quartz, sanidine, plagioclase, biotite, hornblende and

microcline, with this sample holding the highest volume percent of potassium feldspar, and the lowest volume percent of pumice, of any of the Qvset-2 variants.

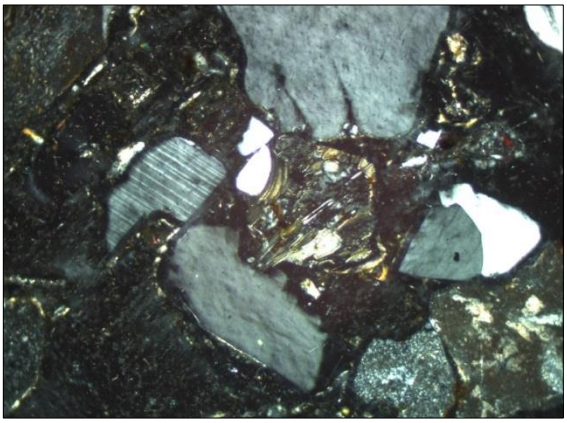

Figure 29. Sample RWVC16-14, from Qvset-2, from site WP-128 under cross polarized light. Note glassy groundmass and variety of phenocrysts.

Many Qvset-2 samples show a spherulitic texture (Figure 30). Devitrification is an alteration process during which volcanic glass, or any previously uncrystallized material, converts to crystallized material, although the term is most commonly used for the formation of spherulites.

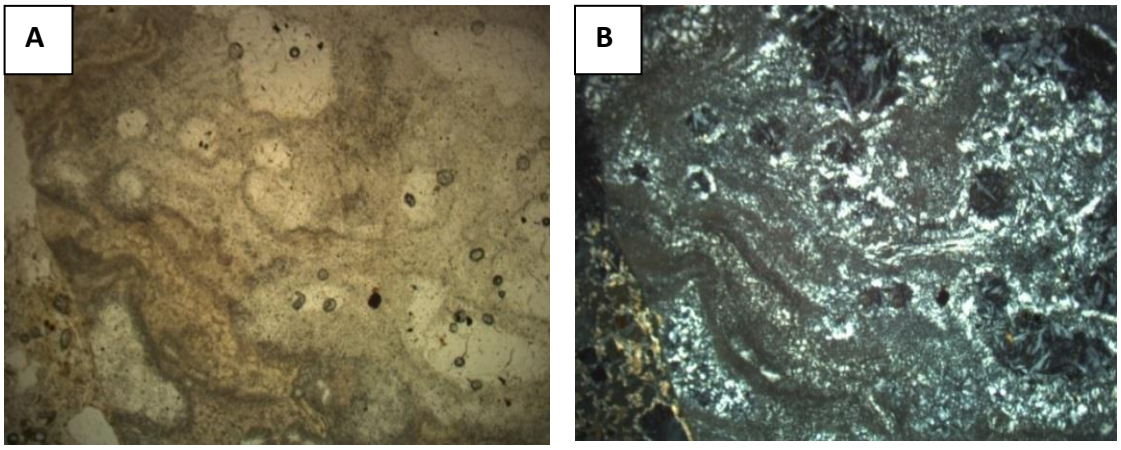

Figure 30. Spherulitic groundmass of Qvset-2, sample RWCV16-14 from site WP-128. The overall composition of this rock suggests that the cryptocrystalline minerals in the spherulites include sanidine and trydimite. (A) Plane-polarized light. (B) Cross polarized light.

Devitrification proceeds radially outward from a nucleus, producing powdery white spheres called spherulites (Figure 31). Spherulites are formed when vapor reacts with glassy groundmass in high temperature conditions, occurring when newly formed glass stays hot for prolonged periods. While the devitrification texture is too fine-grained to identify individual minerals, the growth of the interstitial silica materials of alkali feldspar and trydimite is typical for a rock of this composition. Trydimite is a high-temperature silica polymorph that is thermodynamically stable only at temperatures above 1470°C, and which forms wedge-shaped crystals along the margins of spaces (Cox et al., 1979) (Figure 31).

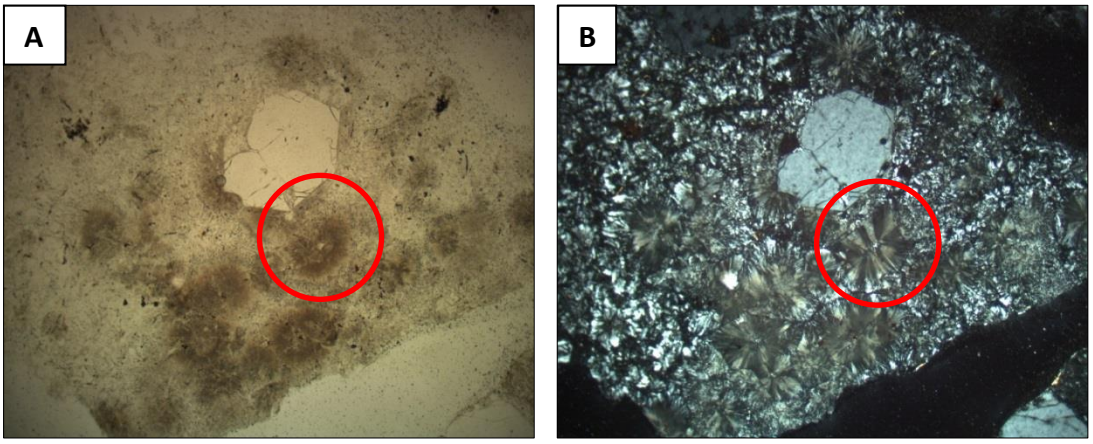

Figure 31. Detail of spherulite in sample RWVC16-12, circled in red, from a conglomeratic lens of Qvset-2. (A) Plane-polarized light. (B) Cross polarized light.

Crystals within Qvset-2 pumices were also counted (Refer to Appendix B). The highest pumice counts in the Qvset-2 samples are from the most distal sites (WP-136 and -049), whereas the highest intra-pumice crystal counts are from samples within a zone of the "apron" along a line of equal elevation closer to the vent.

The two Cerro Seco lavas are geochemically similar, both highly silicic, described by Goff et al. (2011) as flow-banded massive to slightly vesicular lavas containing phenocrysts of quartz, sanidine, biotite and rare hornblende (Refer to Figure 23, Section 3.1.6). Beside flow morphology, the obvious presence of biotite and higher vesicularity are the features that distinguish the first lava (Qvse1) from the second lava (Qvse2). The lavas have a phenocryst assemblage and composition similar to the Seco ignimbrite, but contain almost 60% more total crystals of quartz, sanidine, plagioclase (and biotite in the first lava) than the ignimbrites.

The texture of Seco lavas is best described as containing sinuous glassy ribbons; it is frothy and pumicious. Generally, Qvse1 is less dense than Qvse2, contains more flow-banding and foliation around grains, but is still denser than the lava from the earlier-erupted Cerro San Luis (Qvsl1). Qvse1 contains both biotite and hornblende, not seen in Qvse2. Petrographic analysis of the lava from Cerro San Luis was not performed, but hand sample observations suggest that non-Seco lava units (including San Luis) tend to be finer-grained and less dense than Seco, may be pinkish due to the presence of pink quartz, and tend to contain more biotite.

Other petrographic observations consistently made through the analyses of the Seco units include the presence of feldspar aggregates or glomerocrysts, Carlsbad twinning in sanidine crystals, alteration features in quartz and fragmentation of phenocrysts, conchoidal fracture in the vitrophyre sample, and perlitic texture.

Feldspars glomerocrysts are possibly derived from holocrystalline to partly crystalline material in the magma chamber (Best and Christiansen, 1997). The clusters

may later disaggregate to varying extents during explosive eruption, but some aggregates persist (Figure 32).

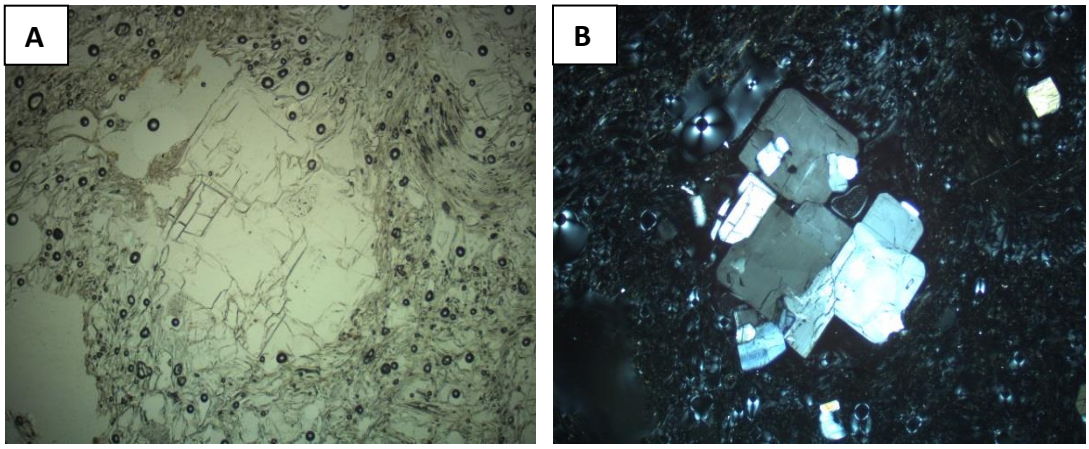

Figure 32. Photomicrograph of feldspar (sanidine and plagioclase) glomeroporphyritic texture in the pumice of ignimbrite Qvset-1, sample from site WP-132. (**A**) Plane-polarized light. (**B**) Cross polarized light.

In many of the Seco units, sanidine phenocrysts may display blue chatoyancy (adularescence) in hand sample, unlike the other moat rhyolites, and typically show Carlsbad twinning in thin-section. A significant percentage of quartz grains are embayed along the crystal margins. In several Qvset-2 samples, both sanidine and quartz phenocrysts are fragmented, and display irregularly shaped fragments with cuspate or embayed outlines.

The vitrophyre from Qvset-1 (RWVC16-02) in hand sample appears as irregularly shaped black fragments within the "host" ignimbrite, ranging in size from 0.5 cm to more discrete, more rounded 10-cm inclusions. Glassy lenses are black, and exhibit vitreous luster and conchoidal surfaces. Conchoidal fracturing and perlitic cracking are also observed in thin section , the glass shards being angular and sharp, clear under PPL and

black under XP. Groundmass is glassy. Plagioclase shows typical albite twinning, but frequently also Carlsbad twinning in the same phenocryst. The biotite is euhedral. Perlite is seen in many of the Cerro Seco hand samples as glassy spheres, or as black, amorphous fields with curved crack lines.

3.3 Geochemistry

ICP-MS and ICP-AES Analyses of Major and Trace Elements

ICP-MS and ICP-AES analyses of major element oxide and element concentrations were conducted on eight whole rock and two Qvset-1 pumice samples of the Cerro Seco volcanic suite (refer to Appendix A for details on methods; to Appendix C for major element oxide data; to Appendix D for trace element data). A total alkali versus silica (TAS) diagram, defined by Le Bas and others (1986) and modified by Le Maitre (1989), illustrates the tight compositional range of the Seco volcanic suite, and compares older and younger rhyolitic rocks from adjacent domes with the Seco rhyolites (Figure 33).

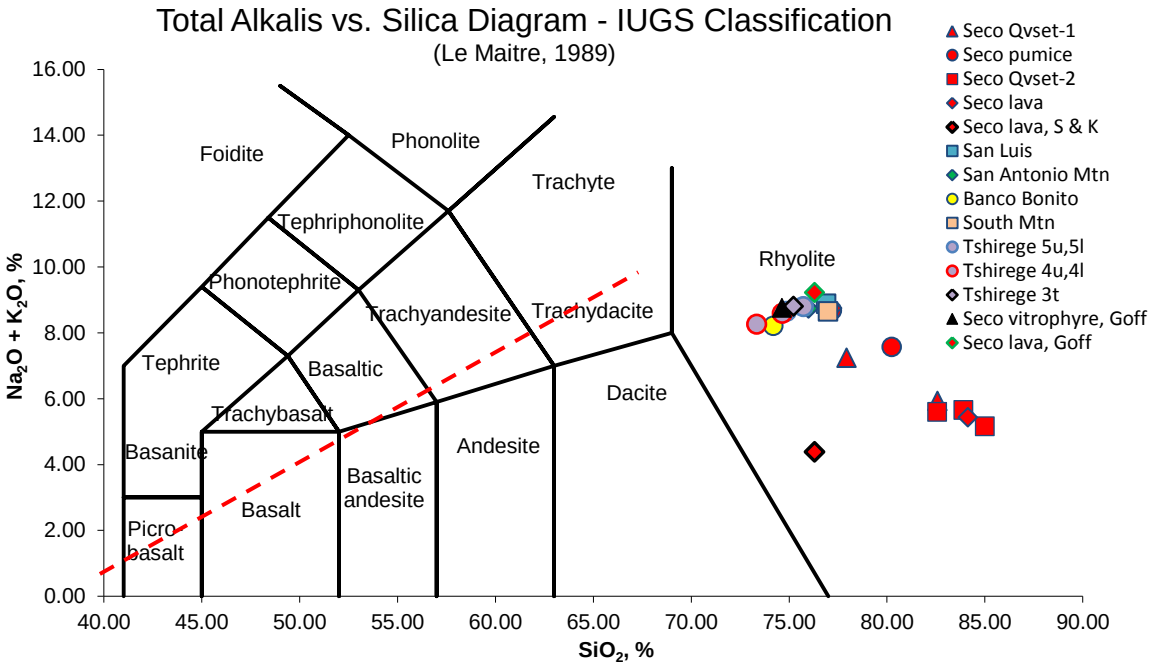

Figure 33. Total alkalis vs. silica diagram of the Cerro Seco volcanic suite. Fields were defined by Le Bas and others (1986) and modified by Le Maitre (1989). The alkaline-subalkaline dividing line (in red) was defined by Irvine and Baragar (1971). All Seco units, pyroclastic and lava flow units, classify as rhyolite, and subalkaline. All data are normalized LOI-free to 100% from analyses in Appendix C.

Irvine and Baragar (1971) defined the dividing line separating alkaline from subalkaline rocks (Figure 33). Alkaline igneous rocks are those rich in potassium or sodium relative to their silica contents.

The subalkaline rocks are further divided into two groups based mainly on iron content, with the iron-rich group called the tholeiitic series and the iron-poor group called calc-alkalic series (Blatt, 2006) (Figure 34); the Seco suite of rocks, enriched in alkali metals, plot in the lower left corner of the diagram, circled in red circle. Each of these groups represents a magma series of compositions that defines the evolution of a mafic magma from its primitive, or unevolved, high magnesium and iron state. Calc-alkaline magmas are oxidized; tholeiitic magmas are reduced. Calc-alkalic volcanic rocks comprise a major part of the continental crust and are primarily generated along subduction zones, becoming emplaced in volcanic arcs (Blatt, 2006). Notably in contrast, initial formation of the Jemez Volcanic Field (JVF), of which the Valles caldera is a later constituent, is dominated by basaltic (alkalic) and andesitic rocks (Gardner, 2010).

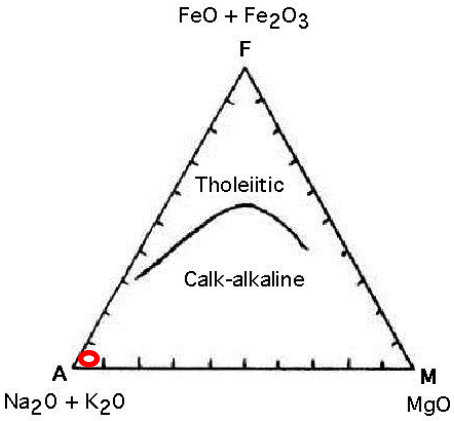

Figure 34. The ternary AFM diagram, as defined by the IUGS, separates tholeiitic and calc-alkaline igneous rocks, by their relative percentages of alkalis (A = $Na_2O + K_2O$), iron (F = FeO *, i.e. the total of all iron oxides), and magnesium (M = MgO). The Seco rocks, enriched in alkali metals, plot in the lower left corner of the diagram, shown by the red circle (from http://usgeologymorphology.com).

The Seco suite of rocks are calc-alkalic, being enriched in alkaline earth metals (magnesium and calcium oxide) and alkali metals (including sodium, potassium). Within the compositional range of Seco rocks, the Qvset-2 samples are apparently the most strongly subalkaline and tightly plotted, the lavas are the least subalkaline, and the ignimbrite and pumices fall between these two end members. The lavas of San Antonio Mountain and Cerro San Luis plot closer to the alkaline dividing line than do any of the Seco units, but are still well within the subalkaline field. For comparison to other Valles caldera rocks, a plot of total alkali vs. silica from the Valles caldera resurgent dome and vicinity is shown in Figure 35 (modified from Goff, 2007 and 2014).

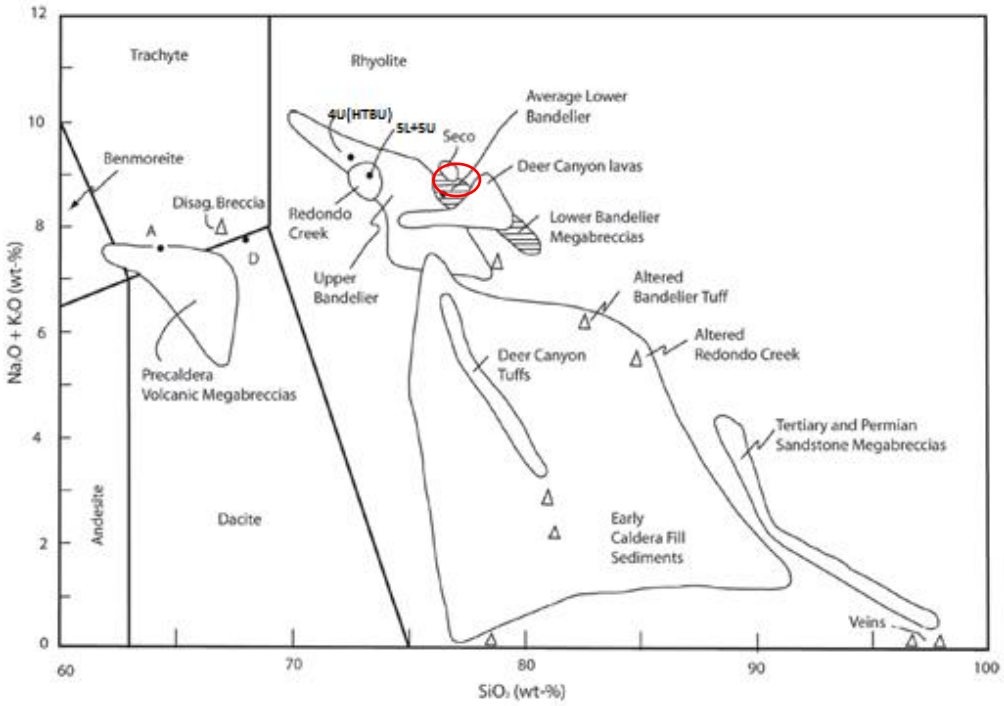

Figure 35. Plot of total alkalis ($Na_2O + K_2O$) versus SiO_2 for rocks of the Valles caldera resurgent dome and vicinity, including Cerro Seco rocks, circled in red; fields enclose related groups of rocks. Plot is from Goff et al., 2007, modified after Le Bas (Le Bas et al., 1986). Units 4U(HTBU) and 5L+5U are updated names from Goff, 2014. All data are normalized LOI-free to 100%. Abbreviations: A = Paliza Canyon andesite; D = Tschicoma dacite; 4U(HTBU) and 5L+5U = subunits of the Upper Bandelier Tuff; triangles = veins, gouge, breccias, and highly altered rocks.

One of the geochemical variables used to further classify igneous rocks is the Agpaicity (Alkalinity) Index (AI), defined by Shand (1947), which characterizes the alkalinity of volcanic rocks. When used with other geochemical variables, the index can be used to determine if volcanic rocks formed by fractional crystallization, or if they evolved by processes other than, or in addition to, fractional crystallization (Frost and Frost, 2008). Agpaitic coefficients of Cerro Seco samples were calculated by dividing the sum of molecular ($Na_2O + K_2O$) by molecular Al_2O_3 (Table 5). Samples with Agpaitic coefficients (AI) greater than one indicate a peralkaline rock, and values less than one are metaluminous or peraluminous rocks. Peraluminous rocks are those having a molecular proportion of Al_20_3 higher than the combination of Na_2O, K_2O and CaO. All samples of the Cerro Seco suite are peraluminous, as are the San Luis and two San Antonio Mountain samples.

Molecular Entity→	CaO	Na_2O+K_2O	Al_2O_3	Na_2O+K_2O+CaO	SiO_2	AI
Seco Samples						
RWVC17-102P	0.53	8.68	11.9	9.21	77.19	**0.729412**
RWVC17-102	1.03	7.24	11.2	8.27	77.94	**0.646429**
RWVC17-132P	0.36	7.57	10.55	7.93	80.24	**0.717536**
RWVC17-138	0.37	5.93	9.4	6.29	82.59	**0.630851**
RWVC17-141	0.39	5.65	8.73	6.05	83.90	**0.647194**
RWVC17-049	0.4	5.15	7.83	5.55	85.00	**0.657727**
RWVC17-136	0.62	5.59	9.33	6.21	82.56	**0.599143**
RWVC16-116	0.34	8.61	12.05	8.95	77.41	**0.714523**
RWVC17-050	0.24	8.74	12.35	8.99	77.20	**0.707692**
RWVC16-121	0.55	5.43	8.66	5.99	84.14	**0.627021**
Non-Seco Samples						
San Luis	0.38	8.88	12.7	9.26	76.90	**0.699213**
San Antonio-1	0.71	8.73	12.9	9.44	76.00	**0.676744**
San Antonio-2	0.64	8.81	12.97	9.45	76.00	**0.679260**

Table 5. **Agpaicity (Alkalinity) Index (AI) for Seco and adjacent dome rocks, bolded.** AI is based on the definition by Shand (1947) to describe alkalinity of volcanic rocks. Agpaitic coefficients of Seco and neighboring dome samples were calculated by dividing molecular ($Na_2O + K_2O$) by molecular Al_2O_3. Peralkaline rocks have AI coefficients > 1, whereas metaluminous and peraluminous rocks have AI coefficients < 1. Peraluminous rocks have a molecular proportion of Al_20_3 higher than the combination of Na_2O, K_2O and CaO.

The Cerro Seco tuffs and lavas are high-silica rhyolites with a range from 77% to 85% SiO_2. An upper limit of 77.4% silica content is generally considered the maximum for igneous rocks (Hildreth, 1981). Unaltered Valles caldera rhyolites contain no more than 79% silica (Goff, personal communication 2017); using this delineation, all of the Qvset-2 samples, plus one pumice and one ignimbrite sample show silica enrichment (Figure 33). The Seco lavas, with silica levels similar to adjacent Cerro San Luis and San Antonio Mountain dome rhyolites, become the "unaffected" benchmark geochemical samples.

All Cerro Seco pyroclastic samples show a general trend toward higher silica, compared to the lava samples. Qvset-2 samples, in particular, are often found in the field coated with opaline rinds, formed by precipitation of silica from groundwater.

Total alkali ($Na_2O + K_2O$) contents of the ten Seco samples range from 5.15% to 8.74% (Appendix C and Figure 36), with the lowest four (5.15-5.65%) being from Qvset-2, and the highest being in the lavas (8.61% and 8.74%). One pumice sample from Qvset-1 (at site RWVC16-102) contained 8.68% total alkalis. Within the Qvset-2 samples tested, highest total alkali concentration is found in the sample most exemplifying a surge deposit. All Qvset-2 samples sit at the same relative stratigraphic elevation, without observable major variation in alkali concentration related to stratigraphy or geographic zonation.

Loss on ignition (LOI) is reported as part of an oxide analysis of a rock, and can indicate volatile materials lost or gained. These volatiles consist mostly of water and carbon dioxide from carbonates. The geochemical analyses of the Cerro Seco pyroclastic rocks reveal high LOIs (2.01 – 6.54 weight percent), an indication that they are hydrated. In contrast, the LOIs for the lavas range from 0.30 – 1.90 weight percent, again rendering them better benchmarks for geochemical comparisons.

Harker variation diagrams are widely used to plot weight percent of all other oxides as a function of one oxide, typically SiO_2 because it is a useful indicator of magma evolution in many cogenetic suites where various magmas are all descended from a single parent (Blatt, 2006). The diagrams not only display the range of petrologic variation, but they are also useful for detecting geochemical and genetic trends in the

petrology of a set of samples. The more primitive members of the series commonly have lower silica content than the more evolved ones; oxide pairs are commonly correlated in linear fashion in fractionation processes (Blatt, 2006).

Each of the plots in Figure 36(a)-(f) illustrates the trends and geochemical comparisons among three main sample sets: the Cerro Seco suite, select older and younger rocks from the Valles caldera (data from Spell and Kyle, 1989), and samples from the Tshirege member of the Bandelier tuff (data from Goff et al, 2014).

Figure 36. (Following) Harker variation diagrams of Cerro Seco and other Valles rocks. Major element oxides have been normalized to 100 %. Major element oxides (a) TiO_2, (b) Al_2O_3, (c) Fe_2O_3, (d) MnO, (e) MgO, (f) CaO, (g) Na_2O, (h) K_2O and (i) P_2O_5 are plotted against silica, on the horizontal axis. Relatively stable oxide levels with increasing silica are noted for TiO_2, Fe_2O_3, P_2O_5, CaO and MgO, whereas levels of Al_2O_3, Na_2O, K_2O and MnO decrease with increasing silica in the Seco samples.

(a)

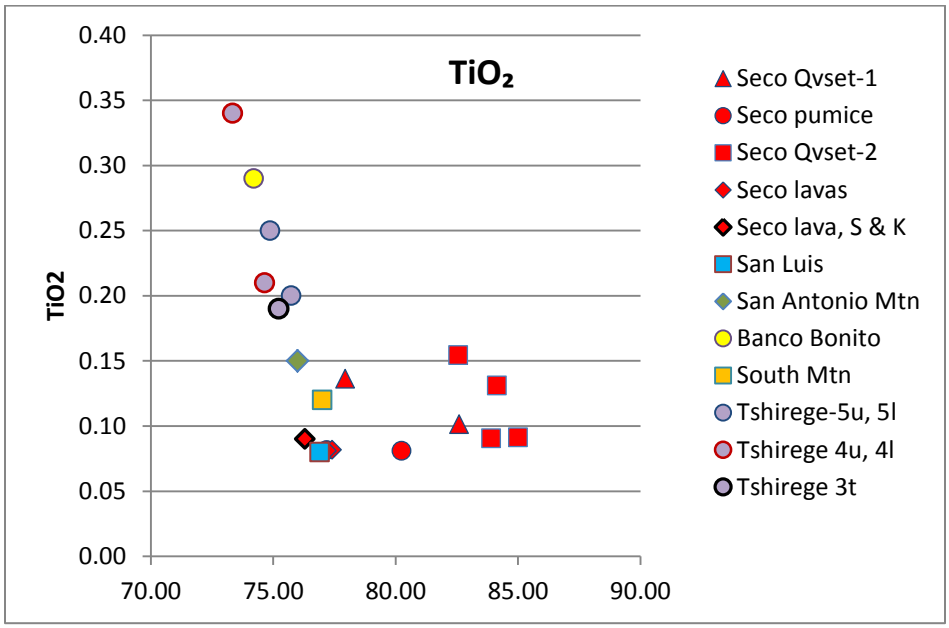

(b)

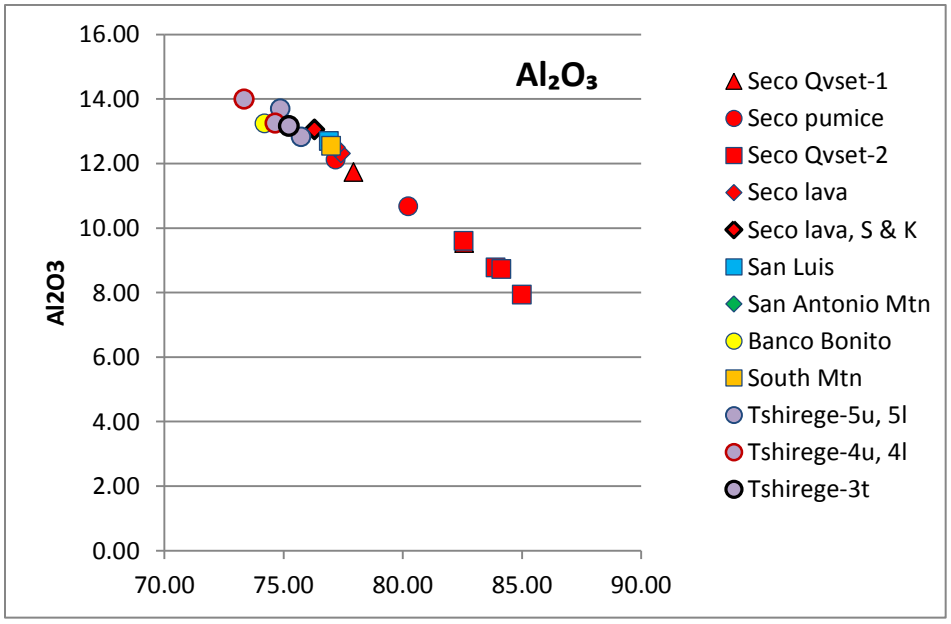

Figure 36. Figure caption on page 55.

(c)

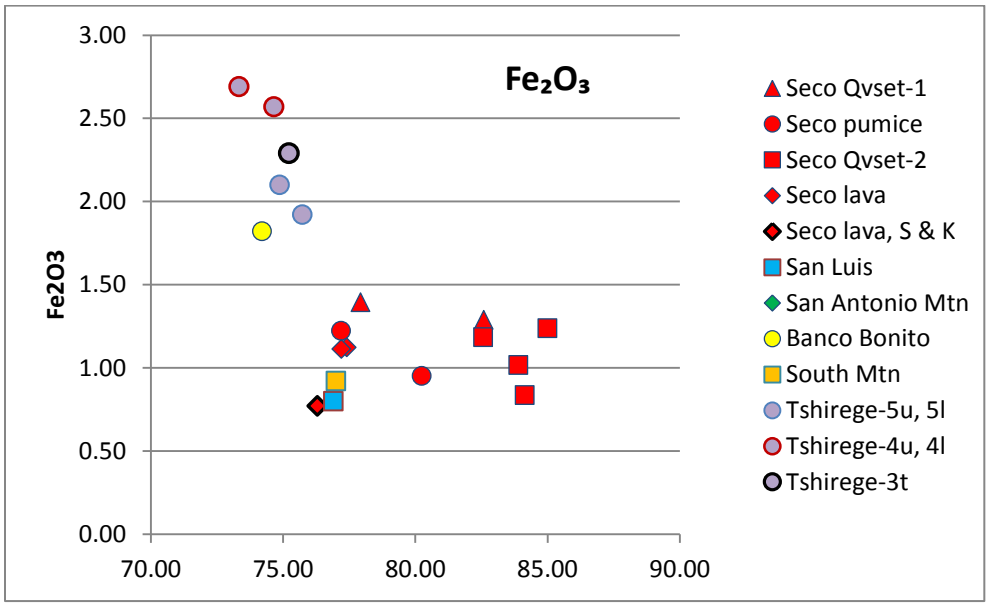

(d)

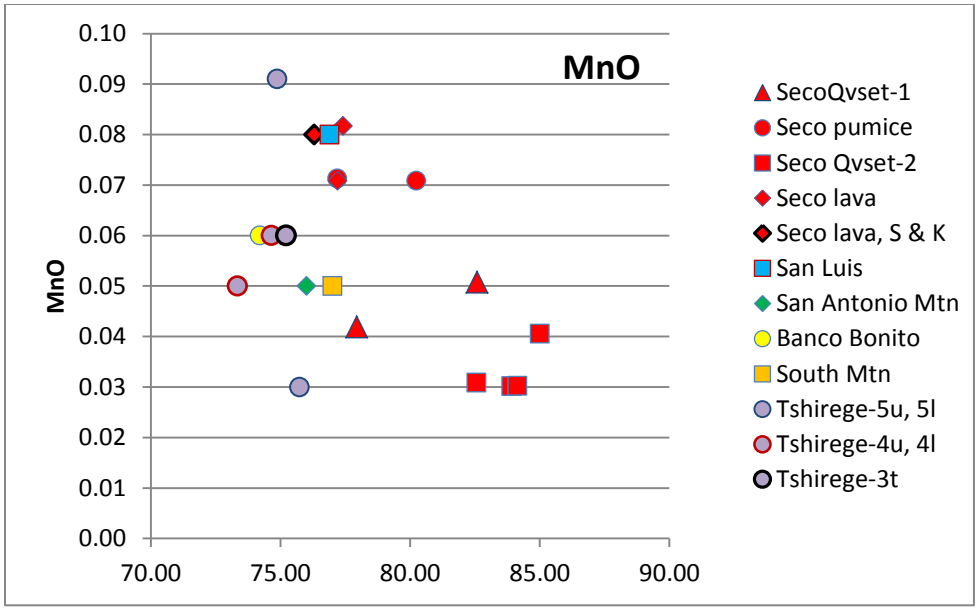

Figure 36. Figure caption on page 55.

(e)

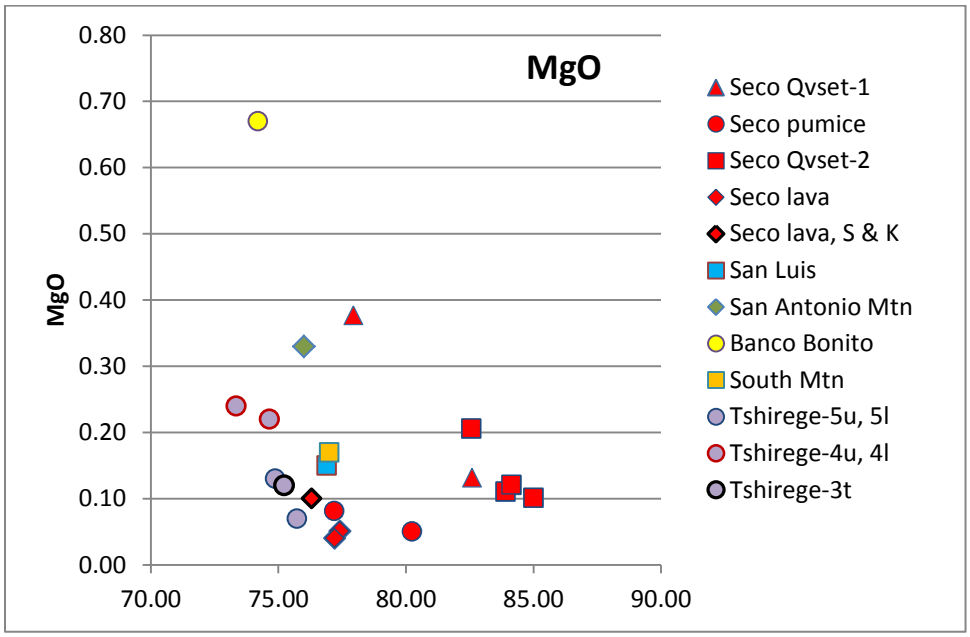

(f)

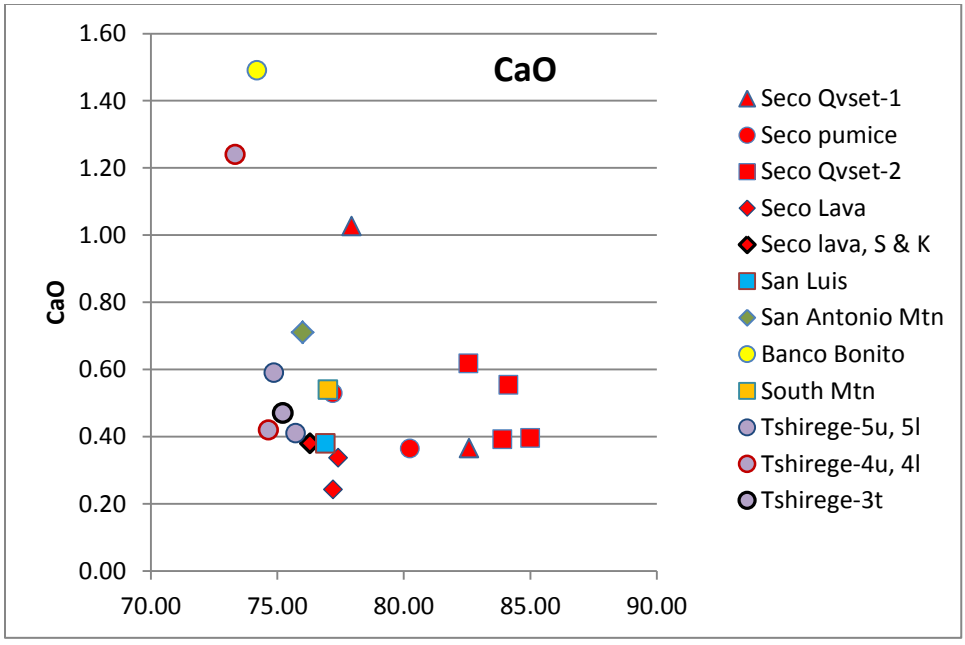

Figure 36. Figure caption on page 55.

(g)

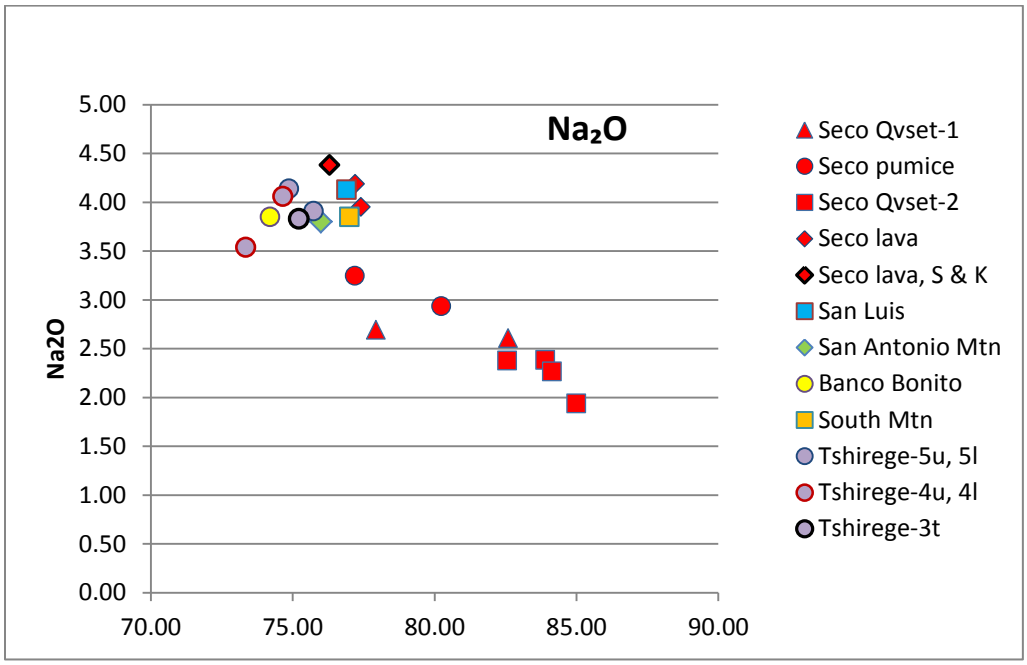

(h)

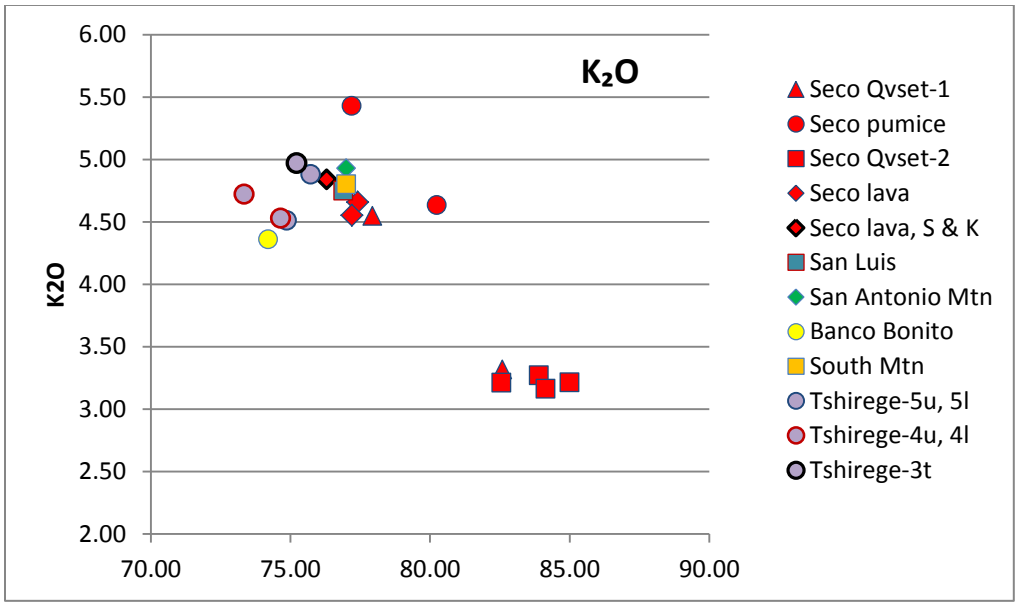

Figure 36. Figure caption on page 55.

(i)

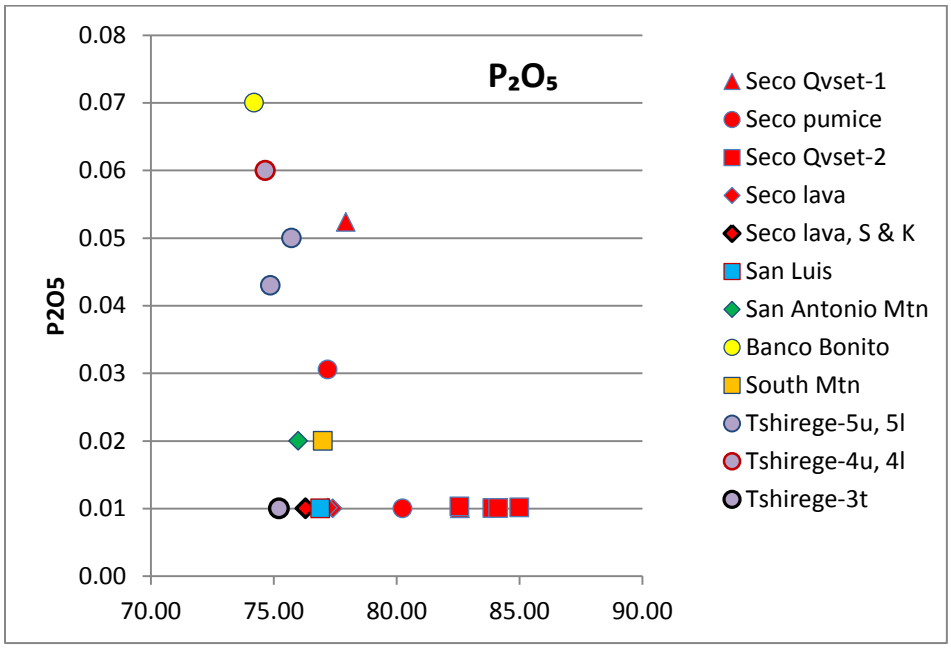

Figure 36. Figure caption on page 55.

The Seco plots for TiO_2, Fe_2O_3, P_2O_5, CaO and MgO show relatively stable levels of oxide with increasing silica, pointing to the immobility of these elements. The only exception is higher Ca and Mg values noted in one Qvset-1 sample. The more immobile elements, such as TiO_2, Fe_2O_3, Zr, and the rare earth elements, can be used to evaluate geochemical characteristics and evolution even in somewhat altered rocks.

In contrast to the relative stability of the Ti, Fe, P, Ca and Mg oxides, the levels of Al_2O_3, Na_2O, K_2O and MnO decrease with increasing Si in the Seco samples. All Seco pyroclastic samples except for one ignimbrite show low potassium levels.

In another binary plot, Ba is plotted against TiO_2 (Figure 37). This plot proved important in analysis of the Valles magmatic system because it indicated mixing of mafic

magma with the high-silica magmatic host magma, particularly in the Bandelier (Tshirege) members, 4u (informally named HTBU, high titanium-barium unit) (Goff et al., 2014). The Seco lava and pumice, as well as the San Luis lava, have low Ba and TiO_2, making them useful benchmark compositions. In contrast, the Seco pyroclastic samples, show higher Ba and TiO_2. San Antonio Mountain shows slightly higher Ba and TiO2 than the Seco units. Notably, Banco Bonito contains higher levels of Ba and TiO_2, almost as high as the Bandelier unit 4u (HTBU).

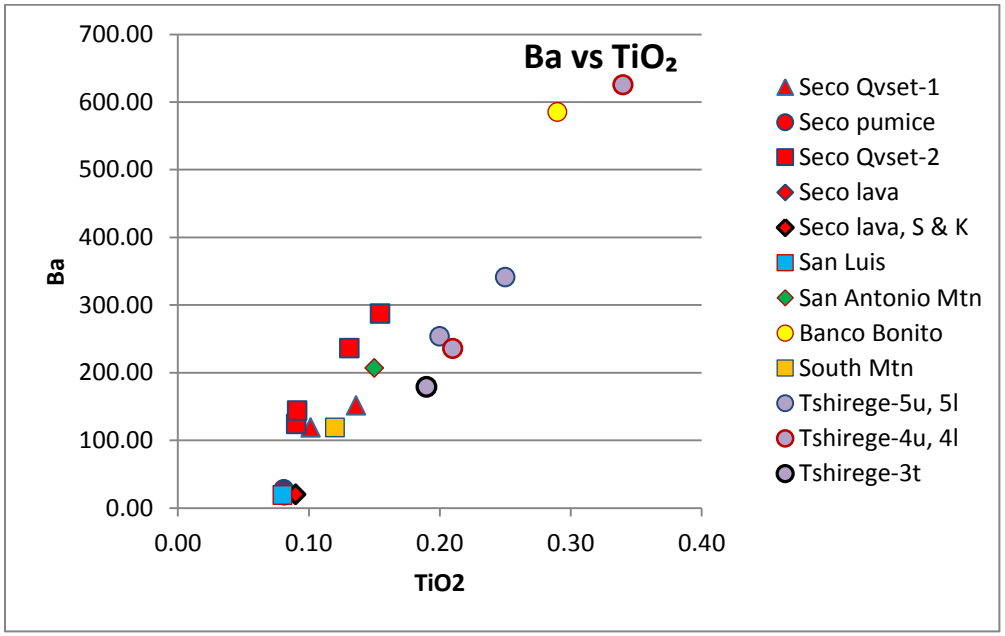

Fig 37. Harker variation diagram of Cerro Seco and other Valles rocks, plotting Ba against TiO_2. Major element oxide has been normalized to 100%, Ba is un-normalized. Seco lava and pumice and San Luis lava have low Ba and TiO_2; Seco pyroclastic rocks show higher levels of Ba and TiO_2.

Additional Harker variation diagrams were plotted to show weight percent of select trace elements as a function of SiO_2 (Figure 38a-d). These trace elements are easy to analyze with reliable accuracy, and are used in various plots to illustrate compatible

and incompatible trends. Ba, Rb and Sr are incompatible trace elements characterized by large ionic radius, making them more mobile, particularly if a fluid phase is involved; Zr tends to be nonreactive.

The plots for Zr, which is resistant to chemical reactions, and Sr, show relative stability in the Seco samples. In contrast, Rb, which often follows K, decreases as silica increases, and Ba increases as silica increases.

Figure 38. (Following) Harker variation diagrams of Cerro Seco and other Valles rocks. Select trace element values are un-normalized. Trace elements (**a**) Ba, **(b**) Rb, (**c**) Sr, (**d**) Zr are plotted against silica. Relatively stable trace element levels with increasing silica are noted for Sr and Zr, whereas levels of Rb decrease, and levels of Ba increase, with increasing silica in the Seco samples.

(a)

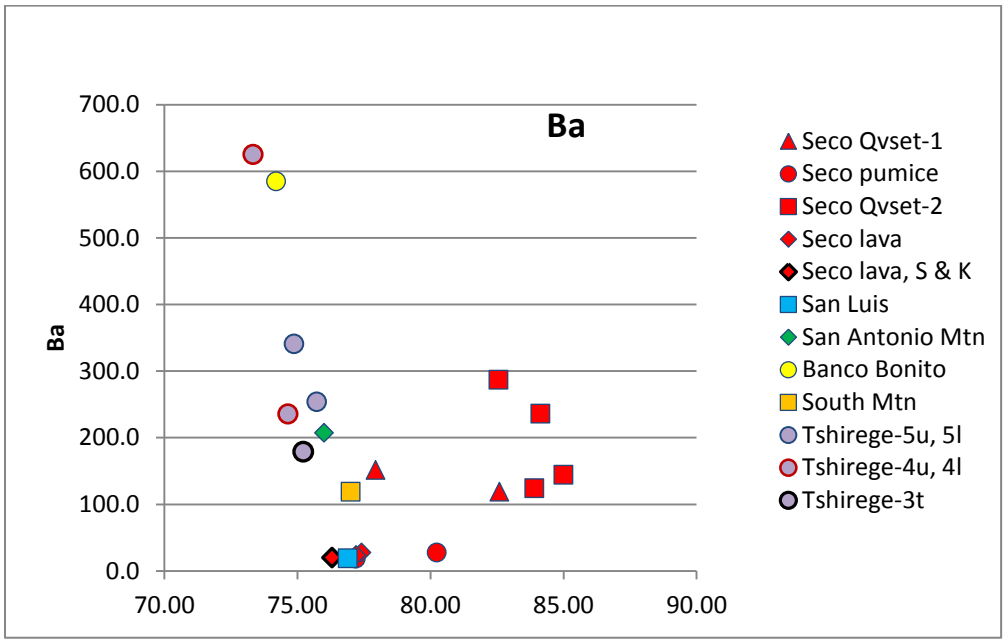

(b)

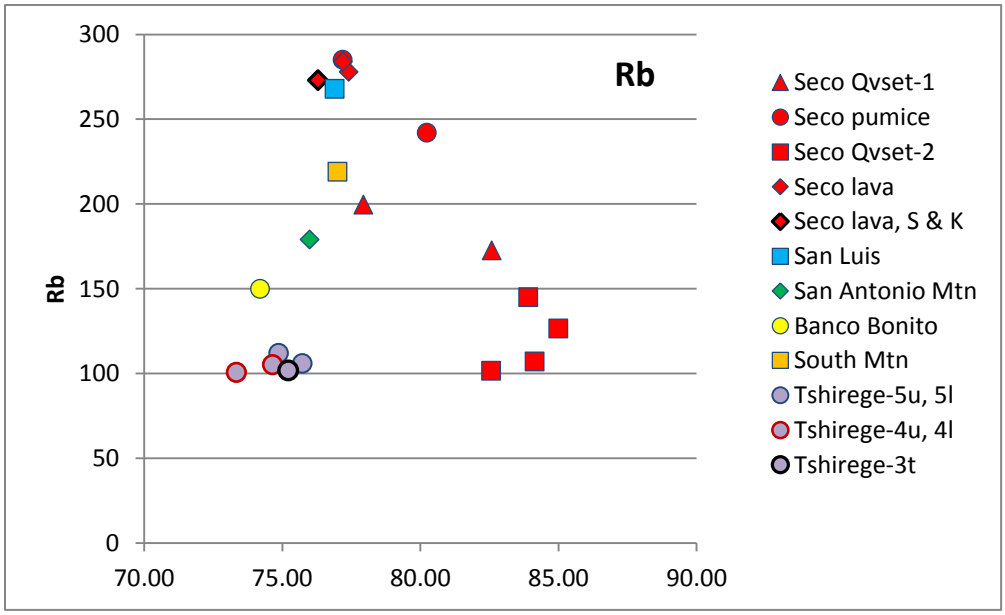

Figure 38. Figure caption on page 62.

(c)

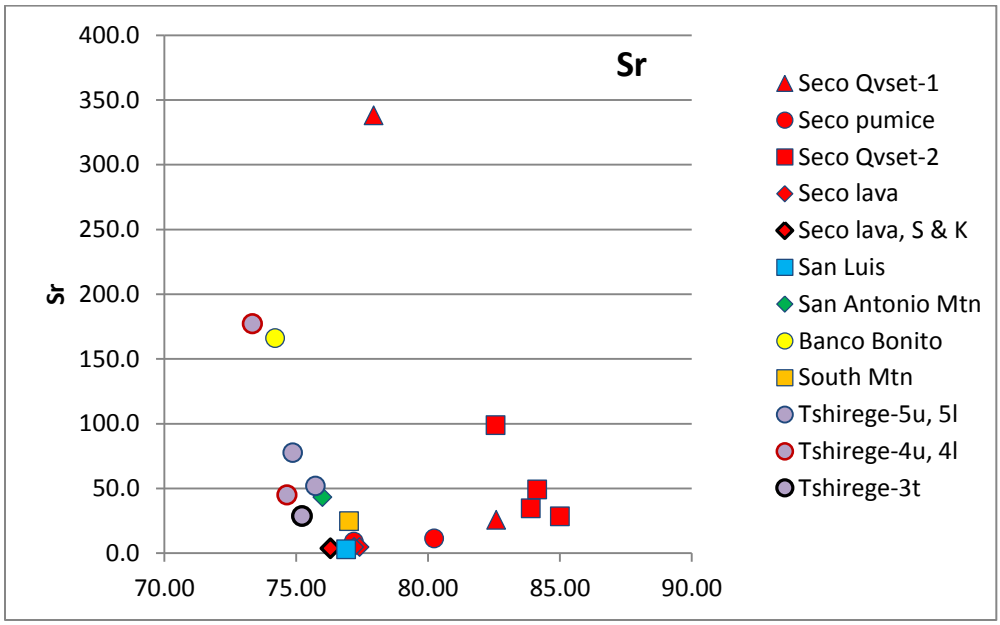

(d)

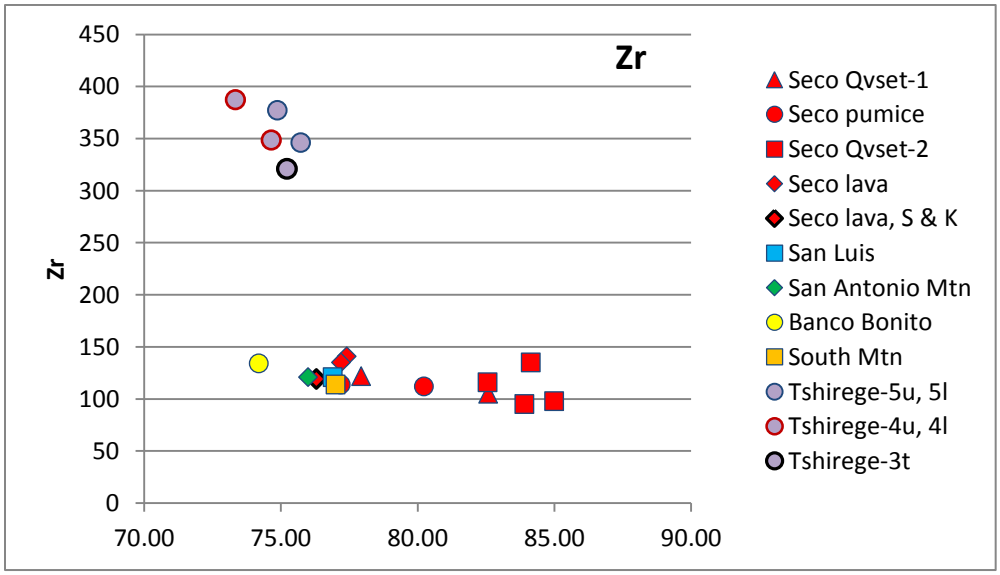

Figure 38. Figure caption on page 62.

CHAPTER 4

DISCUSSION AND INTERPRETATIONS

Field observations, as discussed in section 3.1, have confirmed Goff's observation that Cerro Seco's pyroclastic unit (Qvset) might actually comprise two distinct units (Goff, 2011), one of which may have a hydromagmatic origin. The focus of this study is the second, possibly hydromagmatic, unit, informally named here as Qvset-2. In this section its distribution and character, eruptive chronology and mode of emplacement, as well as evidence for a hydromagmatic origin will be addressed. Secondary emphasis is placed on Seco's first pyroclastic unit, the ignimbrite Qvset-1. The two pyroclastic units are compared, and other related eruptive units are discussed in this section. The strongest lines of evidence leading to a hydromagmatic eruptive model are field relations and observations. Field evidence relates to outcrop morphology, distribution and lithologic content, and indications of lacustrine environment. Petrographic findings support the model of hydromagmatism; while it does not offer primary evidence of hydromagmatism, geochemical data are consistent with the model presented, and offer evidence of post-emplacement processes.

4.1 Sequence of Eruption

Although available dates (Spell and Kyle, 1989, and Goff, et al., 2011) suggest that the Cerro Seco units were emplaced over a short period of time, it is clear from stratigraphic relations in the field, that the Seco ignimbrite overlies the lava of Cerro San Luis, and underlies Qvset-2. The ignimbrite persists as ellipsoidal-shaped ridges that remained after the Qvset-2 deposit flowed around and over them. Ignimbrite outcrop

shape and resistance to weathering and erosion suggests that some degree of cementation, possibly vapor phase mineralization, took place during the emplacement process or afterward.

4.2 Distribution and Volume of Cerro Seco Deposits

Mapping of the Cerro Seco deposits shows that the dominant pattern of pyroclastic deposition is to the north of the vent (Refer to Plate I, Geologic Map). This distribution of deposits can be partly explained by the structural uplift of the Redondo Peak resurgent dome to the south of Seco, which caused a northward shedding of a wedge of debris, now covered by Seco tuffs and lava flows. The resurgent dome lifted all surrounding pre-Seco units, providing a gradient that dictated pyroclastic flow directions. The two Seco pyroclastic units, erupting at separate times, flowed downhill to the north, filling valleys and topographic low areas. In contrast, the highly viscous lavas later piled up in a dome-shaped mass more symmetrically around the vent, and were contained within a roughly concentric configuration; their viscosity rendered them less mobile, lessening gradient influence.

At first glance, the areal extent of Qvset-2 appears to be at least equal to that of the ignimbrite, Qvset-1. Simple volume calculations for the two units, however, show that the volume of the Qvset-2 unit is approximately one third smaller than that of the ignimbrite. Eruptive volume can be estimated using basic geometric methods: simplifying to a circle, with a radius equal to the average distance from the vent. Given that pyroclastic products form an apron, or sector of the circle, the volume can be calculated using the formula $\mathbf{(\pi r^2)(T)(f)}$, where: **r** = average radius for each unit, **T** =

average thickness, taken from the geologic cross section (Plate II), and **f** = area factor, or percentage of the entire circle of the depositional basin, taken from the angle comprising the pyroclastic northern sector of the circle (Refer to sketch in Appendix A). This method yields a total pyroclastic volume of 1.31 km^3 ± 0.470, with an ignimbrite eruptive volume of 0.82 km^3 ± 0.299, and an eruptive volume of 0.49 km^3 ± 0.171 for Qvset-2.

Possible sources of error in volume calculations are related to the nature of pyroclastic flows and emplacement. Pyroclastic flows both deposit and erode, scouring existing topography as they erupt; they also may flow over topographic high points in their fluidized course downslope. This variable, undulatory profile is depicted in lower and upper contacts of the pyroclastic units in the geologic cross-section (Plate II), and renders the determination of average thicknesses problematic. This can be addressed to some extent by increasing the sample size (n) and using an even distribution of measured points. For example, averaging measured thicknesses (T) at 12 equidistant points on the cross section, and by averaging the lengths of 10 equidistant radii (r), the precision is increased. However, given the absence of well data or depth measurements directly beneath Seco, the cross section is, at best, an estimation of subsurface stratigraphy. It is also likely that the ignimbrite was later eroded and planed off to some degree by the subsequent eruption of Qvset-2, and possibly by wave action of a subsequent lake. Thus, the calculated ignimbrite volume should be considered a minimum volume. The results, a total pyroclastic eruptive volume of 1.31 km^3 ± 0.470, reflects an overall error of ± 36% (Refer to Appendix A for more information about this methodology and error calculation).

4.3 Outcrop Morphology

Cerro Seco's pyroclastic rocks, both first-erupted ignimbrite Qvset-1 and second-erupted Qvset-2, have many of the characteristics of sedimentary deposits. Like many pyroclastic deposits, they are composed of magmatic fragments, but laid down generally like sediments (Smith, 1968). Qvset-2 deposits were described in section 3.1.1 as undulatory, creating a mantled outcrop appearance (Figure 18), often strongly bedded and cross-bedded (Figures 19 and 21), graded and clast-supported (Figure 28). Deposits are almost fluvial in appearance, and are devoid of massive structure. The outcrop distribution and morphology of Qvset-2 suggest that it was deposited in a fluidized, highly mobile emplacement process, creating a fan-shaped apron distribution (Plate I). Outcrops display pinch and swell features (Figure 19), and laterally variable bed thickness (Plates III, IV, V and VI). Wet surge from a hydromagmatic eruption is likely, given bed thicknesses of up to 46 m; dry surge beds associated with ignimbrite eruption are rarely thicker than cm to tens of cms (Goff, Wohletz, personal communication, 2018). The ubiquitous presence of cross-bedding, pinch and swell features, graded fluvial-like bed structures and clast-supported stratigraphy are quite suggestive of hydromagmatic surge deposition. Deposits tend to be lithic-rich, but also contain juvenile clasts. The resulting morphology of the second pyroclastic eruption of Cerro Seco is that of a tuff ring, a common vent-type for both hydromagmatic and surge eruptions. The following is a discussion about surges and tuff rings.

4.4 Pyroclastic Surges

Pyroclastic density currents (PDCs) broadly consist of two components, pyroclastic flows and pyroclastic surges. Pyroclastic flows are the main body, or dense, laminar base of the current, whereas surges are the overlying buoyant, dilute cloud of the PDC (Figure 39A).

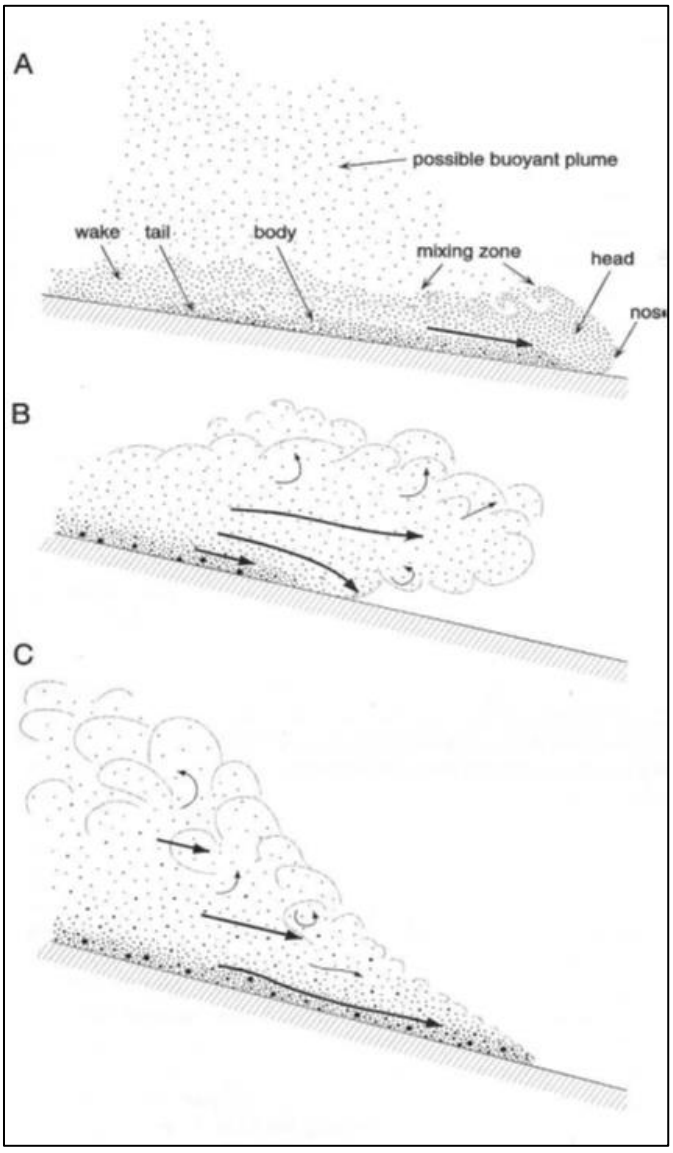

Figure 39. Components of the pyroclastic density current (PDC), illustrating the dilute, buoyant nature of the overlying surge (from Branney and Kokelaar, 2002).

A. Generalized structure of PDC with main body ("flow" in text) and buoyant plume ("overlying dilute cloud" in text).

B. The buoyant, mobile surge current may overhang a more sluggish basal flow.

C. Advance of density-stratified PDC dominated by fast-moving basal layer. Surge cloud is held behind by air resistance.

The pyroclastic surge portion of a PDC is entirely dilute (Fujii and Nakada, 1999) and highly mobile traveling over topographic highs. This makes the effects of surges more widespread and unpredictable. Surges result from a range of environmental conditions, including hot and dry (superheated steam) to cool and wet (condensing saturated steam) (Wohletz, 1998; Sheridan and Wohletz, 1983). Dry surges form at temperatures of >100°C and occur in pyroclastic eruptions with a low water/magma ratio (<0.2 – 0.3), among other conditions (Sheridan and Wohletz, 1983; Vespermann and Schmincke, 2000). The vaporization of water during hotter eruptions leads to the generation of superheated steam, which expands and drives a dry surge. Dry surge deposits show systematic variations in facies, with regard to grain size, sorting and thickness away from the vent. In general, they form larger particles and tend toward massive versus bedded deposits. The dry surge beds in Cerro Seco formed at the base of the ignimbrite Qvset-1 observed in several field sites, and are interpreted to be from unsteady explosive activity, or from the dilute leading edges of the ignimbrite-producing flows (Valentine and Fisher, 2000).

Wet surges, in contrast, form at the lower temperatures characteristic of volcanic events involving higher water/magma ratios (>0.2 - 0.3), where steam is nearly saturated after eruption. It cools and condenses, becoming a three-phase system with water drops, solid particles and gas (Valentine and Fisher, 2000). Wet surge deposits are composed of fine particles (ash and lapilli size) of both juvenile pyroclasts and accidental clasts, though they tend to be rich in lithic components (Vespermann and Schmincke, 2000). Wet surge particles are generally smaller than those of dry surges, and are bedded, clast-

supported, well-sorted and show proximal to distal lateral facies thickness variations, as commonly seen in Cerro Seco's Qvset-2 deposits.

The fact that both dry and wet surge deposits were produced by Cerro Seco indicates that a dynamic set of magma-water conditions existed during eruption, and that pulsed explosivity and transitions occurred, likely over hours to weeks to months.

4.5 Tuff Ring Morphology and Classification

Tuff rings and tuff cones are the most common hydrovolcanic edifices, formed subaerially and/or in shallow water (Vespermann and Schmincke, 2000). The determining factor in forming either a tuff ring or a tuff cone is the degree to which the erupting lateral blasts (surges) are dry (superheated steam media) or wet (condensing steam media), magma to water ratios for which were discussed in the previous section (Wohletz, 1998). As discussed in section 1.5, tuff rings are commonly less than 50 m high, have aspect ratios of 1:10 to 1:30 and low rims (Wohletz, 1998), have beds dipping <25° (Vespermann and Schmincke, 2000), and encounter water at a shallow depth, leading to shallow central craters that are at or above ground level.

The ring of Cerro Seco pyroclastic material has an apparent aspect ratio of 1:15 (maximum thickness = 0.29 km, width = 4.55 km), consistent with tuff ring morphology. Bed attitudes were taken where possible, and where it was felt they were truly representative of bedding structure. Due to the nature of pyroclastic surge deposits, it is often difficult to determine with confidence that the inclined surface is the true dip of a bed, and not an erosional feature. Forty-nine credible dips were measured around the apron of Qvset-2 deposits. They are recorded on the geologic map (Plate I and Appendix

E) and reflect dip directions in all four quadrants: 39% were to the NW, 25% were to each NE and SE, and 12% were to the SW. Taken as a whole, the predominant dip direction is to the north (64%). Dip angles range between 5° and 38°, with an average of 15°, consistent with the <25° dips defining tuff ring morphology. Strike readings were variable, reflective of the undulatory and mantling nature of these deposits, and reveal less about the emplacement history than do dip angles and directions. The volcanic form and deposits resulting from the second pyroclastic eruption of Cerro Seco is consistent with a tuff ring.

4.6 Stratigraphic Variability of Cerro Seco Pyroclastic Flows and Surges

There is wide variability in Qvset-2 bed thickness, and in the order of layering within beds, grading, interbed thickness, degree of clast- versus matrix-supported textures and types of bed features (e.g., cross-bedding) (Refer to Plates III-VI). This variability can be explained by the fact that pyroclastic flows and surges may be emplaced as distinct directional lobes at different times during explosive phases, and are strongly controlled by local topography; this is typical of dome related tephra rings (Wohletz, personal communication, 2017). Therefore, each lobe may be quite different from another, and one location likely will not have deposits that match those at another location. Particularly with PDCs, flows may enhance deposition of a certain feature in one location and not in another. Depending on a variety of factors, such as density current properties, substrate slope, and higher degrees of density stratification, the buoyant surge current may overhang the body (Figure 39B), or the surge cloud may be held behind the dominant, dense basal flow by air resistance (Figure 39C). All gradations

between B and C in Figure 39 can occur (Branney and Kokelaar, 2002), and may explain the wide variability in the stratigraphy, bedding sequences and features of Cerro Seco's hydromagmatic deposits.

Another possible explanation for stratigraphic variability relates to dome size. Small domes (with eruptive volumes of roughly 1 km^3) such as Cerro Seco tend to form deposits with internal stratifications, as their eruptions are more sporadic and pulsed (Wohletz, 1987). Internal stratitifications are common features of tuff rings, as is the subordinate process of reworking, both of which further explain stratigraphic variability within Qvset-2.

Even though correlation with respect to a feature or group of features between one stratigraphic section and another is difficult, particularly if there is significant (> 1 km) distance between them, stratigraphic sections are very useful in describing the emplacement history of a volcanic deposit. Some general trends in stratigraphy that can be relied upon are distal ash and pumice winnowing (presence distally of crystal-rich deposits), gravel-rich intervals near valley floor, lithic-rich deposits proximal to the vent, and cross-bedding where the flow was more highly fluidized (Wohletz, 2017).

An example of lithofacies change and distal winnowing was shown in section 3.1.5, Figure 20. Generally, distal hydromagmatic beds consist of better sorted, more fine-grained and lithic-poor deposits. The distal deposits are farther-travelled and more winnowed, similar to being sieved during transit. Conversely, the deposits more proximal to the vent are more poorly sorted and coarser grained. This lateral facies variation is consistent with processes undergone in water-fluidized, hydromagmatic surge deposition.

Bedded intervals are commonly seen in tuff ring deposits, where segregation of coarse and fine grains into distinct layers points to cohesionless transport (Figure 40) (Vespermann and Schmincke, 2000).

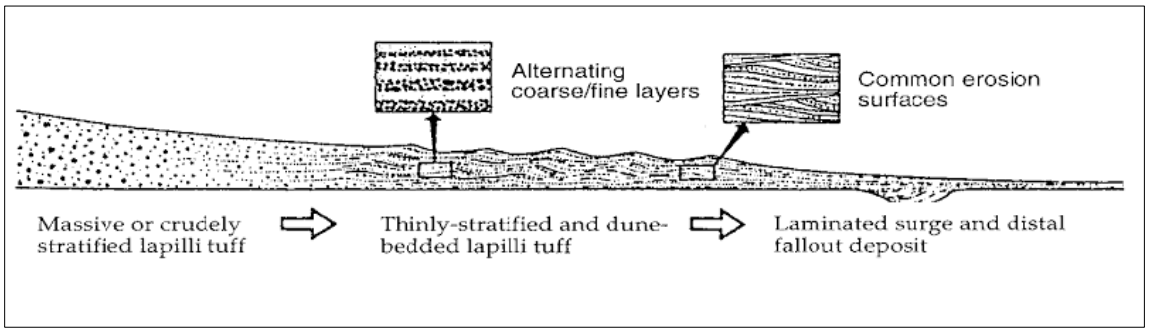

Figure 40. Lateral facies variations of surge, showing crude stratification nearer source, progression to thinly stratified, then laminated bedding distally (modified from Vespermann and Schmincke, 2000).

Detailed mapping revealed conglomeratic intervals of very coarse-grained, subangular gravels within Qvset-2, along a specific topographic horizon. These gravels often contain a distinctive aphyric obsidian, probably from Cerro del Medio several kilometers east. This obsidian is also found in various older sedimentary deposits along and within the drainage system of San Antonio Creek. It is likely that the hydromagmatic surges interacted with the pre-existing sediments near this drainage system. They could have been incorporated into the hydromagmatic surge in the Seco (then lower elevation) conduit and vent area, and as the surges flowed over low-lying surfaces where these intracaldera sediments were previously deposited. The unit Qdf (of Goff et al., 2011), as previously described in section 3.1.1, includes a wide variety of pre-caldera rocks with compositions and ages that constituted the shallow crust at the time of caldera formation,

and is the probable source of most foreign constituents of Qvset-2's conglomeratic intervals.

4.7 Evidence of Lacustrine Environments

There is abundant evidence of the existence of multiple and episodic lacustrine environments in the northern moat of Cerro Seco; the ample supply and availability of water contributes to the proposed model of hydromagmatic eruption. The strongest evidence is the white, fine-grained, laminated, diatom-rich, low-relief beds that uniformly rim the current valley floor, at 2567-2595 m elevation (Figure 11).

Other evidence of a lacustrine environment is found in several outcrops (sites WP-144, WP-123, WP-024) that contain opalized and strongly bedded lacustrine deposits (Figure 13). The presence of opal and alunite is evidence of saturation by low-temperature (sub-boiling, ≈80° C) acidic, silica-rich water (Goff and Janik, 2000). As temperature increases, so does the solubility of silica, thus presence of hydrated silica and sulfates like alunite and jarosite are good indicators of low-temperature geothermal activity, and this activity would be enhanced in the aqueous environment provided by a body of water or an abundant groundwater supply.

However, sands and well-worked, well-sorted sediments are also found at higher elevations, suggesting that lacustrine environments were episodic and spanned a broader time interval. For example, the somewhat isolated pink sand units at sites WP-139 (located at 2674 m), WP-013 (at 2621 m), and WP-028 (at 2621 m) are interpreted as beach-related lacustrine deposits, suggesting a different lake level that pre- or post-dated the lacustrine deposition of the unit Ql in the valley floor elevation of 2560m, 60-100m

below. At site WP-139, the pink sand is partially overlain by Seco lavas Qvse1 and Qvse2, and at site WP-028, the pink sand is located within an outcrop of Qvset-2. This stratigraphic relationship suggests that the sand deposits at both sites existed before the dome lavas erupted, although it is also possible that the lake level was higher than the current valley floor, and that it left sands high against the lavas and Qvset-2 deposit after these units were emplaced. The interdigitation of lacustrine and pyroclastic deposits points undisputedly to episodic volcanic activity with an existing lake or lakes, but the exact timing and stratigraphic relationships of each lake deposit require further study. Refer to Plate I and Table 1 for mapped lacustrine locations and elevations.

4.8 Petrologic Evidence for Hydromagmatism and Explosivity

Petrographic evidence supports a hydromagmatic origin for unit Qvset-2. Angularity of the pumice and lithic clasts within Qvset-2 suggests a non-fluvial mode of transport, although degree of bedding, as described in section 3.1.5, might suggest fluvial deposition. As is typical in hydromagmatic deposits, the grains are predominantly of ash to lapilli size, and show fracture-controlled surfaces with blocky, equant shapes (Figure 28) (Heiken and Wohletz, 1987; Vespermann and Schmincke, 2000). This particle surface is a feature distinguishing these from typical fluvial deposits, which contain clasts that are well-rounded.

Clast morphology or pumice texture is one of the strongest pieces of evidence for a hydromagmatic origin for Qvset-2. Dense pumice, or pumice with low vesicularity, is an indication of a quenching environment. Vesicularity of <70-90% by volume (the theoretical and observed level of gas content needed form fragmentation) indicates that

inadequate magmatic gas existed to form pumice (Wohletz, 2012). Hydromagmatic particles can show a range in vesicularity, from non-vesicular (0-5 vol%) to highly vesicular (60-80 vol%), reflecting the relative timing of vesiculation and water-induced fragmentation (Vespermann and Schmincke, 2000). Deposits can contain some vesicular material, as observed in deposits of Qvset-2, but most clasts have a blocky, compact, structure whose origin is diagnostic of fragmentation formed by rapid quenching (Wohletz, 2012). Large, open-vesicle, frothy, crystal-poor pumice indicates an aerial quenching environment, whereas small, blocky, vesicle-poor and crystal-rich pumice suggests a quenching environment containing water (Goff, 2017). In general, the Seco pumices are dense, blocky and vesicle-poor, consistent with a quenching environment that contained water.

An alternate hypothesis for the origin of Qvset-2 is that the bedded deposits result from a pyroclastic (magmatic versus hydromagmatic) eruption into a body of water. If a pyroclastic density current formed from a magmatic (non-hydromagmatic) eruption and flowed into a standing body of water, the clasts would show high vesicularity, because the fragmentation that produces the flow (and pumice) occurs during eruption (in this example, without external water), before transport and deposition. Ergo, the presence of vesicle-poor pumice, as observed in Qvset-2 thin sections, points to eruption during which external water was present.

Because pumice is a snapshot of quenched magma, the crystal population within the pumice offers a characterization of the magma at eruption. In addition to examining the texture of Seco pumices, crystals and crystal size within the pumices of both

pyroclastic units were also counted, to uncover any evidence of a quenching environment (Appendix B). Crystal-rich (or vesicle-poor) pumice points to the presence of water, or a quenching environment, at the time of eruption, as discussed earlier in this section. The highest pumice counts in the Qvset-2 samples are from the most distal sites (WP-136 and -049), while the highest intra-pumice crystal counts (vesicle-poor) are from samples within a zone of the depositional "apron" along a line of equal elevation closer to the vent; significance of the specific locations of the high-crystal pumice is uncertain.

The petrographic observation was made that Seco feldspars are often aggregated, called glomeroporphyritic texture. The aggregates are possibly derived from holo-crystalline to partly crystalline material in the magma chamber (Best and Christiansen, 1997), and could indicate that the aggregated phenocrysts were not subjected to a highly explosive eruption, or that the eruption was one of pulsed explosivity. The clusters usually later disaggregate to varying extents during explosive eruption, but some aggregates persist, as observed with Seco feldspars (Figure 32).

Cerro Seco's pyroclastic eruptions were highly explosive. In several Qvset-2 and ignimbrite samples, both sanidine and quartz phenocrysts are fragmented, and display irregularly shaped fragments with cuspate or embayed outlines, likely due to vesiculation and decompression during highly explosive eruptions (Best and Christiansen, 1997).

4.9 Petrographic and Geochemical Evidence of Post-emplacement Processes

Several lines of evidence supporting the presence of water at the time of eruption have been presented; however, there is also ample evidence to suggest that water played a role in post-emplacement processes.

The reworking by water likely led to the breakdown of original volcanic material into finer-grained felsic minerals to form the post-depositional opaline silica or clay cement that is ubiquitous in the Qvset-2 thin sections. Clay's relationship to the magmatic process may be close: the last of the fluids and vapors of the magma may react with wall rock to form clay mineral masses (Kerr, 1952). The clay may also have formed after deposition by the action of groundwater, for which there is abundant evidence, saturating the deposit.

Perlite was observed both in hand sample, and in thin section as black, amorphous fields with curved crack lines, in many of the Seco samples. Perlite is formed during the hydration of silicic glass. Given that hydration can take place rapidly when flows get submerged during emplacement, or slowly from the action of groundwater, either or both may have occurred during the deposition of Seco tuff. This is another indication that water likely existed before, during and/or after Cerro Seco eruptions.

The presence of opal is evidence of saturation by low-temperature silica-rich groundwater, as previously discussed in section 4.6. Thin sections showing opaline rinds (Figure 28) surrounding pumice and other grains further supports the model of emplacement into a lacustrine environment, or the evolution of a water-rich environment soon after emplacement of these volcanic units.

An upper limit of 77.4% - 79% silica content is generally considered the maximum for igneous rocks (Hildreth, 1981), and unaltered Valles caldera rhyolites contain no more than 79% silica (Goff, personal communication 2017). Using this delineation, all of the Seco Qvset-2 samples, plus one pumice and one ignimbrite sample

show silica enrichment. This is likely due to leaching of other elemental constituents and/or precipitation of secondary silica, both processes requiring an abundance of water in this setting. The Seco lavas, with silica levels similar to adjacent Cerro San Luis and San Antonio Mountain dome rhyolites, become the "unaffected" benchmark geochemical samples.

Leaching, or the dissolution and loss of soluble substances from a rock, has the effect of enriching the concentrations of other, nonsoluble elements, and resembles silica addition, although no additional silica joins the system. Silicification, the actual addition of mostly opaline silica through percolation of silica-rich groundwater during post-depositional processes, can account for high silica levels; the common source of silica is dissolution of volcanic rocks. In contrast, the Seco lavas are massive and, by virtue of their position above the water table, are not subject to saturation with groundwater; therefore, they are also not subject to rapid leaching. The hypothetical water-rich conditions during the eruption of Qvset-2, as set forth in this thesis, must have changed prior to lava dome emplacement; for some reason the water supply was shut off prior to eruption of Qvse1.

From the variation diagrams (Figure 39a-i), trends involving oxide values with increasing silica may be attributed to four main factors: 1) leaching, discussed above, 2) high concentrations of lithic components, 3) presence of the breakdown or degradation of primary glass, and/or 4) the reaction and dissolution of feldspar.

In plots that show otherwise stable levels of oxides, the only exceptions are high CaO and MgO values noted in one ignimbrite sample (RWVC16-102, Figure 36e and f).

This is likely due to the presence of lithics, which contain andesite, basaltic andesite and dacite; this would generally lead to higher levels of the elements Fe, Ca, Mg, Ba and Sr (Appendix B). The slight elevation in the TiO_2 levels compared to the benchmark lava values may also be due to the presence of lithic components.

In contrast to the relative stability of the Ti, Fe, P, Ca and Mg oxides, the levels of Al_2O_3, Na_2O, K_2O and MnO decrease with increasing silica in the Seco samples. All Seco pyroclastic samples except for one ignimbrite show low potassium levels. This is, again, explained by leaching; the Al, Na, K and Mn were dissolved from the rocks, a process enhanced by a water-rich environment. In the case of Na and K, there could also have been a contribution from the breakdown of feldspar.

In another binary plot, Ba was plotted against TiO_2 (Figure 40). The Seco lava and pumice, as well as the San Luis lava, have very low Ba and TiO_2, making them useful benchmark compositions. In contrast, the Seco pyroclastic units show higher Ba and TiO_2, due to probable contamination by lithic components such as andesites, dacites and previously discussed lithologies present before eruption of Cerro Seco.

Additional Harker variation diagrams were plotted to show weight percent of select trace elements as a function of SiO_2 (Refer to Figure 41). The plots for Zr and Sr show relative stability in the Seco samples. The only exception is one ignimbrite (sample RWVC16-102, Figure 41c), which has higher Sr content than the other Seco samples, likely due to a stronger presence of lithics.

In contrast, Rb, which often follows K, decreases as silica increases, and Ba increases as silica increases. The decreases in Rb may be due to the breakdown of glass

and feldspar. Geochemical processes associated with weathering and soil formation are dominated by alteration of feldspars and volcanic glass. The increases in Ba, as previously discussed, are probably due to the presence of lithics.

4.10 Additional Petrographic Characterization of Cerro Seco Units

A correlation can be made between the sizes of grains (of pumices, crystals, lithic fragments) in deposits and distance from the eruptive source. Generally, the smaller the grain, the greater the distance from the vent, as larger, heavier grains have more time and distance to settle out. As illustrated previously in section 3.1.5 (Figure 20), the rocks closer to the eruptive source contain larger lithic fragments than those more distal, a contrast which is born out petrographically (Appendix B). Thin sections also reveal that the lithic fragments of the more distal sites are highly abraided and weathered, having a "moth-eaten" appearance from extended transport and reworking.

The texture of Seco lavas, which has been described as frothy and pumicious, may indicate degassing near the edge or top of flow (Goff, personal communication, 2017). Lava domes erupt progressively higher viscosity products as the magma chamber empties because of degassing and because of crystal fractionation: the remaining, more silicic magma becomes stiffer and less fluid. This explains the textural differences between the two Seco lavas, and may also partially explain the variability in densities of lavas within the ring fracture rhyolites.

In many of the Seco units, sanidine phenocrysts display blue chatoyance in hand sample, unlike the other moat rhyolites. Chatoyance can develop from thermal stress (such as in fast quenching), chemical impurities (such as in excess iron in the

sanidine), or in sanidine that has compositions near the boundary between true sanidine and anorthoclase. It is uncertain why Seco, uniquely among adjacent dome rhyolites, displays this feature, but chatoyant sanidine is common in the Bandelier Tuff and some of the rhyolite domes in the Toledo embayment (Goff, personal communication, 2017).

Spherulitic texture, an indication of devitrification, was observed in many of Cerro Seco's hydromagmatic and lava samples. Devitrification is an alteration process, common to all crystallized silicic welded tuffs, during which volcanic glass, or any previously uncrystallized material converts to crystallized material, although the term is most commonly used for the formation of spherulites. Rocks, such as sample RWVC16-12 (Figure 31), exhibiting spherulitic texture were likely exposed to high heat and degassing volatiles for a long enough period of time to allow the formation of spherulites. This sample, from one of the conglomeratic gravel lenses, may have been carried from a location very close to eruptive vent, maximizing the time exposed to high temperature.

4.11 Eruptive Model for the Cerro Seco Rhyolite Dome

Based on field observations, petrographic and geochemical anlayses, this study concludes that the Cerro Seco pyroclastic phase was a two-part sequence. Stratigraphy shows that Cerro Seco's first eruption produced the ignimbrite Qvset-1. This highly explosive, likely pulsed, high-silica eruption yielded an estimated 0.84 km^3 of material. The eruption became explosive as the magma rose in the vent because depressurization of dissolved water creates huge quantities of free gas (steam) by virtue of PV=nRT, the ideal gas equation that relates the pressure, volume, and temperature of the gas given a quantity of gas (in this case mostly water vapor).

From the evidence of lacustrine environments in the northern moat, there was abundant external water, defined as any water phase that is not originally dissolved in the magma, such as groundwater or surface water including seawater, meteoric water, hydrothermal water, fluvial water or lake water (Morrissey, et al., 2000).

The fact that no pyroclastic fall deposits were identified in the field may be simply explained by the fact that the ignimbrite exposures are not deep enough to expose co-ignimbrite fall. A too-low volatile content may also preclude a fall deposit, but because the eruption produced a pyroclastic flow, low volatile content does not explain absence of fall deposit. Another explanation lies in the observed low vesicularity of the Seco hydromagmatic pumice. Although density measurements were not made, the tangible and visible field and petrographic observations that the pumice is less vesicular than typical fall-deposit pumice could be explained by the presence of shallow groundwater in this setting. The introduction of water during explosive bursts (quenching) of magma interrupts pumice vesicle growth and expansion, leading to pumice with low vesicularity and high density. The idea that the wet condition impeded pumice vesicle growth might also be applied to infer that conditions were too wet to produce any pyroclastic fall at all.

Once erupted, the mass of pyroclastic debris travelled as a high-particle, fluidized, gas-solid flow that was density-driven. It would have followed topography, becoming channelized in pre-existing valleys and depressions; it possibly surmounted ridges or raised topography, if it had enough energy. The presence of surge layers in some of the ignimbrite outcrops leads to a conclusion that there was energy enough for the medium to

expand into a dilute, turbulent flow, or surge (Cas and Wright, 1992), or that the explosivity of the eruption was unsteady (Valentine and Fisher, 2000). Stratigraphic intervals where shear zones are seen between the pyroclastic flow and the surge layers point to a very dynamic, rapidly changing system.

When all the energy of this first eruption was expended, and the fluidization and gas and steam was spent, the flows filled a shallow basin bounded by the northern caldera wall as an ignimbrite deposit. Given its expansive nature and relatively low volume and thin flows, the ignimbrite did not become welded. The only suggestion of welding in Seco rocks is seen in the presence of clasts of vitrophyre in the non-welded ignimbrite Qvset-1 (sample RWVC16-02, site WP-145), the vitrophyre and ignimbrite being chemically from the same magma. Because vitrophyre is found as fragments within the ignimbrite, it was inferred to have been formed prior to eruption, where it was subject to high enough heat and compression to cause welding.

The presence of water, likely in the form of shallow groundwater or a lake, was the impetus for Cerro Seco's second eruptive/pyroclastic event, one that produced the hydromagmatic unit Qvset-2. After the first pyroclastic phase, the remaining magma interacted with groundwater near the vent, causing massive production of superheated steam to explode, further excavating the vent. Theoretically, this excavation allowed more water to enter the crater, leading to deeper and broader explosions, a process which was repeated many times. The optimum water to magma ratio for hydromagmatic eruptions is 0.2 and 0.3, but other factors such as geometry of the vent and depth of the

interaction, among others, control the explosivity of magma-water interaction (Sheridan and Wohletz, 1983; Vespermann and Schmincke, 2000) (Figure 41).

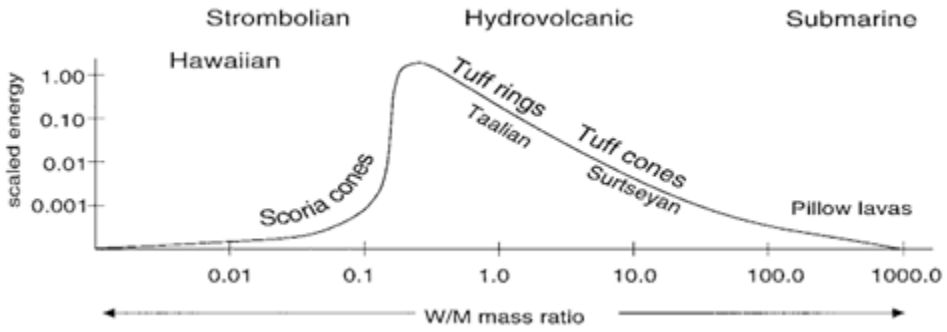

Figure 41. Diagram of water/magma ratios, the primary control on eruption style. Tuff rings results from water to magma mass ratios ranging between 0.2 and 0.3 (modified from Sheridan and Wohletz, 1983).

A poorly understood aspect of hydrovolcanic explosions is the mode of contact between magma and water. Most obvious is the direct pouring of water into an open vent or the movement of magma into a standing body of water. In other cases hydrovolcanic eruptions occur where abundant subsurface groundwater, such as an aquifer, is present. However, water- saturated country rock generally contains insufficient volatiles in pore spaces for the maximum explosive mixing ratios, 30-70% (Sheridan and Wohletz, 1983) (Figure 42).

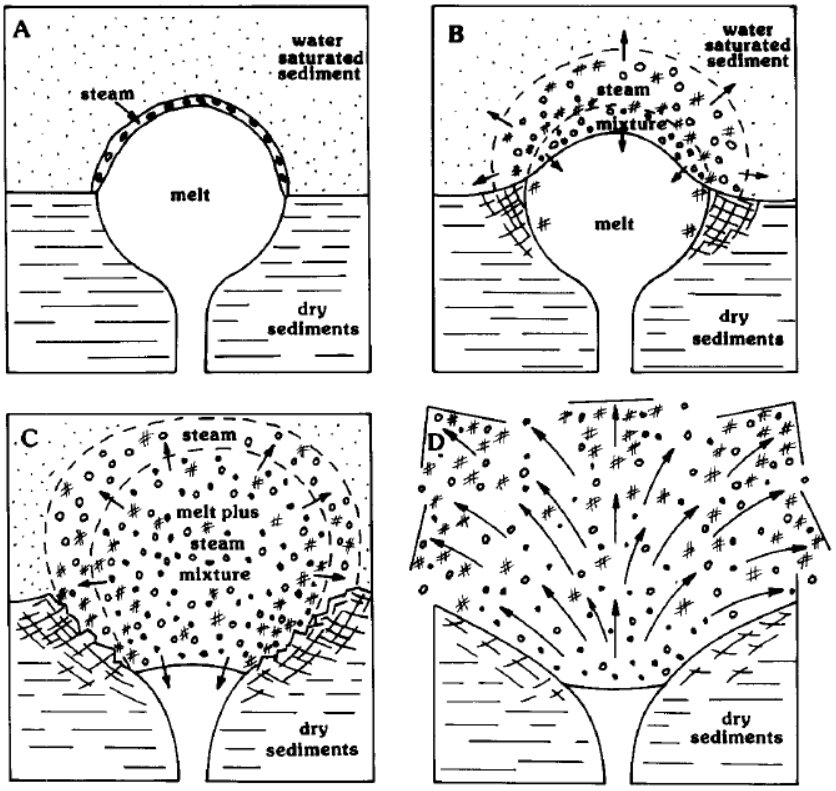

Figure 42. Generalized diagram showing the stages of water-magma interaction within a multi-layered medium. **A.** Magma contacts shallow water-saturated sediments. **B.** Vaporization increases in the high-pressure steam system within the aquifer. Local fracturing of the country rock may occur at this stage. **C.** Large-scale water-magma interaction. Mixing of country rock, steam, and magma. **D**. Explosive rupture of the confinement chamber (from Sheridan and Wohletz, 1983).

Although the mechanics of cold-water egress into the vent are uncertain, the trigger for the transition from the initial pyroclastic event to the hydromagmatic event could be a sudden breach of the crater wall by groundwater, or a conduit that contained both wet and dry sections (Figure 43).

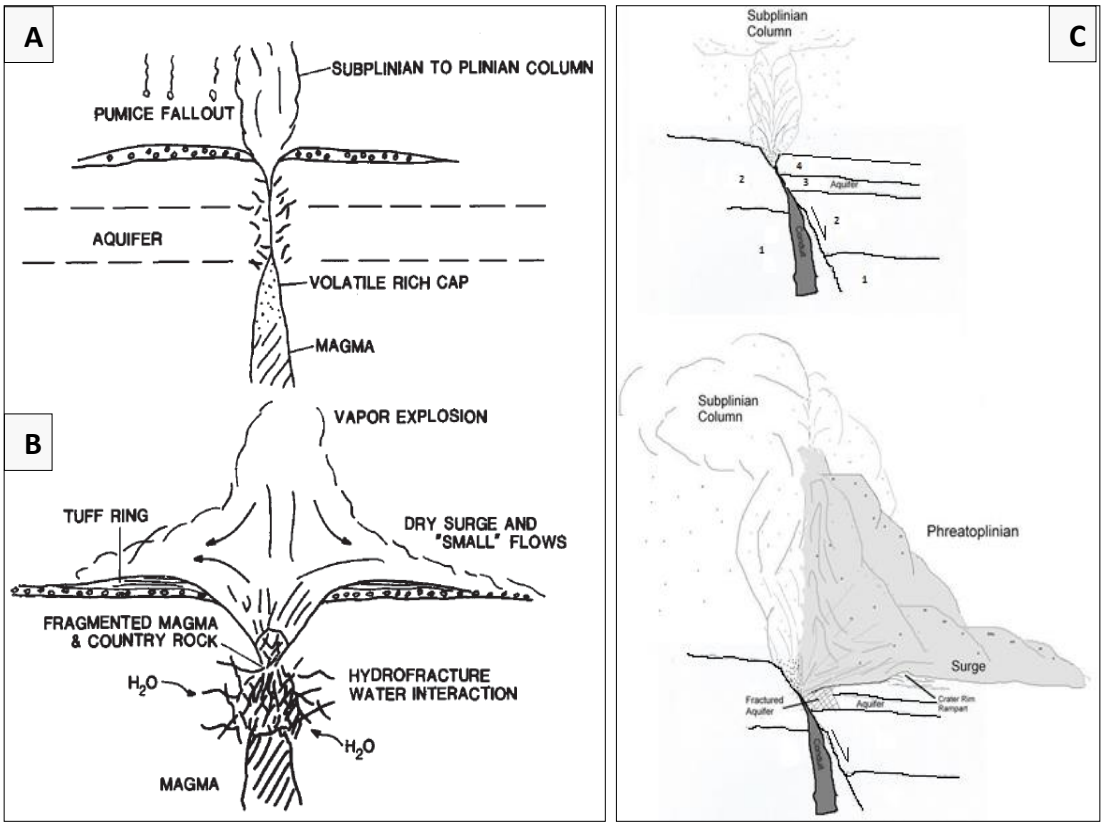

Figure 43. Two schematic models illustrating mechanisms for transition from subplinian pyroclastic to hydromagmatic eruption, as in the eruption of the Cerro Seco hydromagmatic unit Qvset-2. **A.** Tephra production with Plinian stage eruption. **B**. Explosion becomes hydromagmatic with introduction of water. **C**. Water enters conduit on one side of a faulted conduit yielding both wet and dry surges (modified from Sheridan and Wohletz, 1987, and Wohletz, personal communication, 2017).

In this model (Figure 43C) a faulted substrate hosts a pyroclastic eruption, which proceeds until a fracture into the aquifer causes water to enter the conduit. The caldera ring fracture created a faulted zone, rendering the structural conditions for this wet and dry model. As explained previously, the explosion resulting from this magma-water interaction breaches the conduit and further widens the crater, allowing more

groundwater to enter the vent and perpetuate this chain reaction. A low crater rim rampart develops in classic hydromamatic eruptions, forming a ring-like deposit of pyroclastics around the vent. In the field area site WP-38 (section 3.1.4, Figure 16B), an outcrop of ignimbrite is inferred to be the rampart rim given its proximity to vent, morphology and abundance of lithic components.

Field observations indicate that the hydromagmatic unit was emplaced over the ignimbrite, and that it flowed around the more cemented and resistant ignimbrite outcrops. Its course would have been unpredictable, although theoretically, and based on field evidence (Refer to Plate I (site WP-120)), it would have partially filled the shallow basin formed by the caldera wall in the northern moat, as did the ignimbrite. The existing most distal outcrops of Qvset-2 are very thin, less than 0.5m thick (Refer to Plate I and II).

After groundwater was shut off to the vent, the pyroclastic phase ended, and was followed by the growth of a rhyolite lava dome, producing massive to slightly vesicular rhyolite lavas in two separate flows, Qvse1 and Qvse2. The high-silica viscous magma cooled relatively quickly during eruption, resulting in the formation of a contained dome, steep-sided relative to the pyroclastic deposits. In rhyolite systems such as Cerro Seco and other northern moat domes, the evolution from explosive phases to growth of a lava dome is a typical eruptive cycle.

CHAPTER 5

CONCLUSIONS

Cerro Seco (ca. 0.8 Ma) is a post-collapse ring-fracture rhyolite dome of the Valles Caldera, New Mexico and is the only ring-fracture rhyolite that produced hydromagmatic deposits. Field observations, detailed mapping, petrographic observations and geochemical analyses were used to characterize the eruptive dynamics and depositional facies of the Cerro Seco hydromagmatic tuff.

Although new dates for two Cerro Seco units and one unit from the adjacent Cerro San Luis are still pending, stratigraphic relations illustrate that the Seco ignimbrite immediately overlies the Cerro San Luis rhyolite (also about 0.8 Ma), and the Seco hydromagmatic tuff overlies the ignimbrite, followed by two Seco lava flows. Given the existing dates for these units, it is inferred that eruptions were closely-timed. The hydromagmatic tuff deposits form an apron over a northern sector of Cerro Seco, so positioned because of the broad gradient created by pre-Seco uplift of the Valles resurgent dome, and overlying post-resurgence sediments.

Field relations and observations provide the strongest evidence for a second pyroclastic eruption which had a hydromagmatic origin. Outcrop morphologies reveal hydromagmatic tuff deposits that are highly variable, exhibit laterally variable pinch and swell morphologies, and include fine-grained and coarse-grained deposits, thinly-laminated surge layers, gravel intervals, and bedded and cross-bedded, often lithic- or pumice-rich, deposits that are distributed along a 4.5-km depositional apron around the northern sector of the Cerro Seco dome. The total eruptive volume for both pyroclastic

units is estimated at 1.34 km^3, placing Cerro Seco in the Vulcanian-Subplininan explosivity category (VEI 4-5).

Petrographic analysis of hydromagmatic deposits, including grain size and textures, crystal componentry and lithic concentrations reveal an eruptive source that is consistent with previous mapping. Pumice clast morphology shows low vesicularity and fracture-controlled surfaces, strong indications of hydromagmatic eruption. Generally, distal outcrops display finer-grained, more pumice-rich, winnowed and reworked beds, whereas proximal deposits are more crudely bedded, more crystal-rich and contain larger lithic clasts.

Post-depositional opaline silica rinds and clay cement are ubiquitous in the hydromagmatic thin sections, indicating precipitation of silica from groundwater, and the reworking and breakdown of original volcanic material into finer-grained felsic components. This is strong evidence for a lacustrine or shallow-aquifer depositional setting.

ICP-MS and ICP-AES geochemical analyses were conducted on Cerro Seco whole-rock ignimbrites, pumices from the ignimbrites, hydromagmatic tuff and the two Seco lavas. The lava analyses are considered most representative of unaltered and uncontaminated Seco magma. Major oxide concentrations show that Seco pyroclastic deposits, particularly the hydromagmatic deposits, have undergone silica enrichment by precipitation from groundwater. Other major elements (Na, K, Al, Mn) are depleted with respect to silica through the process of leaching of pumiceous glass and chemical breakdown of feldspars. The elements Ti and Ba, show enrichment with respect to silica

due to incorporation of mafic volcanic rocks (from older pre-Seco lithologies) into the pyroclastic deposits. The chemical differences between the various types of Seco pyroclastic deposits point mainly to differences in modes of eruption and to post-depositional alteration, not to compositional changes in the underlying magma chamber.

Cerro Seco initially developed in a water-rich environment, where evidence points to the existence of a lake or, likely, a series of lakes, which saturated the substrate with groundwater. Seco's emergence began as a pyroclastic event, producing an ignimbrite with an estimated volume of 0.82 km^3. Conditions changed that allowed groundwater from the water-rich substrate into the vent, leading to steam-rich conditions, and an explosive event involving an optimum water-to-magma mass ratio. The hydromagmatic eruptions, which were likely pulsed, ultimately yielded an estimated volume of 0.49 km^3 via a fluvial-like mode of deposition over and around the topography of previously-emplaced ignimbrite. Based on the eruptive, transport and depositional models of pyroclastic lithofacies, as described by multiple authors, the eruptive sequence of the Cerro Seco pyroclastic units was described; models of the eruption of the hydromagmatic unit are presented in Figures 42 and 43.

The findings and conclusions put forth by this study have not been identified or postulated until now, largely because the hydromagmatic deposits of Cerro Seco are relatively inconspicuous in the field. Seco's hydromagmatic low-lying and highly variable bedded outcrops are not always easily located or identified. Furthermore, hydromagmatism in the Valles, especially during early mapping of the Valles caldera, was unexpected. The relatively uncommon constellation of conditions leading to the

sequence of pyroclastic eruption followed by hydromagmatic eruption yielding a tuff ring, which then became hidden by lava flows and dome emplacement, is unique within the Valles caldera system. Given the evidence presented here, it is proposed that the Cerro Seco pyroclastic unit Qvset should be reclassified into two distinct units: Qvsig, an ignimbrite unit and Qvshy, a hydromagmatic unit.

APPENDIX A

Methods

Geologic Mapping

Previous geologic maps (Goff et al., 2011, Goff et al., 2006) covered all or parts of nine U.S. Geological Survey topographic 15' quadrangles: Bland, Redondo Peak, Jemez Springs, Seven Springs, Valle San Antonio, Valle Toledo, Polvadera Peak, Cerro del Grant and Jarosa. Detailed geologic mapping for this project covers portions of the Valle San Antonio quadrangle, and has remapped in more detail certain areas of this quad.

Field objectives included mapping the Cerro Seco pyroclastic unit (and to determine if the pyroclastic phase included one or more separate eruptions), two Cerro Seco lavas, portions of the first Cerro San Luis lava (Qvsl1), lacustrine and terrace deposits, debris flow and other related volcanics, contacts and faults, and other important features useful for establishing geospatial relationships. Cerro Seco pyroclastic units crop out around the northern half of the Cerro Seco dome. Therefore, detailed mapping was focused on the northwest to northeast quadrants of the dome. The ring fracture and vent area were approximated based on previous mapping, map patterns, and unit distributions and thicknesses.

To determine eruptive volumes, geometric calculations were done using measured radii directly from map units, extrapolated unit thicknesses, and an area factor. The formula $V = (\pi r^2)(T)(f)$ (where V = volume, r = radius or runout of deposit, T = average unit thickness, and f = fractional part of the circle circumference or sector occupied by

the units) was used for volume calculations. Constraints on overall depth of deposits post-dating the Redondo Creek Member Qrc was offered by well-log cuttings from Baca-7 (Lambert and Epstein, 1980). Refer to Plate II, Geologic Cross-section of Cerro Seco for well-log unit depths and unit thicknesses, and to Figure 44, to accompany the calculation results shown in Table 6.

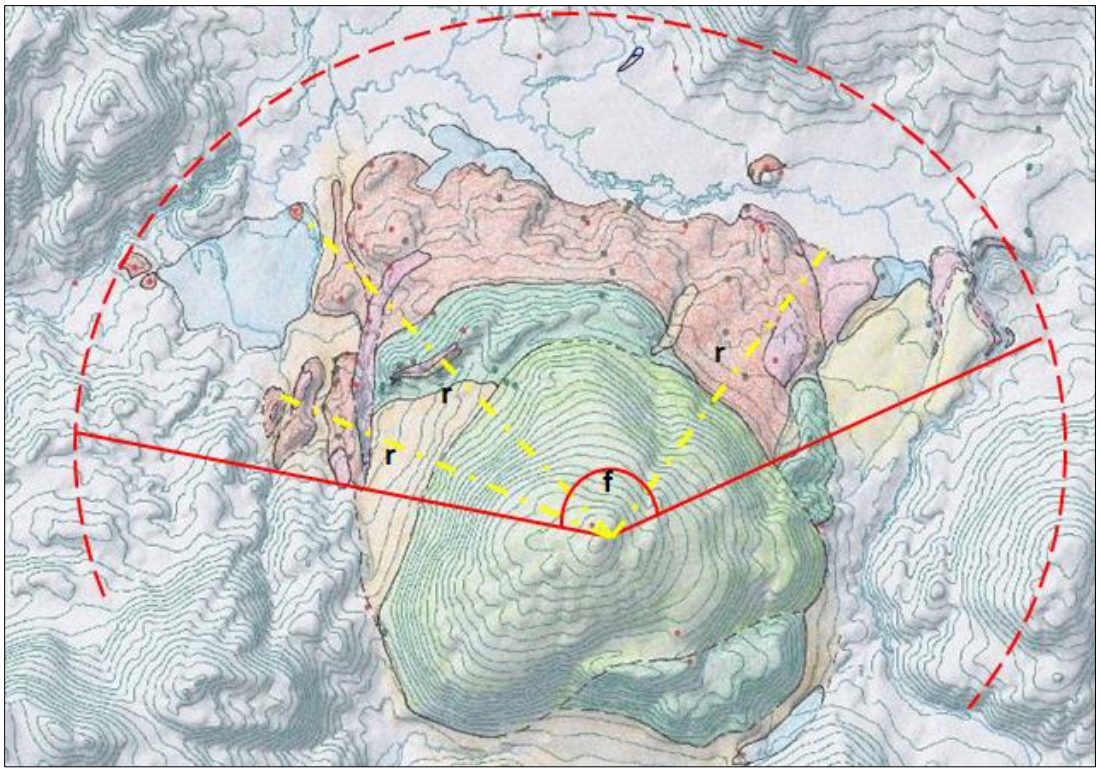

Figure 44. Sketch showing methodology used in calculating eruptive volumes. Map of Cerro Seco illustrates dimensions and concept used in the pyroclastic eruptive volume calculation. Large dashed red line = circumference of the conceptual circle representing the basin into which Seco products were emplaced. Solid red lines = the outer-most arms of the sector in which the Seco ignimbrite Qvset-1 and the hydromagmatic unit Qvset-2 were deposited, and which create the angle 148°; f = the area factor (having a value of 0.411, the quotient of 148°/360°); and r = radii to the various outcrop extents, shown as yellow dashed lines.

Unit	Avg radius r (km)	Avg thickness T (km)	Sector %	V (km^3)
Qvset-1	2.31 ± 0.27	0.120 ± 0.015	0.411 ± 0.014	0.82 ± 0.299
Qvset-2	2.26 ± 0.15	0.074 ± 0.007	0.411 ± 0.014	0.49 ± 0.171
			Total	**1.31 ± 0.470**

Table 6. **Volumes and standard error values calculated using formula $V = (\pi r^2)(T)(f)$.** See text for details.

Standard deviation (**σ**) was calculated using the formula: $\sqrt{\sum}$ (m-i)2/n-1, where m = mean of all measurements; n = sample size. Standard error calculations followed the formula: **σ** /√n**.**

Unit	Depth range (m)	Thickness (m)	Thickness (ft)
Qdf	0-152	152	500
Qrc	152-457	305	1000
Qdf	457-701	244	801
Qbt	701-976	275	902
Tsf	976-1128	487	1598
Mpu	1189-1677	214	702
p€	1677-1687	10	33
Total Depth (TD)=1687 m (5536 ft)			

Table 7. Unit thickness data from geothermal well Baca-7 (Lambert and Epstein, 1980), used in creation of the Geologic Cross-section (Plate II).

Petrographic Analysis

Multiple hand samples of each mapable unit were collected. Collection sites were recorded using a handheld GPS, a hand-held Garmin GPSmap 60CSx, downloaded to Garmin's MapSource software, version 3.02, United States TOPO for the Western United

States. Petrographic descriptions were derived from both hand specimens and thin sections; 60 hand samples were gathered from 82 outcrops mapped in the field. Petrographic descriptions include mineralogy, modal percentages, colors, and textures from volcanic and depositional processes.

From collected samples, 11 standard 30-micron thin-sections were made at California State University, Sacramento, 14 are previous sections that were made by High Mesa Petrographics (HMP) of White Rock, New Mexico but never studied, and 5 are new sections made by HMP. Detailed petrographic descriptions of mapped units were recorded from these thin-sections and included modal percentages of phases derived through point-counting 200 points per section, phenocryst assemblages, micro-textures of crystals and groundmass, presence of lithic, pumice and glass fragments, and other notable petrographic features (refer to Appendix B). A Leitz Laborlux petrographic microscope fitted with a manual Leitz point counter was used for analysis. Photomicrographs were taken with a Leitz photographic adaptor set up on a Meiji petrographic scope and projected for visualization and focus.

Geochemical Analysis

Samples of the Seco ignimbrite, pumice, Qvset-2 unit and lavas were analyzed by ALS Minerals in Reno, Nevada and Vancouver, BC laboratories. Inductively coupled plasma -mass spectroscopy (ICP-MS) using the Agilent 7700, and Inductively coupled plasma - atomic emission spectroscopy (ICP-AES) using an Agilent Vista 725-ES were performed for elemental analysis. The analyzed samples consisted of seven whole rocks and three single pumices (10 samples total) from the Cerro Seco volcanic suite.

Each hand sample was cleaned of weathered surfaces, lichen, dirt and soil, factors that may alter the analytical results. Fresh pieces were broken off, and chips of the hand sample were selected. Approximately 24 grams were required for proper analysis of each sample. Resulting data of major element oxides were reproduced in a spreadsheet, normalized to total 100 %, and plotted.

Using ICP-MS analyses, 31 elements were analyzed, including 13 trace elements and 16 rare earth elements (REEs). Using ICP-AES, 10 elements were analyzed, including the rare earth element Sc (Appendices C and D). Geochemical procedures are specified to have a precision of ±10%. Data analysis is certified, complying with the requirements of the International Standards ISO/IEC 17025:2005 and ISO 9001:2008.

APPENDIX B. Petrography of Cerro Seco Volcanic Suite, Grouped by Deposit Type

Modes, in volume-%, void free; the percentage of each mineral is listed after the "Total %"

Sample	Loc: UTM Easting/Northing	Unit/Waypoint	Total points	GM	pum	glass	Total Xls	Lith frags	Total %	qtz	sa	pl	bt	hbl	ksp	Pheno size (mm)	Xls in Pum	Notes
Seco Units																		
Ignimbrites																		
RWVC16-02	0355964/3981490	Qvset-1-Vitrophyre/WP-145	200	28.5	0.5	40.0	27.0	4.0	100.0	23.5	0.5	1.0	1.5	0.5	0.0	0.25 - 1.5	NA	glassy gm, rhyo LFs
RWVC16-24	0359308/3980511	Qvset-1-ig/WP-138	201	38.3	22.4	2.0	17.9	19.4	100.0	1.9	2.5	3.0	0.0	0.0	0.5	0.25 - 3.5	22	glassy gm; large pum (2.5 mm)and LF; pum contains 18 qtz, 4 sa phenos; highest lithic count of igs; hbl seen
RWVC16-132	0359114/3981527	Qvset-1-ig/WP-132	199	56.8	21.1	0.0	16.6	5.5	100.0	5.0	10.6	0.5	0.0	0.5	0.0	0.25 - 2.5	9	1.75 mm sa, contains green hbl; lots of "oxidized" sa (yellow squares); pum: 6 mm, 1.2 cm, 1.0 cm; xls in pum
RWVC16-132P	0359114/3981528	Qvset-1-pum/WP-132	159	86.8	0.0	0.0	13.2	0.0	100.0	3.8	9.4	0.0	0.0	0.0	0.0	0.5 - 2.25	NA	swirly gm; "ring aggregate"
RWVC16-102	0356358/3980440	Qvset-1-ig/WP-102	177	54.2	18.8	0.0	17.5	8.5	100.0	5.1	9.0	2.3	1.1	0.0	0.0	0.6 - 1.5	16	a 5 and a 6-mm pumice, 1.5 mm sa; "bare edges" on pum; 12 pl, 2 sa, 1 qtz, 1 bt in pumices
F05-137*	0356358/3980441	Qvset-1-pum/WP-102	195	83.6	1.0	0.0	15.4	1.0	101.0	9.7	2.1	3.1	0.0	0.0	0.5	0.25 - 2.0	NA	aggregates of phenos within 1 pum
Pyroclastic-2																		
RWVC16-03	0359186/3982009	Qvset-2-WP-049	199	20.1	51.8	1.5	24.0	2.5	99.9	19.0	0.0	4.0	0.5	0.5	0.0	0.25 - 2.0	13	all xls in pum are qtz; flow-banded grain (hbl or bt andesite), rimmed qtz
RWVC16-10	0356125/3981341	Qvset-2-WP-121	199	33.2	28.6	4.0	20.7	13.6	100.1	18.7	1.0	0.5	0.5	0.0	0.0	0.15 - 2.0	57	pum contain addl: 44 lg qtz, 11 pl, 1 sa, 1 bt; RF= rhyo; wasted qtz
RWVC16-12	0356625/3981384	Qvset-2-WP-125-cgl	200	41.5	10.0	4.0	18.0	26.5	100.0	8.0	9.5	0.5	0.0	0.0	0.0	0.25 - 2.0	1	fine-grained variant; pum contain 1 qtz; 13 rounded LFs, spherulitic grains
RWVC16-14	0357376/3981601	Qvset-2-WP-128	195	21.5	13.3	4.1	30.8	30.3	100.0	9.2	5.6	12.3	1.0	0.5	2.0	0.25 - 2.0	5	coarse-grained variant; pum contain 1 qtz,2 pl, 2 bt; microcline, a flow-banded grain; rhyo & and
RWVC16-16	0358680/3981407	Qvset-2-WP-131-"classic"	182	23.6	28.6	2.7	29.1	15.9	99.9	15.9	3.8	3.3	0.5	0.0	5.5	0.25 - 1.75	76	pum contain 31 qtz, 19 sa, 10 pl, 9 bt, 5 ksp, 1 px,1 hbl; rhyo-and LFs; 1 lg olivine xl (1.5 mm)
RWVC16-28	0356365/3980356	Qvset-2-WP-141-"day 1"	199	50.0	31.2	2.0	5.5	11.0	99.7	3.0	1.0	1.0	0.5	0.0	0.0	0.15 - 1.5	17	pum contain 10 qtz, 6 sa, 1 pl
RWVC17-136	0354835/3981124	Qvset-2-WP-136-west. distal	201	35.3	13.9	1.5	11.4	36.8	98.9	4.5	4.5	1.9	0.5	0.0	0.0	0.35 - 2.25	8	pum size range: 0.5 - 3.0 mm; lithic-rich (VRFs); xls in pum (3 qtz, 5 sa); LFs incl rhyo and large striped sandstone
F05-151*	0354798/3981095	Qvset-2-WP-136-west. distal	191	18.3	45.0	5.8	15.1	15.7	99.9	11.0	1.0	1.6	0.5	0.0	1.0	0.5 - 2.0	1	
F95-45a*	0395241/3981838	Qvset-2-WS-large grain	182	13.2	56.6	8.8	15.3	6.0	99.9	9.9	2.2	1.6	0.5	0.0	1.1	0.25 - 1.75	17	pum contains: 10 qtz; 1lpl; 5 sa; 5 bt; 2.5 mm sa
F95-45b*	0395241/3981839	Qvset-2-WS-sm grain	199	50.3	2.5	1.0	25.6	20.6	100.0	19.6	1.5	2.5	2.0	0.0	0.0	0.15 - 1.75	7	
F05-154*	0359278/3981376	Qvset-2-near WP-113-fossil	192	41.7	18.8	2.6	20.3	15.6	100.0	15.6	2.1	1.6	0.5	0.0	0.5	0.2 - 2.0	16	pum contains some very large xls
Lavas																		
RWVC16-21	0358718/3978505	recount Qvse1	189	75.1	0.0	0.0	25.0	0.0	100.1	10.6	12.2	1.1	1.1	0.0	0.0	0.15 - 2.15	NA	rhyo LFs, hbl present; huge sa and pl phenos; 5% vs 1% (in Qvse2) voids, 2.15 mm bt, 2.5 mm sa
RWVC17-050	0356585/3978700	Qvse2 not summit	197	73.1	0.0	0.0	26.9	0.0	100.0	11.7	14.2	0.5	0.0	0.0	0.5	0.1 - 1.85	NA	minor spherulite; 1 aggregate/sa
Non-Seco Units																		
F80-75*	0356994/3978728	Qvsa2-SAM rhyo lava	196	77.0	0.0	0.0	22.9	0.0	99.9	14.8	5.1	2.0	0.5	0.0	0.5			contains feldspar aggregates; bt may be understated (present but all did not fall in points counted)
F83-10*	0359133/3981721	Qvsw-WS rhyo lava	200	80.0	0.0	0.0	20.0	0.0	100.0	12.0	8.0	0.0	0.0	0.0	0.0			2.25 mm sa
F02-47*		Qsc-rhyo lava	187	82.4	0.0	0.0	17.1	0.5	100.0	0.0	3.5	6.5	2.5	0.0	2.5			uniquely, no qtz
F05-150*	0354841/3981365	Qbo-Bandelier, faulted	199	76.9	3.5	0.0	18.6	1.0	100.0	16.6	1.5	0.5	0.0	0.0	0.0			
F93-SS18*	0356492/3978903	Qdf-Fnet lithic	202				100.1	0.0	100.0	38.7	2.0	45.0	2.0	0.0	16.8			combined ksp and microcline. PLUS px: 0.5. A 2-mica granite
F95-40b*	0357708/3981852	Ql-S/road VC08; underQvset	195	76.9	0.0	1.5	11.3	10.3	100.0	10.3	0.5	0.5	0.0	0.0	0.0			
F05-147*	0355521/3981822	Qsp-Megabreccia, PalitaQry	195	74.5	0.0	0.0	25.6	0.0	100.1	1.5	2.6	19.5	0.5	1.0	0.5			
F05-149*	0355472/3981725	Qvs(or QT)-f-gr mud sandst	182	30.8	2.2	1.1	41.7	24.2	100.0	32.4	2.2	6.6	0.0	0.0	0.5			200 point w/ voids
F06-02*	0358572/3981138	Ql lac	130	60.0	6.1	2.3	11.5	2.3	97.6	6.9	2.3	2.3	0.0	0.0	0.0			diatom: 10.1%; organics: 1.5%; 15.4% diatoms (?)68 voids removed

*Previous sections provided by Fraser Goff

Robin Wham 2016-2017

Abbreviations: WP=waypoint; ig=ignimbrite; WS=Warm Springs; GM=groundmass; pum=pumice; xls=crystals; LF=lithic fragment; sa=sanidine; pl=plagioclase; qtz=quartz; bt=biotite; hbl=hornblende; ksp=potassium feldspar; pheno=phenocryst; rhyo=rhyolite; and=andesite

APPENDIX C. ICP-AES DATA: MAJOR ELEMENT OXIDES OF 10 SAMPLES FROM THE CERRO SECO VOLCANIC SUITE

kUnit	Sample (Type)	Easting	Northing	SiO_2	Al_2O_3	Fe_2O_3	CaO	MgO	Na_2O	K_2O	TiO_2	MnO	P_2O_5	Total	Na_2+K_20
Qvset-1	RWVC17-102P (SP)	0356337	3980495	77.19	12.12	1.22	0.53	0.08	3.25	5.43	0.08	0.07	0.03	100.98	8.68
Qvset-1	RWVC17-102 (WR)	0356337	3980495	77.94	11.73	1.39	1.03	0.38	2.69	4.55	0.14	0.04	0.05	102.00	7.24
Qvset-1	RWVC17-132P (SP)	0359114	3981527	80.24	10.67	0.95	0.36	0.05	2.93	4.63	0.08	0.07	0.01	101.67	7.57
Qvset-1	RWVC17-138 (WR)	0359308	3980511	82.59	9.54	1.29	0.37	0.13	2.61	3.32	0.10	0.05	0.01	101.31	5.93
Qvset-2	RWVC17-141 (WR)	0356365	3980356	83.90	8.78	1.02	0.39	0.11	2.38	3.27	0.09	0.03	0.01	101.95	5.65
Qvset-2	RWVC17-049 (WR)	0359135	3981772	85.00	7.94	1.24	0.40	0.10	1.94	3.22	0.09	0.04	0.01	101.30	5.15
Qvset-2	RWVC17-136 (WR)	0354835	3981124	82.56	9.60	1.18	0.62	0.21	2.38	3.21	0.15	0.03	0.01	100.62	5.59
Qvset-2	RWVC16-121 (WR)	0356325	3981341	77.41	12.31	1.12	0.34	0.05	3.95	4.66	0.08	0.08	0.01	101.25	8.61
Qvse1	RWVC16-116 (WR)	0357078	3980914	77.20	12.50	1.11	0.24	0.04	4.19	4.55	0.08	0.07	0.01	99.82	8.74
Qvse2	RWVC17-050 (WR)	0356585	3978700	84.14	8.73	0.84	0.55	0.12	2.27	3.16	0.13	0.03	0.01	99.13	5.43

Appendix C. ICP-AES data of major element oxides determined by ALS (Reno, NV. Reported values are total weight percent and normalized to 100%. (Type) indicates material analyzed: (SP)=single pumice; (WR)=whole rock

APPENDIX D. ICP-MS and ICP-AES DATA: TRACE AND RARE EARTH ELEMENTS OF THE CERRO SECO VOLCANIC SUITE

(Values continued on next page)

Unit	Sample (Type)	Ba	Ce*	Cr	Cs	Dy*	Er*	Eu*	Ga*	Gd*	Ge	Hf	Ho*	La*	Lu*	Nb	Nd*	Pr*	Rb
Qvset-1	RWVC17-102P (SP)	18.5	71.7	10	10.85	10.20	6.90	0.08	21.6	7.51	<5	6.2	2.23	35.7	1.17	88.1	28.8	8.61	285
Qvset-1	RWVC17-102 (WR)	151.5	76.7	10	38.90	7.14	4.74	0.22	18.7	6.09	<5	5.6	1.66	41.7	0.85	59.6	29.1	8.92	199.5
Qvset-1	RWVC17-132P (SP)	27.6	63.5	10	9.59	9.01	6.29	0.08	19.7	6.53	<5	6.0	2.03	31.7	1.08	79.8	25.2	7.52	242
Qvset-1	RWVC17-138 (WR)	119	56.2	10	8.37	6.64	4.48	0.21	16.1	5.15	<5	5.1	1.50	30.4	0.75	55.2	23.2	6.93	172.5
Qvset-2	RWVC17-141 (WR)	124	46.4	10	11.95	5.02	3.33	0.21	14.1	4.12	<5	4.0	1.11	24.6	0.57	42.1	18.4	5.46	145
Qvset-2	RWVC17-049 (WR)	144	58.0	10	4.94	4.76	3.20	0.17	12.7	3.98	<5	3.8	1.07	33.1	0.54	40.3	22.4	6.91	126.5
Qvset-2	RWVC17-136 (WR)	287	46.3	10	5.19	3.45	2.26	0.28	14.8	3.07	<5	4.3	0.75	25.5	0.38	31.0	17.3	5.20	101.5
Qvset-2	RWVC16-121 (WR)	236	70.9	10	4.57	3.33	2.13	0.28	11.8	2.98	<5	4.3	0.72	41.1	0.39	28.8	23.4	7.65	107
Qvse1	RWVC16-116 (WR)	27.4	67.5	10	9.81	10.65	7.28	0.10	22.6	7.90	<5	7.3	2.37	35.4	1.22	91.2	30.4	8.98	278
Qvse2	RWVC17-050 (WR)	23.6	67.9	<10	6.95	8.91	6.06	0.12	22.8	6.29	<5	7.1	1.95	30.5	1.06	89.5	26.9	8.10	284

Appendix D. ICP-MS and ICP-AES geochemical data for un-normalized rare-earth elements (REE-indicated by *) and trace elements of the Cerro Seco volcanic suite. Values are reported in ppm (parts per million). (Type) indicates material analyzed: (SP)=single pumice; (WR)=whole rock.

(Values continued from previous page)

Unit	Sample (Type)	Sm*	Sn	Sr	Ta	Tb*	Th	Tm*	U	V	W	Y*	Yb*	Zr	Ni	Pb	Sc*	Zn
Qvset-1	RWVC17-102P (SP)	7.98	6.00	8.80	6.80	1.58	29.30	1.13	10.40	<5	6.00	68.60	7.80	114.00	2.00	30.00	1.00	41.00
Qvset-1	RWVC17-102 (WR)	6.61	5.00	338.00	4.90	1.17	22.50	0.80	5.12	8.00	2.00	48.00	5.55	122.00	4.00	23.00	2.00	33.00
Qvset-1	RWVC17-132P (SP)	7.11	6.00	11.20	6.20	1.42	26.70	1.01	10.95	<5	5.00	61.90	6.88	112.00	1.00	27.00	1.00	35.00
Qvset-1	RWVC17-138 (WR)	5.85	4.00	25.70	4.30	1.03	19.35	0.73	7.39	6.00	4.00	44.10	4.91	105.00	3.00	22.00	2.00	33.00
Qvset-2	RWVC17-141 (WR)	4.31	3.00	34.60	3.10	0.77	14.80	0.55	21.00	5.00	3.00	33.10	3.74	95.00	3.00	18.00	1.00	25.00
Qvset-2	RWVC17-049 (WR)	4.73	3.00	28.40	3.10	0.76	16.35	0.51	5.50	5.00	3.00	31.40	3.48	98.00	3.00	16.00	1.00	23.00
Qvset-2	RWVC17-136 (WR)	3.98	2.00	98.80	2.20	0.56	11.55	0.37	3.66	12.00	3.00	21.60	2.44	116.00	3.00	19.00	2.00	27.00
Qvset-2	RWVC16-121 (WR)	4.31	3.00	49.10	2.30	0.53	14.30	0.37	19.50	7.00	2.00	20.70	2.41	135.00	4.00	16.00	2.00	17.00
Qvse1	RWVC16-116 (WR)	8.54	7.00	4.60	7.20	1.67	30.40	1.23	11.00	<5	6.00	71.10	8.16	141.00	1.00	32.00	1.00	39.00
Qvse2	RWVC17-050 (WR)	7.23	3.00	4.60	7.30	1.40	31.00	1.02	10.95	<5	5.00	51.20	6.96	135.00	4.00	33.00	1.00	35.00

Appendix D. ICP-MS and ICP-AES geochemical data for un-normalized rare earth elements (REE- indicated by *) and trace elements of the Cerro Seco volcanic suite. Values are reported in ppm (parts per million). (Type) indicates material analyzed: (SP)=single pumice; (WR)=whole rock.

APPENDIX E. BEDDING ATTITUDES OF SELECTED CERRO SECO ERUPTIVE UNITS

WP	Unit	Strike	Dip	Azimuth
49	Qvset-2	N28W	9NE	152
	Qvset-2	N29W	11NE	153
	Qvset-2	N10W	8NE	
	Qvset-2	N24E	11NW	
99	Qvset-2	N15E	26NW	195
112/132/010	Qvset-2	N80W	22SW	
	Qvset-2	N64E	18SE	
	Qvset-2	N60E	15SE	
	Qvset-2	N40E	12SE	
	Qvset-2	N65E	18SE	
	Qvset-2	N70E	18SE	
113	Qvset-2	N52E	20NW	232
	Qvset-2	N68E	19NW	248
121	Qvset-2	N23E	13NW	203
	Qvset-2	N78W	4SW	
	Qvset-2	N10E	15SE	
122	Qvset-2	N46W	7NE	
bet 127-128	Qvset-2	N89W	22NE	269
	Qvset-2	N28E	25NW	
	Qvset-2	N50E	28SE	
128	Qvset-2	N10E	30SE	190
	Qvset-2	N2E	36NW	
	Qvset-2	N6E	38NW	
bet 128-130	Qvset-2	N70W	14SW	
	Qvset-2	N80W	14NE	
	Qvset-2	N90W	17N	90
	Qvset-2	N39E	9NW	219
	Qvset-2	N22W	25NE	
		N60W	25NE	240
131	Qvset-2	N56E	16NW	
	Qvset-2	N80E	14NW	
	Qvset-2	N53E	15NW	
	Qvset-2	N55W	7NE	
139	Ql	N80W	11SW	
141	Qvset-2	N50E	25NW	
	Qvset-2	N38E	26NW	

WP	Qvset-2	N50E	22NW	
	Qvset-2	N50E	29NW	
behind 102	Qvset-2	N10E	18NW	
17-009	Qvset-2	N14E	22SE	
	Qvset-2	N19E	22SE	
115	Qvset-2	N25E	9NW	
	Qvset-2	N58W	5SW	
14	Qvset-2	N52W	23NE	
30	Qvset-2	N40W	23SW	140
33-foliation	Qvse1	N34E	55SE	34
34-foliation	Qvse1	N18E	60SE	18
40-foliation	Qvse1	N34E	65SE	34
	Qvse1	N55E	40SE	55
48	Qvset-2	N90E	28N	90

Appendix E. Strikes and dips measured on appropriate bedding planes of Qvset-2. Strikes were measured using quadrant method, then converted to azimuth. Note: All measurements taken in 2016 are shown in black; 2017 data is shown in red. Abbreviation: WP=waypoint.

ILLUSTRATIONS

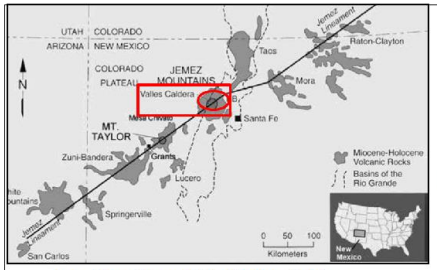

Location Map of the Valles Caldera

Plate I

Geologic Map of Cerro Seco, Valles Caldera, New Mexico

Explanation

Line Symbols

- Cross-section line A-A'
- Contact, approx. located
- Contact, certain
- Normal fault, approx. located

Point Symbols

- ★ Location of radiometric dated sample (age in Ma)
- ⊙ Geothermal well
- Structure points (strike/dip)

Lithologic units

- Ql
- Qa, Qc
- Qto
- Qvsa
- Qvse2
- Qvse1
- Qvset-2-gravel
- Qvset-2
- Qvset-1
- Qvsl2
- Qvsl1
- Qrc
- Qbt
- Qxp
- Qbo

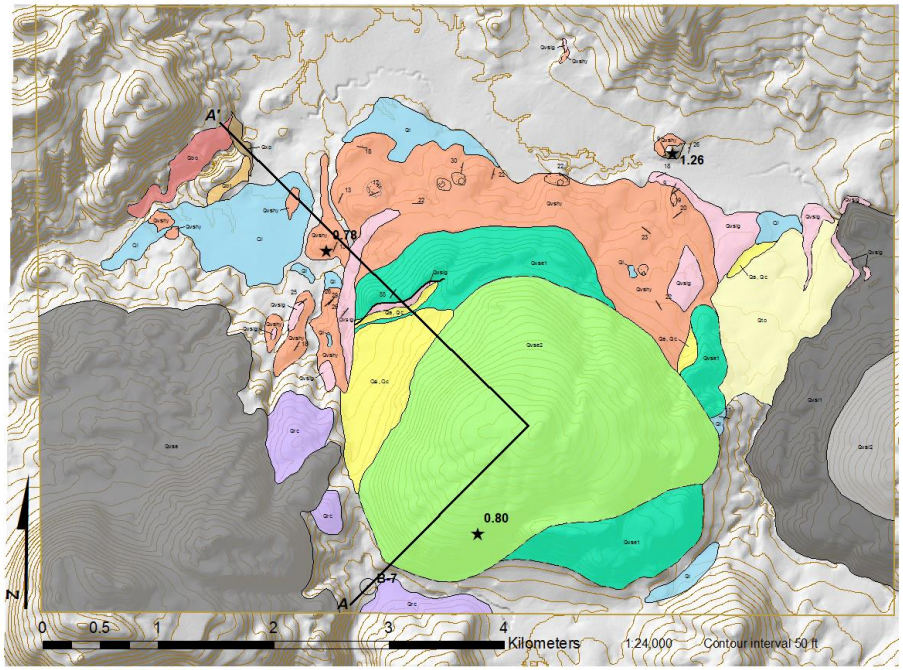

Plate II - Geologic Cross-section of Cerro Seco

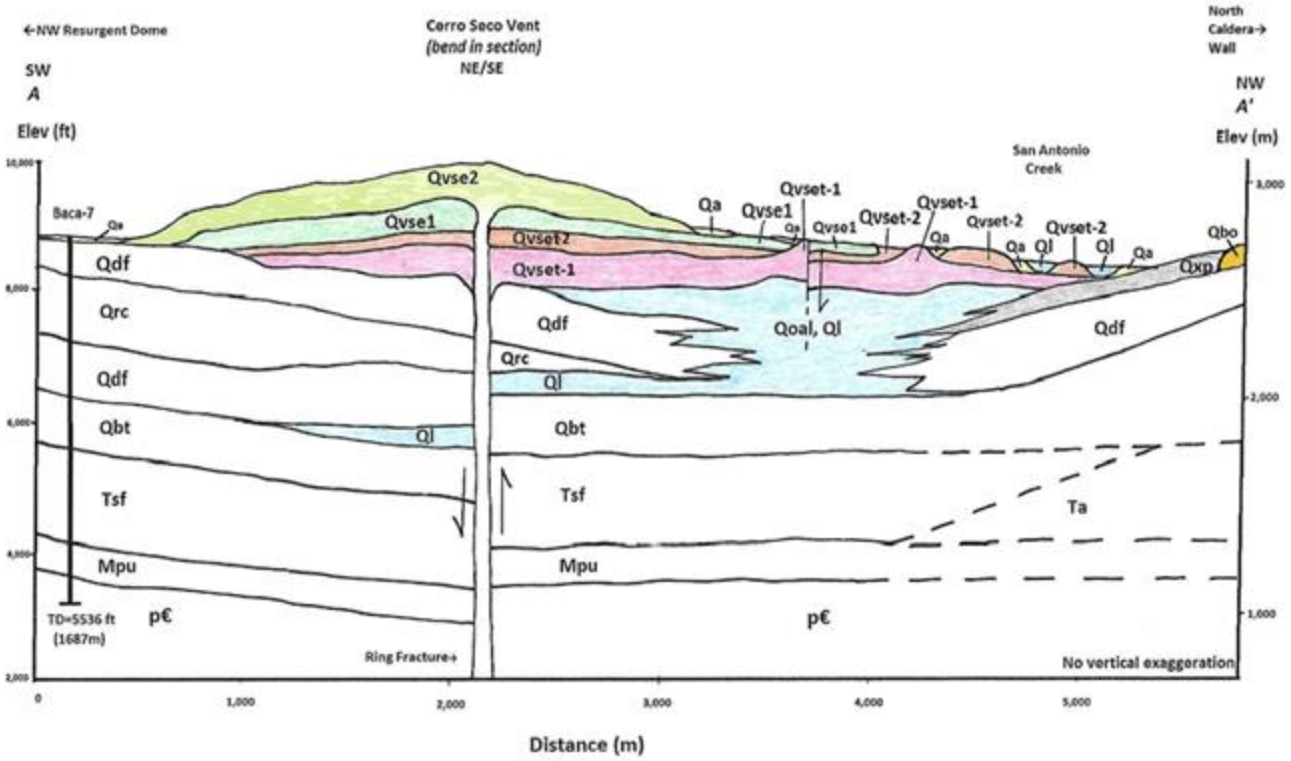

Explanation

Ql	Lacustrine deposits	Qvset-2	Seco pyroclastic unit, second
Qa	Alluvial, colluvial deposits	Qvset-1	Seco ignimbrite
Qvse2	Seco lava, second	Qxp	Caldera collapse breccia, Paliza Fm
Qvse1	Seco lava, first	Qbo	Bandelier Tuff, Otowi Member

Contact, certain

Contact, approximated

Normal fault sense of motion

TD Total depth, Baca-7 well

Plate III. STRATIGRAPHIC SECTION OF CERRO SECO HYDROMAGMATIC UNIT (Qvset-2) Waypoint-141

Location: 3980356/0356365, UTM NAD 27
Attitude: N50E 26NW

Total thickness: 7.7 m minimum section

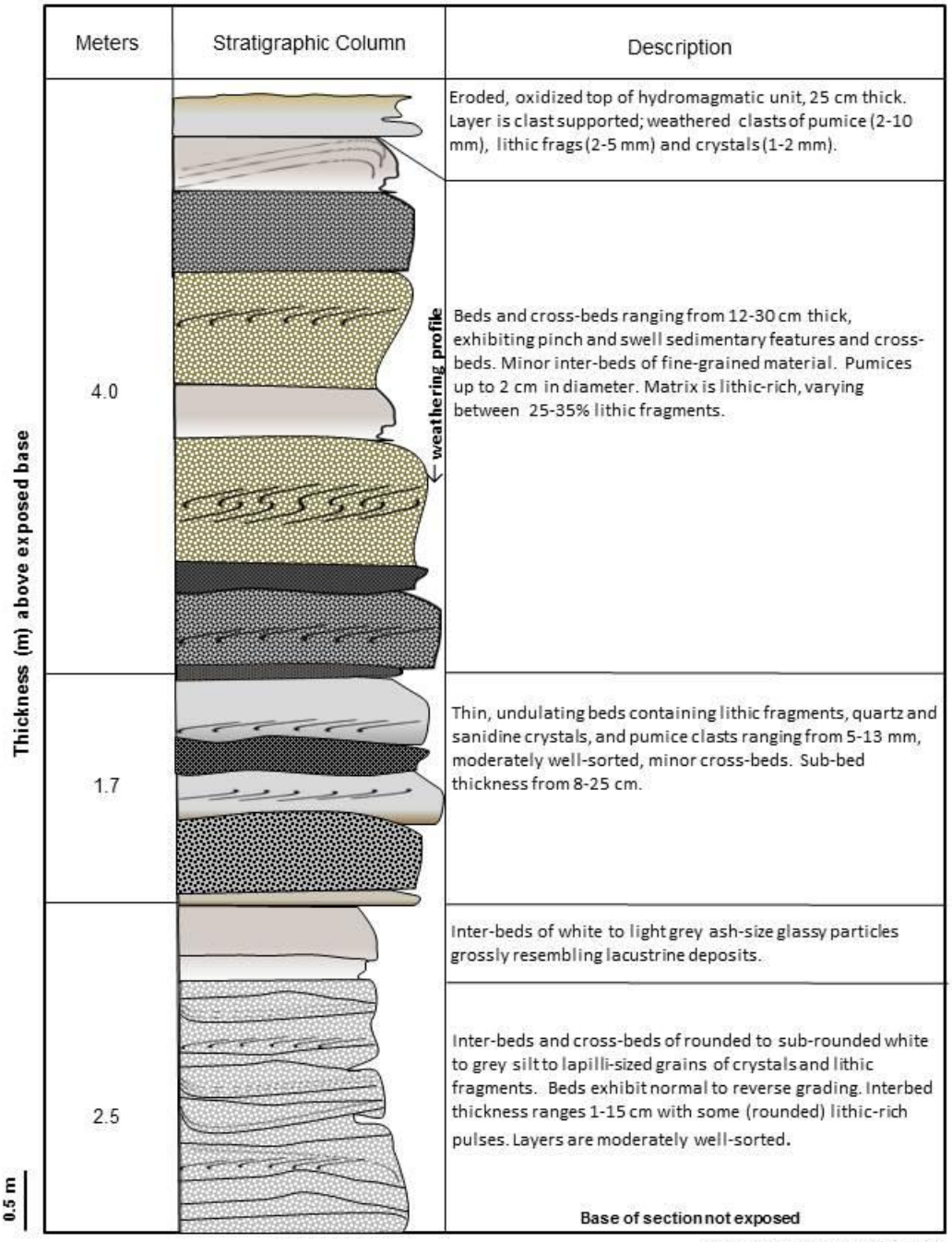

Measured by Robin Wham, 2017

Plate IV. STRATIGRAPHIC SECTION OF CERRO SECO HYDROMAGMATIC UNIT (Qvset-2) WP-136

Location: 3981124/0354835, UTM NAD 27
Attitude: N76E 37 NW

Total thickness: 4.9 m minimum section

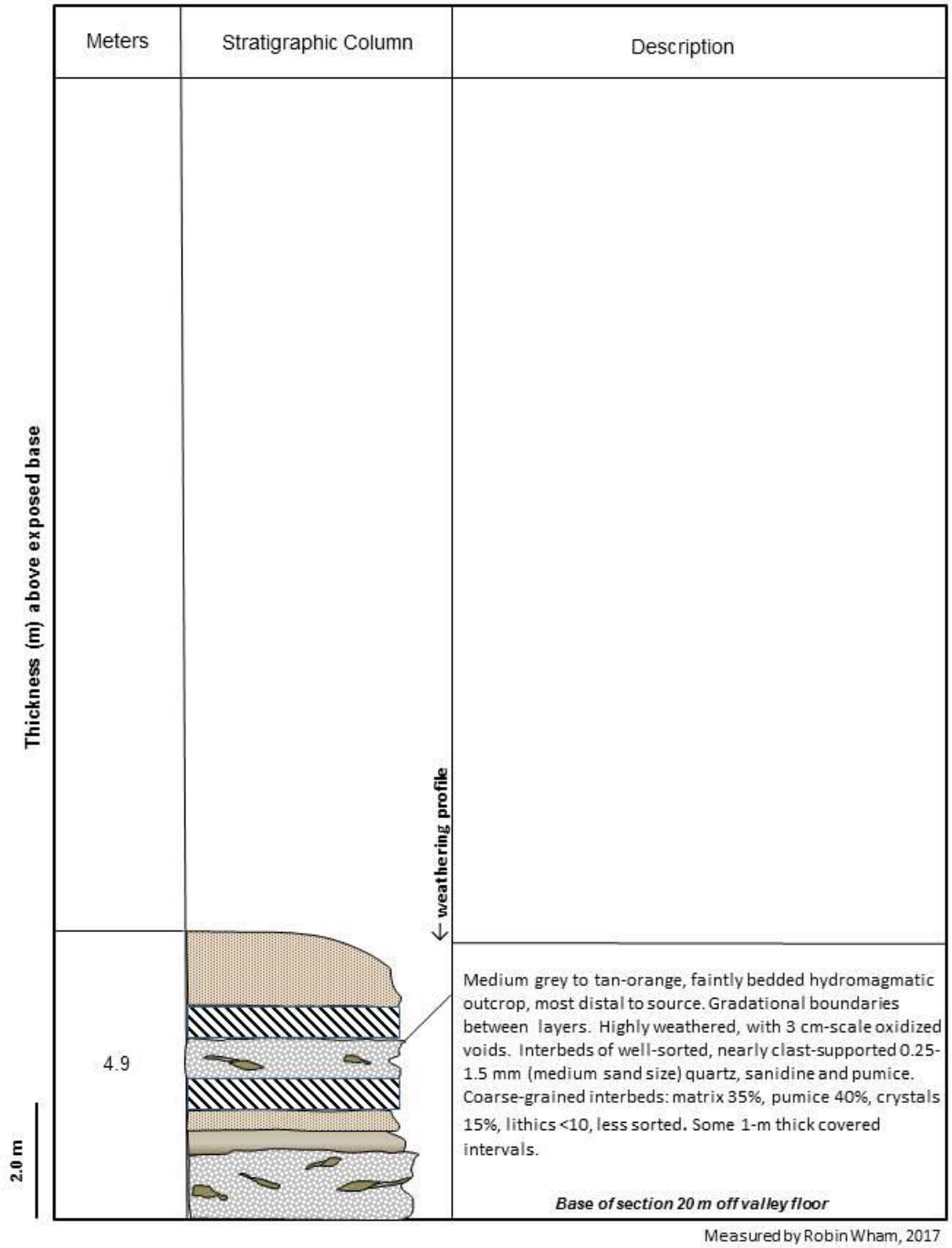

Measured by Robin Wham, 2017

Plate V. STRATIGRAPHIC SECTION OF CERRO SECO HYDROMAGMATIC UNIT (Qvset-2) Waypoint-049

Location: 3981772/0359135, UTM NAD 27 Total thickness: 6.1 m minimum section
Attitude: variable (N24E 11NW; N15E 26NW; N30W 14NE)

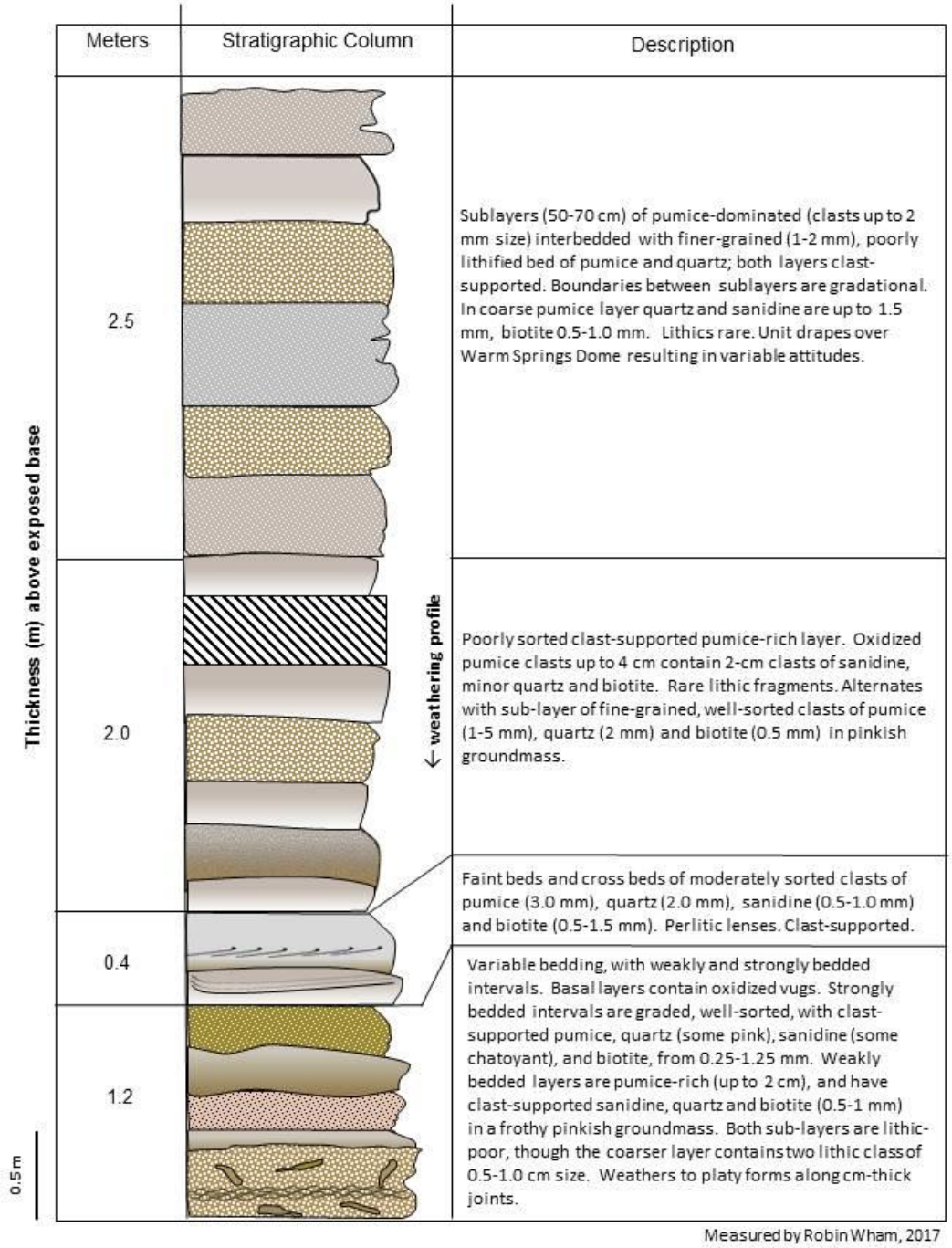

Measured by Robin Wham, 2017

Plate VI. STRATIGRAPHIC SECTION OF CERRO SECO PYROCLASTIC UNITS (Qvset-1+Qvset-2) WP-132

Location: 3981527/0359114, UTM NAD 27
Attitude: N60E 18 SE

Total thickness: 46 m minimum section

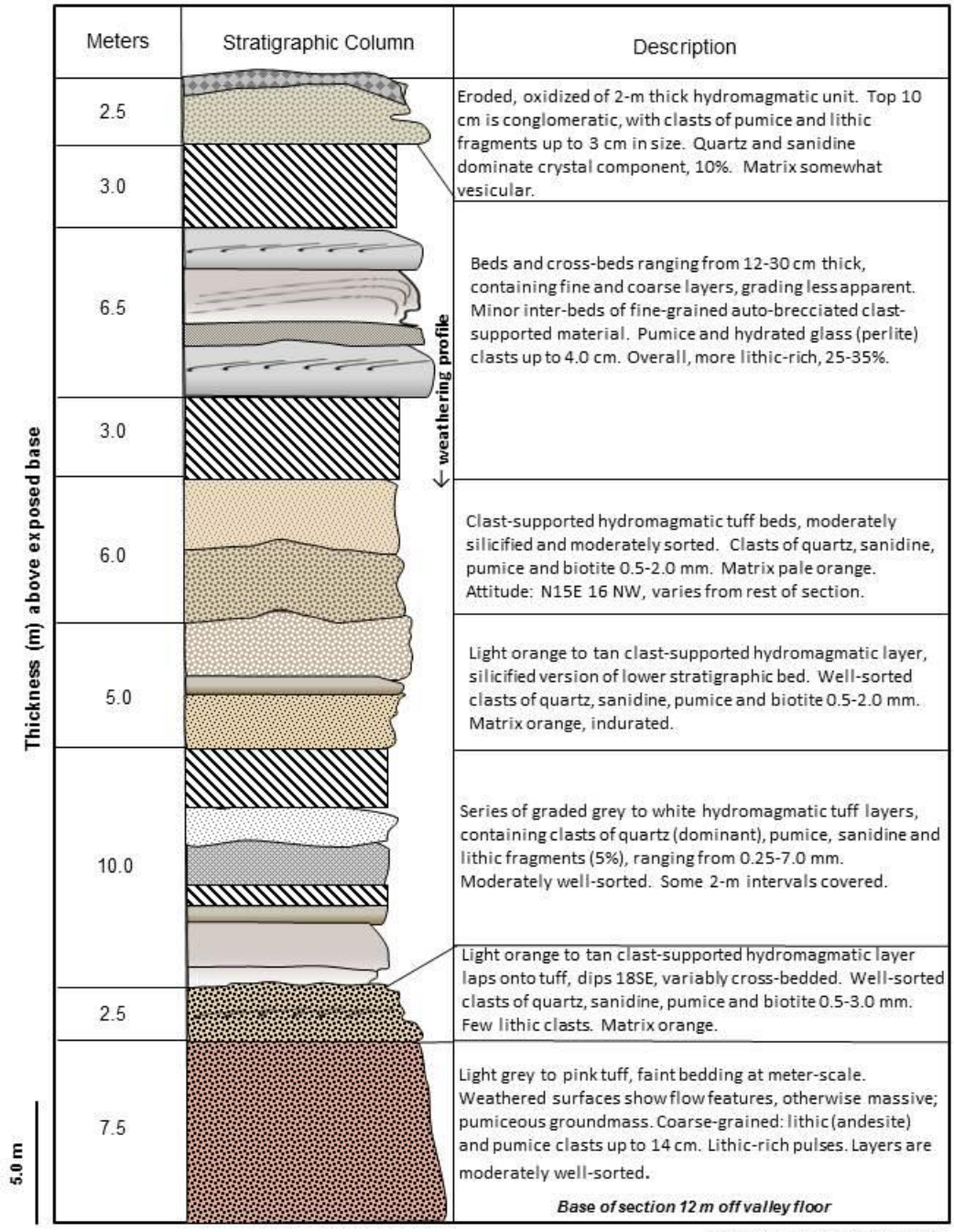

Measured by Robin Wham, 2017

REFERENCES

Aldrich, M. J. and Laughlin, A. W., 1984, A Model for the tectonic development of the Southeastern Colorado Plateau Boundary: Journal of Geophysical Research, v. 89, no. B12, p. 10,207-10,218.

Bailey, R. A., Smith, R. L., and Ross, C. S., 1969, Stratigraphic Nomenclature of Volcanic Rocks in the Jemez Mountains, New Mexico: U. S. Geological Survey Bulletin 1274-P, 19 p.

Best, M.G., and Christiansen, E.H., 1997, Origin of broken phenocrysts in ash-flow tuffs: Geological Society of America Bulletin, v. 109, p. 63-73.

Blatt, H. and John M. Christie, J. M., 1963, Undulatory extinction in quartz of igneous and metamorphic rocks and its significance in provenance studies of sedimentary rocks: Journal of Sedimentary Research, v. 33, p.559-579.

Blatt, H., Tracy, R. J. and Owens, B. E., 2006, Petrology: Igneous, Sedimentary and Metamorphic: New York, W. H. Freeman and Company, 530 p.

Branney, B.J. and Kokelaar, P**.,** 1992, A reappraisal of ignimbrite emplacement: progressive aggradation and changes from particulate to non-particulate flow during emplacement of high-grade ignimbrite: Bulletin of Volcanology, v. 54, p. 504-520.

Branney, B.J. and Kokelaar, P**.,** 2002, Pyroclastic density currents and the sedimentation of ignimbrite: Geological Society Memoir, p. 1-141.-

Cas, R. A. F., and Wright, J. V., 1992**,** Volcanic Successions: London, Chapman & Hall, 528 p.

Cashman, K.V. and Sparks, R. S. J., 2013, How volcanoes work: A 25 year perspective: GSA Bulletin, v. 125, no. 5/6, p. 664–690.

Chipera, S., Goff, C. J., Goff, F., Fittipaldo, M., 2008, Zeolitization of intracaldera sediments and rhyolitic rocks in the 1.25 Ma lake of Valles caldera, New Mexico, USA: Journal of Volcanology and Geothermal Research, v. 178, Issue 2, 317-330.

Cole, P.D., 1991, Migration direction of sand-wave structures in pyroclastic surge deposits: Implications for depositional processes: Geology, v. 19, p. 1108-1111.

Cox, **K. G**.; Bell, J. D., and Pankhurst, R. J., 1979, The Interpretation of Igneous Rocks: London, George Allen & Unwin, 450 p.

David, **C.P**., Dulce, R.G., Nolasco, D.D., Zamoras, L.R., Jumawan, F.T. and Newhall, C.G., 1999, Changing proportions of two pumice types from the June 15, 1991, Eruption of Mount Pinatubo: pubs.usgs.gov/pinatubo/david.

Fisher, R. V. and Smith, G. A., (editors), Sedimentation in Volcanic Settings, Society for Sedimentary Geology Special Publication No. 45.

Fisher, R.V., Orsi, G., Ort, M., Heiken, G., 1993, Mobility of a large-volume pyroclastic flow--emplacement of the Campanian ignimbrite, Italy, Technical Report, Journal of Volcanology and Geothermal Research, v. 56 (3), p. 205-220.

Frost, B. R. and Frost, C. D., 2008, A geochemical classification for feldspathic igneous rocks: *Journal of Petrology*, v. 49, p. 1955–1969.

Fujii, T. and Nakada, S. **,** 1999, The 15 September 1991 pyroclastic flows at Unzen Volcano (Japan): a flow model for associated ash-cloud surges: *Journal of Volcanology and Geothermal Research*, v. 89, p. 159-172.

Fujinawa, A., Ban, M., Ohba, T., Kontani, K., Miura, K., 2008, Characterization of low-temperature pyroclastic surges that occurred in the northeastern Japan arc during the late 19th century: *Journal of Volcanology and Geothermal Research*, v. 178, p. 113–130.

Gardner, J. N., Goff, F., Kelley, S., and Jacobs, E., 2010, Rhyolites and associated deposits of the Valles-Toledo caldera complex: New Mexico Geology v. 32, Number 1, 3-18.

Gardner, J. and Goff, F., 1986, Stratigraphic relations and lithologic variations in the Jemez volcanic field, New Mexico: Journal of Geophysical Research 91:1763-78.

Goff, F. and Gardner, J. N., 2004, Late Cenozoic geochronology of volcanism and mineralization in the Jemez Mountains and Valles caldera, north central New Mexico in The Geology of New Mexico – A geologic history: New Mexico: Geological Society Special Publication 11, ed. G. Mack and K. Giles, 295-312. Socorro: New Mexico Geological Society.

Goff, **F**., Wolff, J. A., and Fellah, K., 2013, Mount Taylor dikes, New Mexico Geological Society Guidebook, 64th Field Conference, Geology of Route 66 Region: Flagstaff to Grants, 2013, p. 159-165

Goff, F., Warren, R. G., Goff, C. J., Whiteis, J., Kluk, E., and Counce, D., 2007, Comments on the geology, petrography, and chemistry of rocks within the resurgent dome area, Valles caldera, New Mexico, in Kues, B., Kelley, S., and Lueth, V., (eds.), Geological of the Jemez region II: New Mexico Geological Society Guidebook 58, p. 354-366.

Goff, F., Reneau, S. L., Goff, C. J., Gardner, J., N., Drakos, P. G., Katzman, D., 2006, Geology of the Valle San Antonio 7.5 Minute Quadrangle, Sandoval and Rio Arriba Counties, New Mexico, New Mexico Bureau of Geology and Mineral Resources, scale 1:24,000, 1 sheet.

Goff, F., Warren, R. G., Goff, C. J., and Dunbar, N., 2014, Eruption of reverse-zoned upper Tshirege Member, Bandelier Tuff from centralized vents within Valles caldera, New Mexico: Journal of Volcanology and Geothermal Research, v. 276, p. 82-104.

Goff, F., 2009, Valles Caldera, A Geologic History, University of New Mexico Press, p. 114.

Goff, F., Gardner, J. N., Hulen, J. B., Nielson, D. L., Charles, R., WoldeGabriel, G., Vuataz, F-D., Musgrave, J. A., Shevenell, L., and Kennedy, B. M., 1992, The Valles caldera hydrothermal system, past and present, New Mexico, USA, Scientific Drilling, v. 3, p. 181-204.

Goff, F., Gardner, J. N., Reneau, S. L., Kelley, S. A., Kempter, K. A., and Lawrence, J. R., 2011, Geologic map of the Valles caldera, Jemez Mountains, New Mexico, New Mexico Bureau of Geology and Mineral Resources, scale 1:50,000, 1 sheet.

Goff, F. and Janik, C. J**.,** 2000, Geothermal Systems, in Sigurdsson, H., ed., Encyclopedia of Volcanoes, p. 817-834.

Heiken, G., 1972**,** Morphology and Petrography of Volcanic Ashes: Geological Society of America Bulletin, v. 83, p. 1961-1988.

Heiken, G. and Wohletz, K., 1987, Tephra deposits associated with silicic domes and lava flows, Geological Society of America Special Paper 212.

Hildreth, W., 1981, Gradients in silicic magma chambers' implications for lithospheric magmatism: Journal of Geophysical Research, v. 86, no. B11, p. 10153-10192.

Hudson, M. R. and Grauch, V. J. S., 2013, Introduction in New perspectives on Rio Grande rift basins: from tectonics to groundwater, Geological Society of America Special Papers 2013, v. v-xii, p. 494.

Irvine, T.N. and Baragar, W.R.A., 1971, A guide to the chemical classification of the common volcanic rocks: Canadian Journal of Earth Sciences, v. 8, p. 523-548.

Karlstrom, K. E. and Humphreys, E. D, 1998, Persistent influence of Proterozoic accretionary boundaries in the tectonic evolution of southwestern North America: Interaction of cratonic grain and mantle modification events: Rocky Mountain Geology, v. 33, no. 2, p. 161-179.

Kerr, P.F., 1952, Formation and Occurrence of Clay Minerals: Clays and Clay Minerals, v. 1, no. 1, p. 19-32.

Lambert, S. J. and Epstein, S., 1980, Stable isotope investigation of an active geothermal system in the Valles caldera, Jemez Mountains, New Mexico, Journal of Volcanology and Geothermal Research, v. 8, p. 111-129.

Le Maitre, R.W., 1989, A Classification of Igneous Rocks and Glossary of Terms: Recommendations of the International Union of Geological Sciences Subcommission on the Systematics of Igneous Rocks. Blackwell, Oxford, 193 pp.

Le Bas, M. J., Le Maitre, R. W., Streckeisen, A., and Zanettin, B., 1986, A chemical classification of volcanic rocks based on the total alkali-silica diagram: Journal of Petrology, v. 27, p. 745-750.

Lipman, P. W., Chapin, C. E., and Dungan, M. A., 1989, Cenozoic Volcanism in the Western United States, A Volume of Selected Reprints, American Geophysical Union, Library of Congress, Washington, D. C.

Martin, R.C., 1959, Some field and petrographic features of American and New Zealand ignimbrites: New Zealand Journal of Geology and Geophysics, v. 2, p. 394-411.

Miyashiro, A., 1978, Nature of alkalic volcanic rock series: Contributions to Mineralogy and Petrology, v. 66, p. 91-104.

Morrissey, M., Zimanowski, B., Wohletz, K., and Buettner, R., 2000, Phreatomagmatic Fragmentation, in Sigurdsson, H., ed., Encyclopedia of Volcanoes, p. 421-445.

Nesse, W. D., 1991, Introduction to Optical Mineralogy, Second Edition: New York, Oxford University Press, 335 p.

Olsen, K. H., ed, 2006, Continental rifts: Evolution, structure, tectonics in Developments in Geotectonics, v. 25, p. 3-466.

Reneau, S. L., 2007, Post-resurgence lakes in the Valles caldera, New Mexico, in Geology of the Jemez Mountains Region II (58th Field Conference Guidebook), ed. B. S. Kues, S. A. Kelley, and V. W. Lueth, p. 398-408. Socorro: New Mexico Geological Society.

Schmincke, H. U., 2004, Volcanism, Springer 2004 (book in library QE 522 S295 2004)

Shand, S.J., 1947, The Eruptive Rocks, 3rd edition. New York: John Wiley, 444 p.

Sheridan, M. F. and Updike, R. G., 1975, Sugarloaf Mountain Tephra — A Pleistocene Rhyolitic Deposit of Base-Surge Origin in Northern Arizona, Geological Society of America Bulletin, v. 86, p. 571-581.

Sheridan, M. F. and Wohletz, K. H., 1981**,** Hydrovolcanic Explosions: The Systematics of Water-Pyroclast Equilibration, Science, v. 212, pp. 1387-1389.

Smith, R. L., 1960, Zones and zonal variations in welded ash flows: Geological Survey Professional Paper 354-F, Reprinted from USGS Professional Papers 345-F and 366, New Mexico Geological Society No. 9, 1980.

Smith, R. L., 1961, Ash-flow tuffs: their origin, geologic relations and identification: Geological Survey Professional Paper 366, Reprinted from USGS Professional Papers 345-F and 366, New Mexico Geological Society No. 9, 1980.

Smith, R. L. and Bailey, R. A., 1968, Resurgent Cauldrons; ***in*** Coats, R. R., Hay, R. L., and Anderson, C. A. (eds.), Studies in volcanology: Geological Society of America, Memoir 116: 613-662.

Smith, R. L., Bailey, R. A., and Ross, C. S., 1970, Geologic map of the Jemez mountains, New Mexico, Miscellaneous Investigations Series: U. S., Geological Survey, scale 1:125,000, 1 sheet

Smith, R.L., 1979, Ash-flow magmatism: Geological Society of America Special Paper 180, p. 5-27.

Spell, T. L., 1987, Geochemistry of Valle Grande Member ring fracture rhyolites, Valles Caldera, New Mexico, M.S. thesis, 213 pp., N.M. Inst. of Min. and Technol., Socorro.

Spell, T. L. and Kyle, P. R., 1989, Petrogenesis of Valle Grande Member rhyolites, Valles caldera, New Mexico: Implications for evolution of the Jemez Mountains magmatic system, Journal of Geophysical Research, v. 94, No. B8, p. 10, 379-10, 396.

Trainer, F. W., Rogers, R. J., and Sorey, M. L., 2000, Geothermal hydrology of Valles caldera and the southwestern Jemez mountains, New Mexico, USGS Water-Resources Investigations Report 00-4067, 115 p.

Valentine, G.A. and Fisher, R.V**.,** 2000, Pyroclastic surges and blasts. In: Sigurdsson, H., Houghton, B., McNutt, S. R., Rymer, H., and Stix, J., eds., Encyclopedia of Volcanoes, p. 545–554.

Vespermann, D., and Schmincke, H. U., 2000, Scoria Cones and Tuff Rings, *in* Sigurdsson, H., Houghton, B., McNutt, S. R., Rymer, H., and Stix, J., eds., Encyclopedia of Volcanoes, p. 683-694.

West, M., Ni, J., Wilson, D., Aster, R., Baldridge, S., Gao, W., Grand, S., Gok, R., 2003, Passive rifting and support for high elevation in the Southwest U.S.: kiska.giseis.alaska.edu /input/west/ presentations/iris2003-miniposter.

Wilson, C.J.N. and Houghton, B.F**.,** 2000, Pyroclast transport and deposition, in Sigurdsson, H., Houghton, B., McNutt, S. R., Rymer, H., and Stix, J., eds., Encyclopedia of Volcanoes, p. 545–554.

Wohletz, K.H., 1998, Pyroclastic surges and compressible two-phase flow. In: From MAGMA to TEPHRA Modelling Physical Processes of Explosive Volcanic Eruptions, A. Freundt (Ed.), Elsevier Science Publications, Amsterdam, p. 247-312.

Wohletz, K.H. and Sheridan, M.F., A Model of Pyroclastic Surge, Geol. Soc. Amer. Sp. Paper 180, 1979.

Wolff, J. A., Rowe, M. C., Teasdale, R., Gardner, J. N., Ramos, , and Heikoop, C. E., 2005, Petrogenesis of pre-caldera mafic lavas, Jemez Mountains Volcanic Field (New Mexico, USA): Journal of Petrology, v. 46(2), p. 407–439.

Zoback, M. L., Anderson, R. E. and Thompson, G. A., 1981, Cainozoic evolution of the state of stress and style of tectonism of the Basin and Range province of the western United States: Philosophical Transactions of the Royal Society of London A 300, p. 407-434.